Establishment and application of a FRET sensor for VRAC activity reveals a key role for diacylglycerol signaling in channel regulation

Inaugural-Dissertation
to obtain the academic degree
Doctor rerum naturalium (Dr. rer. nat.)
submitted to the Department of Biology, Chemistry and Pharmacy
of Freie Universität Berlin

by
Benjamin König
from Berlin

2019

This work was prepared under the supervision of PD. Dr. Tobias Stauber at the Freie Universität Berlin from May 2015 until October 2019.

1^{st} Reviewer:	PD. Dr. Tobias Stauber, BCP Freie Universität Berlin
2^{nd} Reviewer:	Prof. Dr. Helge Ewers, BCP Freie Universität Berlin

Date of defense: 12.08.2020

Preface

Part of this work has been published in the following publication:

Benjamin König, Yuchen Hao, Sophia Schwartz, Andrew JR Plested, Tobias Stauber,
A FRET sensor of C-terminal movement reveals VRAC activation by plasma membrane DAG signaling rather than ionic strength.
eLife, 2019. 8: p. e45421

Part of the experiments shown in this thesis were performed in collaboration with Yuchen Hao from the AG Plested, FMP Berlin. All electrophysiological recordings were exclusively performed by him and patch-clamp fluorometry experiments in collaboration with me.

Acknowledgments

First of all, I want to thank my boss and supervisor Dr. Tobias Stauber. Not just for hiring me in general, but as well for being supportive or annoying depending on what the situation demanded (to quote my wife: “I think he knows how to deal with you!”). Especially for just letting me do and discover what is possible and what not. This hell of a ride would not have been the same with someone else. Thank you.

I want to thank Yuchen Hao and Prof. Dr. Andrew Plested for collaborating with us/me in a very productive way. This thesis and the insights gained with the FRET sensor were tremendously improved by the work we did together.

As well I have to thank Lisa von Kleist and Antje Buttgereit for all the support, fun, and tears we shared for the last four years. We built up a lab together; no one can take that from us. I am grateful for all the things I learned from you guys, professionally and personally.

I thank the members of AG Stauber, Stricker, Freund, Ewers, and Knaus in general for the support and advice. Special thanks to Prof. Dr. Helge Ewers for letting me restore and work with his microscope and the fruitful discussions we had (of course, as well for being my second reviewer!). In more detail, I want to thank Anja, Wiebke, Jonas, Sophia, Miguel, Lisa, Frank, Miriam, Anna, Katharina, Susanne, Sophie, George, Pedro, Hylkje, Jia, and all I might have forgotten for the role they played in bringing me here.

Last but not least, I have to thank my family and friends. Without my family nothing of this would have been possible. The rougher the seas, the smoother we sail, but only with the crew formed by TSUZ, “dem braunen Auge” and “der Tropenschatzbande.” The last words (as this work and everything beyond) shall be dedicated to my heart and soul, Nici and Melissa. Thank you!

Contents

List of Figures

List of Tables

List of Abbreviations

a.u.	arbitary unit
adPROM	affinity-directed protein missile
aFRET	cFRET normalized to acceptor concentration
APB	acceptor photobleaching
AVD	apoptotic volume decrease
BFA	brefeldin A
C3	three-fold rotational symmetry
C6	six-fold rotational symmetry
CAMK	Ca^{2+}/calmodulin-dependent protein kinase
CFP	cyan-fluorescent protein
cFRET	corrected FRET
DAG	diacylglycerol
DCPIB	4-[(2-Butyl-6,7-dichloro-2-cyclopentyl-2,3-dihydro-1-oxo-1H-inden-5-yl)oxy]butanoicacid
dFRET	cFRET normalized to donor concentration
DIC	differential interference contrast
DOG	dioctanoylglycol
ebo	ébouriffé
ECD	extracellular domain
EAA	excitatory amino acids
EL	extracellular loop
ER	endoplasmic reticulum
FM	self-dimerizing domains of the FK506-binding protein
FOV	field of view
FRET	Förster-resonance energy transfer
GABA	gamma-aminobutyric acid

GFP	green-fluorescent protein
GPCR	G-protein coupled receptors
HEK 5x KO	HEK293 cells with all 5 LRRC8 proteins depleted
HPLC	high-performance liquid chromatography
$\mathbf{I}^{AA}$	intensity measured with acceptor excitation and acceptor emission, acceptor channel
$\mathbf{I}^{DA}$	intensity measured with donor excitation and acceptor emission, FRET channel
$\mathbf{I}^{DD}$	intensity measured with donor excitation and donor emission, donor channel
$\mathbf{I}^{DD}_{AB}$	intensity measured with donor excitation and donor emission after bleaching of YFP
ICD	intracellular domain
IL	intracellular loop
IP3	inositol-1,4,5-triphosphate
KO	knock-out
LatB	latrunculin B
LRRC8	leucine-rich repeat-containing protein family 8
LRRD	leucine-rich repeat domain
LUT	look-up table
NPPB	5-nitro-2-(3-phenylpropyl-amino)benzoic acid
NTC	N-terminal coil
OAG	1-oleoyl-2-acetyl-sn-glycerol
PA	phosphatic acid
PDBu	phorbol 12,13-dibutyrate
PIP2	phosphatidylinositol-4,5-bisphosphate
PIP3	phosphatidylinositol-3,4,5-triphosphate
PKC	protein kinase C
PKD	protein kinase D
PLC	phospholipase C
PM	plasma membrane
PMA	phorbol-12-myristate-13-acetate

PTK	protein tyrosine kinase
PTP	proteine tyrosine phosphatases
RFP	red-fluorescent protein
ROI	region of interest
ROS	reactive oxygen species
RVD	regulatory volume decrease
RVI	regulatory volume increase
s.e.m.	standard error of the mean
S1P	sphingosine-1-phosphate
S1PR	sphingosine-1-phosphate receptor
SCL12A	solute-carrier family 12 A
seFRET	sensitized-emission FRET
siRNA	small interfering RNA
TMD	transmembrane domain
TMH	transmembrane helix
TNFα	tumor necrosis factor α
unFRET	cFRET without normalization
VAAC	volume-activated anion channel
VRAC	volume-regulated anion channel
VSOAC	volume-sensitive organic osmolyte/anion channel
VSOR	volume-sensitive outwardly rectifying anion channel
YFP	yellow-fluorescent protein

SI units and SI prefixes are used according to the International System of Units. Nomenclature and symbolism for amino acids and peptides follows the guidelines of the IUPAC-IUB Joint Commission on Biochemical Nomenclature (JCBN): "Nomenclature and symbolism for amino acids and peptides. Recommendations 1983."

Abstract

The volume-regulated anion channel (VRAC) is a crucial part of the regulatory volume decrease in vertebrate cells with various other proposed roles as, for example, in apoptosis, differentiation, and auto/paracrine signaling. Their modular architecture with differing biophysics and potential functions, as well as the lack of specific inhibitors, led to VRAC's activation mechanism being elusive until today. Furthermore, current methods to study VRACs fail to account for the diversity of these channels.

In this thesis, the movement of fluorophores at the C-termini of the VRAC forming protein family LRRC8 upon activation was proven by Förster-resonance energy transfer (FRET) microscopy. Patch-clamp fluorometry validated that FRET variations reflect channel gating. FRET microscopy of fluorescently labeled LRRC8 proteins was, therefore, exploited as a new optical sensor for VRAC activity.

The optical sensor revealed isotonic activation of VRAC by the diacylglycerol analog phorbol-12-myristate-13-acetate (PMA), an effect abolished by the whole-cell configuration. VRACs trapped on endomembranes by the reverse dimerization system cannot be activated by decreased intracellular ionic strength. Furthermore, are VRACs rendered active under isotonic conditions by inhibition of the diacylglycerol kinase (DAGK) by dioctanoylglycol. Activation of VRAC by hypotonicity was impaired by the PKD inhibitor CRT 0066101.

Concludingly, ionic strength is not the critical regulator of VRAC activity in living cells. Instead, they are activated by diacylglycerol mediated PKD recruitment. Electrophysiological approaches might obscure the effects of drugs and protein manipulations, as seen for PMA. The here established FRET-based optical sensor opens new possibilities to detect activation of VRACs in living cells in a non-invasive, subunit-specific manner.

Zusammenfassung

Der Volumen regulierte Anionenkanal (VRAC) spielt eine zentrale Rolle im Prozess der regulierten Volumenverringerung von Wirbeltierzellen nebst anderen vermuteten Rollen in Prozessen wie der Apoptose, Differenzierung und der auto/parakrinen Sekretion. Sowohl der modulare Aufbau, der zu unterschiedlichen biophysikalischen Eigenschaften und vermutlich Funktionen führt, als auch das Fehlen spezifischer Inhibitoren hat dazu geführt, dass der Aktivierungsmechanismus von VRAC bis heute ungeklärt ist.

In dieser Arbeit beweise ich mithilfe von Förster Resonanz Energie Transfer (FRET) Mikroskopie, dass sich fluoreszente Proteine, die an den C-Terminus der VRAC formenden LRRC8 Proteinfamilie fusioniert sind, bei der Aktivierung des Kanals bewegen. Mithilfe von patch-clamp Fluorometrie konnte ich zeigen, dass FRET Änderungen tatsächlich das Öffnen und Schließen des Kanals wiederspiegeln. Ich habe daher FRET-Mikroskopie von fluoreszierenden LRRC8 Fusionsproteinen als optisches Werkzeug genutzt, um die Aktivierung von VRACs zu detektieren.

Mit diesem Werkzeug konnte ich die Aktivierung von VRAC unter isotonen Bedingungen durch das Diacylglycerol Analogon Phorbol-12-myristat-13-acetat (PMA) nachweisen und gleichzeitig zeigen das die whole-cell Konfiguration diesen Effekt unterdrückt. VRACs die in Endomembranen lokalisiert sind können nicht durch intrazellulär reduzierte Ionenstärke aktiviert werden. Desweitern, bleiben bereits aktivierte Kanäle auch unter isotonen Bedingungen aktiv, wenn das Enzym Diacylglycerolkinase (DAGK) durch Dioctanoylglycol (DOG) inhibiert wird. Die Aktivierung von VRAC durch Hypotonizität konnte auch durch den PKD Inhibitor CRT 0066101 eingeschränkt werden.

Ich folgere daraus, dass die intrazelluläre Ionenstärke nicht maßgeblich an der Aktivierung von VRAC beteiligt ist. Stattdessen werden die Kanäle durch Diacylglycerol rekrutierte PKDs aktiviert. Wie am Beispiel von PMA gezeigt werden konnte, können elektrophysiologische Methoden die Effekte von applizierten Chemikalien oder Manipulationen auf Proteinebene verschleiern. Das neue, hier etablierte optische Werkzeug eröffnet neue Möglichkeiten um VRAC auf eine nicht-invasive, Untereinheit spezifische Weise in lebenden Zellen zu untersuchen.

1 Introduction

1.1 Cellular ion homeostasis- A story of swelling and shrinking

Cells, as the smallest unit of life, are a confined space of defined composition striving at all times to maintain their intrinsic properties in a defined range. A plethora of mechanisms underlie the homeostasis keeping cells and their properties in balance with their environment. Among those properties of cells is their volume, dictated by the concentration interplay of ions and osmolytes intra- and extracellularly. To maintain their volume, cells need mechanisms to counteract imbalances of osmolytes leading to either swelling or shrinkage. This thesis deals with a critical player of the process of regulatory volume decrease (RVD) following swelling of cells: the volume-regulated anion channel (VRAC). To understand VRAC's role in RVD, the principles of ion and volume homeostasis shall be introduced in the first section of this thesis, before I focus on VRACs themselves and the struggle of their investigation.

Metazoan cells are encapsulated by a semipermeable membrane, which is highly permeable to water compared to the main inorganic osmolytes of a cell being K^+, Na^+ and Cl^-. Water will, therefore, flow along its osmotic gradient created by concentration differences of intra- and extracellular osmolytes, in or out of the cell. Whereas the intrinsic permeability of cellular membranes for these inorganic osmolytes is small, they can pass the membrane through ion transporting proteins. There are three groups of them: pumps, transporters, and channels. While pumps and transporters actively transport ions even against their electrochemical gradient, by either using metabolic energy or the gradient of a different osmolyte, channels form pores in the plasma membrane. Osmolytes can diffuse through those pores as soon as the channel is in an open conformation. Apart from the named inorganic osmolytes that can pass the membrane, cells contain a significant amount of non-permeable charged proteins and other osmolytes as sugars, DNA, etc. This high content of intracellular non-permeable osmolytes would lead, together with extracellular osmolytes entering the cell down their concentration gradient to reach zero chemical potential, to an influx of water to "dilute" the cytosol to extracellular levels. Cells cannot achieve these levels due to the named non-permeable species. The

steady-state equilibrium of diffusible and non-diffusible species is described by the Gibbs-Donnan equilibrium. At this equilibrium, the osmolyte content of cells would be higher than that of the extracellular space (caused by the impermeable colloids), creating an osmotic pressure. This pressure is defined as the force needed to stop water from entering a compartment with a higher concentration of osmolytes. Plant, bacterial, and yeast cells have a rigid cell wall that can withstand exactly this osmotic pressure, protecting them from harmful water influx and bursting. Animal cells lack this protective cell wall and would, therefore, swell until membrane rupture without further cellular intervention [1]. To counteract the osmotic pressure caused by intracellular non-permeable species, the Na^+-K^+-ATPase extrudes under consumption of energy three molecules of Na^+ for the intake of two molecules of K^+. So, cells sacrifice metabolic energy to render Na^+ an extracellular non-permeable species counterbalancing the intracellular organic ones. This, as "pump and leak" denoted concept, stabilizes cell volume in the presence of the non-permeable osmolyte content [2, 3]. Apart from thereby diminished Na^+ concentrations, intracellular levels of Cl^- are reduced as well compared to the extracellular space, which again creates "osmotic space" for the cellular organic osmolytes [1].

As a consequence of an established osmotically neutral equilibrium, metazoan cells accumulate negative charge intracellularly, creating a potential difference between the cytosol and the extracellular space (the membrane potential). Eukaryotic cells have resting membrane potentials between -40 to -95 mV. Ions are thereby affected by two forces: their chemical potential, depending on the intra- and extracellular concentration of that ion and their electrical potential depending on the repulsion of equally and attraction of oppositely charged species. The net force that will either lead to ions flowing out or into a cell can be estimated with the Nernst equation, calculating the Nernst potential. At this equilibrium potential, the respective ion would have no net exchange anymore. Exemplary concentrations of K^+, Na^+, and Cl^- measured in HeLa cells [4] were (in mM) 170, 32 and 43 with extracellular concentrations of the same ions of 5.5, 152, and 129 mM. Thus, the chemical gradient would lead to an influx of Na^+, and Cl^- and efflux of K^+. Due to the electrical potential, though, an opening of respective channels would lead to the efflux of Cl^-. As well would K^+ leave the cell, while Na^+ would enter it. Apart from K^+, Na^+ and Cl^-, cells contain significant amounts of uncharged organic osmolytes as well that are used for volume regulation, such as taurine, myo-inositol, betaine, sorbitol, and myo-inositol [5]. Since they do not carry any charge, their direction of flow is dictated only by their concentration gradient, being usually highly concentrated intracellularly compared to the extracellular fluid.

The described osmolyte balance renders animal cells capable of reacting to volume and osmolyte perturbations in several ways. The osmolarity of the extracellular fluid

is tightly regulated and varies only in a narrow window (reviewed in [6]). Extracellular changes of osmolarity are, therefore, usually limited to cells of the intestines and kidney. Intestinal epithelial, blood and kidney medullar cells can be exposed to solutions with highly varying osmolarities. These cells need mechanisms to counteract swelling induced by extracellular hypotonicity by RVD and shrinkage induced by extracellular hypertonicity by regulatory-volume increase (RVI). Cells embedded in a tightly regulated tissue rather experience osmotic perturbations by intracellular changes created by transepithelial transport, and catabolic or anabolic processing of macromolecules (reviewed in [7]). An increase in intracellular osmolarity by, e.g., break-down of polysaccharides leads to water influx and cell swelling. Returning to basal volume is accomplished by RVD through the efflux of K^+, Cl^-, and organic osmolytes with obliged water following the osmolytes for both extracellularly hypotonic and intracellularly hypertonic induced swelling. To increase the permeability of these osmolytes, a plethora of different channels and transporters is embedded in the plasma membrane that can be opened to allow their conduction [8]. A hypothesis for an elegant sorting mechanism for which species (ions or organic osmolytes) are allowed to flow out of the cell to restore the volume is linked to the ionic strength of the cytoplasm (discussed in [9]). The ionic strength of a solution is the sum of the solved ions in it and is kept stable by cells to retain, e.g., the functionality of proteins, and the membrane potential. Swelling induced by hypotonicity of the surrounding medium leads to water influx into the cells, diluting the cytoplasm and lowering the ionic strength of it. An opening of ion channels would, therefore, be counterproductive in two different ways: firstly the driving force for the respective ion to leave the cell would be lowered already by the decreased concentration after swelling, and their efflux would even further decrease the already lowered ionic strength. To achieve RVD without further loss of ions, the efflux of organic osmolytes would be more advantageous for the overall cell fitness. Vice versa would it be beneficial to activate channels and transporters for inorganic osmolytes if cells swell isosmotically (for example, by increased uptake of salts). This was shown for a swelling activated KCl-cotransporter in dog red blood cells, which showed an increased volume sensitivity with increased ionic strength [10]. Similarly, in trout red blood cells RVD was either accomplished by the efflux of amino acids when intracellular ionic strength was low or by KCl efflux if the ionic strength was high [11, 12].

There are several different channels and transporters known to be involved in RVD. Many of them are expressed simultaneously in the same cell, and some are exclusive to certain cell types. The electroneutral efflux of inorganic osmolytes, being K^+ and Cl^- for volume regulation, is either directly coupled by, e.g., KCl-cotransporters or indirectly by seperate K^+ channels and Cl^- channels. There are four KCl-cotransporters encoded in eukaryotic genomes: the solute-carrier family 12

A (SCL12A) with members 4-7, also known as KCC1-4. Their expression profiles differ, with KCC2 being specific to neurons and constitutively activated to use the driving force of K^+ to lower the concentration of Cl^- in neurons below the Nernst equilibrium of Cl^- [13, 14]. KCCs are known to play important roles in steady-state volume-regulation and RVD [15]. As a major property for this task, all isoforms are known to be activated by cell swelling [16–20]. In mouse erythrocytes, it was even shown that KCCs are responsible for the majority of RVD in these cells [21]. Besides the electroneutral cotransport by one transporter, cells lower their volume by parallel activation of individual K^+ and Cl^- channels. Known K^+ channels are the calcium-activated K^+ channels containing the small, intermediate, and bid conductance K^+ channels (SK, IK, and BK) or, .e.g, the two-pore domain channels TRAAK,TREK, and TASK2 (reviewed in [8, 22]). For electroneutrality, efflux of either K^+ or Cl^- necessitates the respective other ions to leave the cell as well. Therefore, there must be several accompanying Cl^--channels. One group is the calcium-activated Cl^--channel group, containing the bestrophin and TMEM16 family (reviewed in [23, 24]). It needs to be noted that their activation by swelling is also dependent on Ca^{2+} levels, which is not changed upon swelling in all cell types (reviewed in [8]). Another group is the long-time enigmatic "group" of volume-regulated anion channels.

1.2 The volume-regulated anion channel VRAC

In 1988 two groups described for the first time chloride currents with VRAC characteristics involved in volume regulation [25, 26]. In the following years, comparable currents were detected in basically every vertebrate cell line under investigation. VRAC seems to be ubiquitously expressed throughout a single organism, and throughout the whole vertebrate subphylum [27, 28]. The unknown molecular identity of the channel responsible for these currents led to nonuniformeous nomenclatures and unknown functions for the mysterious VRAC. Today it is known that descriptions of channels called volume-sensitive outwardly rectifying anion channel (VSOR), volume-sensitive organic osmolyte/anion channel (VSOAC), and volume-activated anion channel (VAAC) were indeed all of VRACs, explainable by its modular nature described in section 1.2.2. In 2014, two groups found independently the leucine-rich repeat-containing protein family 8 (LRRC8) to form VRACs, starting a new era with now known protein targets to decipher the mystery of VRAC [29, 30]. In all the years between 1988 and 2014, various groups worked on the identification and characterization of VRAC, leading to a defined biophysical characterization of VRACs but unclear physiological functions and regulatory mechanisms.

1.2.1 VRAC's role in regulatory volume decrease and beyond

As described above, cells can decrease their volume by efflux of Cl^-. The first identified function of VRACs was precisely that: the release of chloride upon cell swelling to induce RVD. Knock-out and knock-down approaches after identification of the LRRC8 protein family forming VRACs could verify that RVD is impaired without functional VRACs in several cell types from different organisms [28–33]. Besides their ability to conduct Cl^-, VRACs are known to conduct organic osmolytes as taurine and glutamate as well. Nevertheless, there was a controversy about the physiological role of VRACs for taurine release upon RVD (reviewed in [8]). With the discovery of the LRRC8 protein family, this controversy was ended by experiments not suffering from unclear VRAC diversity and unspecific pharmacology. Mediation of taurine and other organic osmolyte efflux through VRAC could be clearly shown for neuronal [34] and non-neuronal cells [30, 35]. VRAC is, therefore, not a pure anion channel, as it was suspected to be for a long time. The diversity of conducted species and VRACs themselves (see section 1.2.2) renders these channels capable of more physiological functions than RVD.

Channels and transporters involved in RVD usually have more physiological roles than RVD. This is true for VRACs as well, with proposed involvement in physiological processes like apoptosis, migration, proliferation, auto- and paracrine signaling, to name a few (reviewed in [36]). As for many aspects concerning VRACs, there exists ambiguous data for these roles. The three mechanisms by which VRACs could fulfill their proposed tasks are shown in figure 1.1 (reviewed in [36]).

Programmed cell death is often accompanied by a reduction of cell volume; the apoptotic volume decrease (AVD) [37, 38]. Having a pivotal role in RVD, VRACs were thought to be involved in AVD as well (reviewed in [39]). Indeed, several groups could show the involvement of VRACs in AVD, e.g., in colonic epithelial cells, myocardial cells, and chondrocytes [40–42]. Besides, VRAC currents can be evoked isosmotically with known apoptosis inducers, as staurosporine, FAS ligand, and cisplatin [43, 44]. The importance of cell-type dependency when analyzing VRACs, in general, reveals itself in their (missing) activation by staurosporine. Whereas apoptosis in HCT116 cells could be reduced by knock-out of the obligatory LRRC8A subunit, HeLa cells did not show this reduction by knock-down of the same subunit [43, 45]. As is the role of AVD in general, the involvement of VRACs in apoptosis is not fully understood yet.

Volume regulation is not only necessary as a reaction to altered osmolarity but is also part of physiological processes as proliferation [46]. VRACs were suspected to be involved in cell cycle progression and proliferation due to unspecific pharmacological hints [47–49]. Used inhibitors as tamoxifen,5-nitro-2-(3-phenylpropyl-amino)benzoic

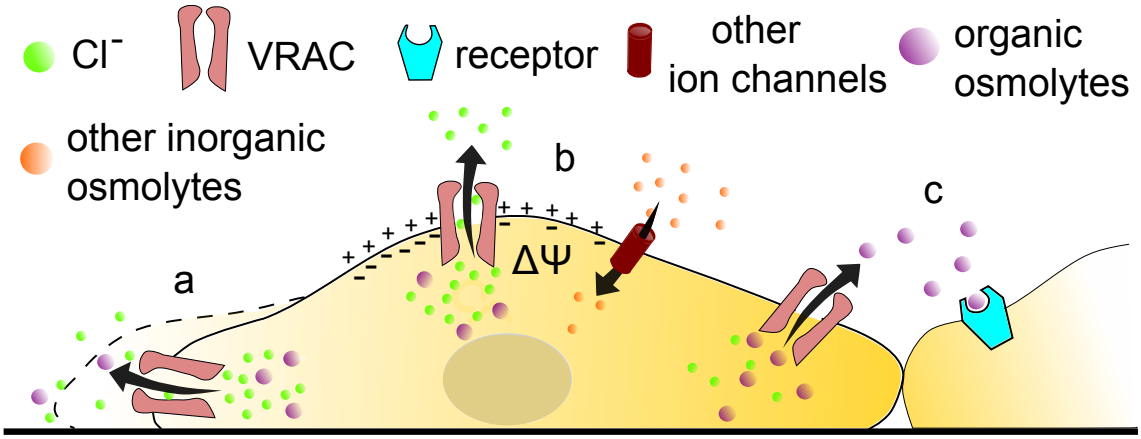

Figure 1.1: Mechanisms underlying VRACs physiological functions
Schematic presentation of the three mechanisms of VRACs to fulfill their physiologicals tasks. Modified from [36]. (**a**) Release of Cl^- and other organic osmolytes to reduce cell volume by obliged water efflux. (**b**) Release of Cl^- leads to changes of the membrane potential (Ψ) which alter the nernst potentials of other ions and the activity of other ion channels. (**c**) Release of organic osmolytes that act as extracellular signaling molecules.

acid (NPPB), 4-[(2-Butyl-6,7-dichloro-2-cyclopentyl-2,3-dihydro-1-oxo-1H-inden-5-yl)oxy]butanoic acid (DCPIB), and quinine were all shown to affect several targets apart from VRACs, weakening the conclusion of their involvement [50–52]. Indeed, all existing data based on depletion of LRRC8 proteins show no role of VRAC for proliferation. Neither do knock-out cell lines show impaired proliferation nor did knock-down ones [29, 30, 45, 53]. It is safe to assume, that VRACs do not play a pivotal role in proliferation, eliminating one often-cited role of these channels. Of course, either a species or tissue-specific involvement cannot be excluded yet, but having protein depletion tools at hand enables future experiments to finally answer this question.

Another often mentioned potential role for VRACs is in cell migration [54]. The hypothesis for the involvement of ion channels in cellular migration is their asymmetrical opening at the leading and trailing edge of a migrating cell, reducing the volume at the trailing edge for an amoeba-like movement. It was shown that glioblastoma cell line's and HCT116 cell's migration could be impaired by either application of VRAC inhibitors or knock-down of LRRC8A [55, 56]. Nevertheless, our lab could not reproduce the impairing effect of VRAC inhibition, knock-out, and knock-down on migration in all these cell lines [53]. As for proliferation, the role of VRAC in cell migration is, thereby, at least questionable.

A fascinating field is the potential role of VRACs in auto- and paracrine signaling. Conducting excitatory amino acids (EAA) as glutamate and aspartate, VRAC was thought to play a role in EAA signaling in the brain (reviewed in [57, 58]). Indeed, the physiological role of VRACs in astrocyte-neuron communication could be confirmed [34, 59, 60]. Glutamate signaling is important for neuronal excitability,

plasticity, and ultimately learning processes in the central nervous system. Being usually released in vesicles by neurons, astrocytes are believed to be involved in glutamate secretion as well (reviewed in [61]). Nevertheless, there is an intense debate over the molecular mechanism behind the proposed glutamate release by astrocytes (reviewed in [62]). Having VRAC confirmed to be the entity for EAA release not only in cultured astrocytes but even in an astrocyte-specific LRRC8A knock-out mouse (showing learning and memory deficits) clearly shows VRACs importance beyond RVD [59, 60].

VRACs importance is further underlined by the severity of the phenotype of *Lrrc8a*$^{-/-}$ knock-out mice [63]. Knock-out of LRRC8A leads to increased pre- and postnatal mortality, with born pubs dying latest at the age of 100 days. Born mice show severe growth retardation, defective organ development comprising kidney and muscle abnormalities, and impaired T-cell function. Interestingly there is a spontaneous mouse mutant known, that shows the same (but milder) phenotype, namely *ébuoriffé* (ebo) [64]. Only recently the cause for the ebo phenotype was found to be a depletion in *Lrrc8a* truncating the leucine-rich repeat-domain [65]. The infertility of ebo/ebo mice is indeed due to the abolished conducting ability of VRACs, as a germline-specific knock-out of LRRC8A was shown to lead to male infertility as well in mice by impaired spermatogenesis [31].

Another tissue-specific role for VRACs was found in glucose sensing and insulin secretion. Swelling is a known result of glucose uptake and metabolization by pancreatic β-cells [66]. Indeed, anion currents with VRAC characteristics were measured in β-cells stimulated with glucose and roles beyond RVD of these currents proposed before the identification of the LRRC8 family (reviewed in [67]). Recently two groups verified VRACs involvement in glucose sensing and insulin secretion in LRRC8A knock-out mouse models [33, 68]. The electrogenic release of Cl^- by VRACs upon glucose uptake depolarizes the membrane potential. This opens voltage-gated Ca^{2+} channels and leads to an influx of Ca^{2+} into β-cells, which ultimately leads to insulin release. Even though both studies disagree on the severity of LRRC8A depletion on insulin secretion, they do agree in a general role of VRACs for membrane depolarization and insulin secretion.

1.2.2 The modular architecture of VRAC(s?) formed by the LRRC8 protein family

For a long time, it was not understood how a single channel, if it only was one, could potentially fulfill such diverse tasks and conduct different species as VRAC was suspected of doing. With the identification of the leucine-rich repeat-containing protein family 8 (LRRC8) to be forming VRACs finally a possible answer to the question of

diversity was found [29, 30]. The LRRC8 family comprises five members, LRRC8A-E. LRRC8A is the obligatory subunit needed for channel formation. Knock-out of LRRC8A, with all four other genes still functional, leads to the same loss of chloride current upon cell swelling as knocking out all five LRRC8 genes. Without the A subunit, overexpressed LRRC8B-E are stuck in the endoplasmic reticulum (ER) [30]. To form functional and conducting VRACs, at least LRRC8A and one other family member is needed. Recently, four groups solved the cryo-EM structure of LRRC8A homomers [69–72]. As impressively precisely predicted by Abascal and Zardoya in 2012, VRACs form hexamers [73]. VRACs share, therefore, topology and channel structure with pannexins, connexins, and innexins.

The five paralogs are formed by around 800 amino acids, with a moderate sequence similarity of on average 45.92 % [73]. They comprise four transmembrane domains, with the C- and N-terminus located intracellularly. Nearly half of the amino acids of LRRC8 proteins form the intracellular, C-terminal leucine-rich repeat domain (LRRD). These domains comprise up to 17 leucine-rich repeats, that are known protein-protein interaction motifs. Until now, no direct interaction partners of the LRRDs of VRAC subunits are known, but it is conceivable that protein interaction motifs in a channel fulfill regulatory tasks.

The topology of a single LRRC8 protein and the structure of a LRRC8A homomer are shown in figure 1.2. The four transmembrane helices of every subunit (TMH1-4) are connected by two extracellular loops (EL1 and 2), and an intracellular loop (IL1) between TMH2 and 3. Intracellular loop 2 (IL2) is connecting TMH4 with the LRRD (Figure 1.2A). The LRRD of a subunit has the, for that domain type, typical horseshoe shape, with the concave side of every LRRD facing the pore axis. Interestingly there are some discrepancies concerning the overall channel symmetry in the four solved structures (discussed in [74]). Three structures show a six-fold rotational symmetry (C6) for all regions except the LRRD [69, 71, 72] and one a three-fold symmetry (C3) [70]. As a possible reason for the C3 symmetry was discussed that the detergents used to reconstitute the channels are bigger than plasma membrane lipids, forcing themselves in fitting pockets and rearranging the channel to this symmetry [72]. The symmetry of the LRRDs is less clear compared to the other regions. Two groups propose a C3 symmetry, leading to a trimer of dimer formation, with two neighboring subunits having tight interaction interfaces between their LRRDs and wider interfaces to the next pairs (example of C3 arranged LRRDs shown in figure 1.2B) [69, 71]. The other two structures hint towards a disordered, heterogeneous LRRD arrangement [70, 72].

An LRRC8A homohexamer can be divided into four regions: the extracellular domain (ECD), the transmembrane domain (TMD), the intracellular domain (ICD), and the LRRD. The pore of the channel is lined with hydrophilic and positively

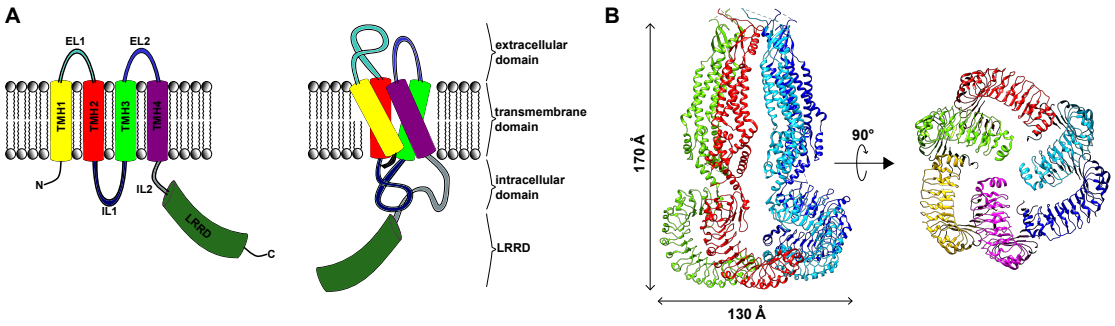

Figure 1.2: Structure of VRACs
(**A**) Topology of a single LRRC8 protein (left) and schematic representation of the structure of a single subunit within a hexamer (right). Folded structure resembles the light blue subunit shown in **B** (**B**) Solved cryo-EM structure of an LRRC8A hexamer (PDB:5ZSU [70]). Shown is the channel viewed parallel to the plasma membrane (left) and from the intracellular side (right). Individual subunits are differntly coloured. Two subunits in the left structure were removed for better visualization. Figure modified from [74].

charged residues. The domain architecture forming the pore starts with the first resolved stretch of EL1 of all subunits. El1 of the subunits are slanted towards the pore axis and form the narrowest, resolved part of the osmolyte permeation pathway in all structures. R103 protrudes into the pore and is believed to be responsible for the charge selectivity towards anions of VRAC heteromers [69]. In the TMD, the extracellular space facing part of TMH1 and the intracellular space facing part of TMH2 further form the pore. Whereas, TMH3 and TMH4 face the lipid environment of the plasma membrane. Membrane lipids were shown to directly interact with several ion channels, modifying their function and regulating their activity [75]. If such an interaction is influencing VRACs as well, it will, therefore, probably be by the interaction of lipids with TMH3 and 4. Unfortunately, the N-terminus is not resolved in all four structures. The structurally closely related connexins and innexins were shown to have an N-terminal coil (NTC) protruding into the central channel axis, creating a constriction with selectivity instances and size restriction tasks [76, 77]. Even though the possible NTCs of LRRC8A hexamers were not resolved, mutagenesis studies with the first 15 amino acids of LRRC8 proteins revealed their importance for general conductance, ion permeability, and inactivation gating [78]. Thus, it is likely that VRACs, as do connexins and innexins, have an NTC that is folded into the permeation pathway of the channel. Past the potential NTC, the lowest part of the pore is finally formed by a meshwork of helices of IL2. The involvement of the LRRDs in pore formation is unclear due to their unsure localization in the solved structures.

Knock-out of three of the five LRRC8 genes and overexpression of LRRC8A and another subunit leads to functional VRACs that conduct ions [30]. These het-

eromers show different biophysics and conduct different species (see section 1.2.3). Combinations of two subunits, therefore, gives rise to several different VRACs. In living cells, the situation is probably even more complicated since it was shown by co-immunoprecipitation and TIRF based bleaching experiments, that functional VRACs could contain more than two different subunits [79, 80]. Mapping of the conservation scores for the respective residues between the five paralogs on the solved structure of LRRC8A homomers hints towards the domains and amino acids that are responsible for the biophysical differences of heteromers [70]. Pore architecture forming domains, namely ECD, TMH1 and 2, and ICD, are highly conserved between the different family members, implying that these structures are equally arranged in different VRAC heteromers. Variability of VRACs, thereby, arises from diversified regions, being TMH3 and 4, non-pore forming parts of the ECD, the LRRDs, specific residues in the NTC and the constriction forming residues at the permeation pathway entrance (R103 in LRRC8A).

1.2.3 Biophysical characterization of VRACs - a matter of subunit composition

Decades of research on VRACs without knowing their molecular identity led to a detailed electrophysiological and biophysical fingerprint to discriminate them from other channels. Under basal conditions, VRAC currents are not detectable but start seconds after an activating stimulus, such as hypotonicity, and develop over minutes to reach their maximum. A hallmark of VRAC currents is the deactivation at positive potentials above 40 mV, that discerns them from other Cl^- channels as, e.g., the already mentioned bestrophins, which show no deactivation at positive potentials [81]. Even though being a characteristic property of VRACs, the varying degree of inactivation between different cell lines was unexplainable for a long time (reviewed in [48, 82]). The reason for these variations in inactivation is again the subunit dependence of this property [30]. VRACs formed by LRRC8A and another subunit show significantly different inactivation kinetics at positive potentials, with, e.g., LRRC8E inactivating very fast compared to LRRC8C [30]. Since there seems to be a different expression profile of LRRC8 proteins in tissues and cell lines, detected variations of inactivation are probably due to different subunit compositions in that cell line under investigation [83, 84].

Whereas VRACs do not display significant cation permeability, their permeability towards anion corresponds to Eisenmann's sequence I for weak field strength: $I^- > Br^- > Cl^- > F^-$ (reviewed in [48]). Estimates of the permeability of VRACs towards taurine compared to Cl^- ($P_{taurine}/P_{Cl}$) yielded permeation ratios of 0.15-0.4 [85–88]. These studies were done in different cells from different organisms

and lacked, due to the LRRC8 protein family being not identified yet, controls of subunit expression in the investigated cell lines. Today it is known, that the subunit composition of VRACs leads to different conducting preferences as well. LRRC8D is the main subunit needed for taurine efflux upon cell swelling [43]. This underlines the importance of taurine for RVD in general, and specifically, the subunit dependence for VRAC activity and function, since Cl^- currents in *LRRC8D*$^{-/-}$ cells were unaltered to WT cells, whereas their RVD was impaired [43]. Interestingly, the preference of LRRC8D for taurine is linked to taurine baring no net charge at physiological pH [59]. Raised extracellular pH levels lead to more anionic taurine molecules, which were conducted by other subunit compositions lacking LRRC8D [59]. Besides taurine, LRRC8D was shown to be essential for the conduction of myo-inositol, gamma-aminobutyric acid (GABA), glycine, and lysine [35, 80]. The permeation of ATP was increased for VRACs formed by either LRRC8E or C [80]. All LRRC8 subunits can conduct Cl^-, besides the other named osmolytes. Only for LRRC8B, no other conducted species apart from Cl^- could be identified yet.

Another hallmark of VRAC's electrophysiological fingerprint is its mild outward rectification. Per definition, current is the net outside movement of positive charge. For an anion channel, this means that high outward current reflects an inward flux of Cl^-, whereas, an inward current is the outward flux of Cl^-. By being outwardly rectifying, VRACs conduct, therefore, more chloride at positive potentials (into cells), than at negative potentials (out of cells). As for many other aspects of VRACs, this property is again subunit dependent. Reconstituted combinations of LRRC8A with another LRRC8 protein revealed that complexes containing LRRC8D have a stronger outward rectification then complexes of LRRC8C or E [79].

1.3 Techniques to study VRACs

1.3.1 Electrophysiology- The gold standard

Electrophysiology assesses the flow of ions through biological membranes by using electrodes in cells or at their plasma membrane [89]. Over the last century, the methods around electrophysiology developed to a sophisticated toolset for various applications. Indeed, electrophysiological measurements are the most used method to study VRACs yet. In general, there are two different ways of measuring the electrical behavior of a cell: either by holding the voltage of the plasma membrane constant (voltage-clamp) and measuring the occurring flow of charged species or by holding the current of a cell constant (current-clamp) to measure the membrane potential. Assessment of the membrane potential is a typical application in neuro-science, where action potentials of neurons are measured. Investigation of

ion channels in mostly non-neuronal cells is usually done by voltage-clamp, where the flow of ions can be readily measured since injected currents to hold the voltage constant directly reflect flux of charged species through the plasma membrane after a short capacitive loading of the plasma membrane (reviewed in [90]). There are four different configurations in which voltage-clamp experiments can be performed: whole-cell, inside-out, outside-out, and cell-attached configuration (reviewed in [91]).

To perform a voltage-clamp experiment, a glass tip, containing an electrode, is brought into physical contact with the plasma membrane of a cell. The lipids of the membrane attach to the glass surface, forming a tight seal that, hopefully, electrically shields the pipette interior from the extracellular solution with a resistance of several giga ohms. The name for this seal is derived from this high resistance and is called giga-seal. Having established a giga-seal leads to the easiest mode for electrophysiological experiments, the cell-attached configuration. Channels that are in the enclosed membrane patch in the pipette tip can be measured in their cellular environment this way, physically and electrically isolated from other channels. Electrophysiological measurements of patches of the plasma membrane are, therefore, used for either single-channel or at least measurements of a small subset of channels. These patch-clamping techniques for small numbers of channels comprise the inside-out, outside-out, and cell-attached configuration. Cell-attached measurements suffer from hardly controllable voltage levels, so only a few groups managed to detect VRAC currents in this configuration [79, 80, 92, 93].

The other methods potentially assessing single-channel events are the outside-out and the inside-out configuration. Those are established after successful cell-attached mode, by either withdrawing the pipette tip slowly from the plasma membrane, excising a patch of it with the cytosolic side facing the bath solution (inside-out) or by rupturing the plasma membrane before withdrawal of the pipette tip for the membrane patch residing at the tip to form a vesicle with the cytosolic side facing the pipette internal solution (outside-out). This way, single channels can be investigated outside of their cellular context. Furthermore, it creates the possibility to directly bring either the intracellular or the extracellular side of a channel into contact with defined drugs or signaling molecules, only measuring the specific channels in the membrane patch. To my knowledge, there is no publication yet showing single-channel currents of VRACs in inside-out patches. In pre-swollen cells, though, single-channel currents of VRACs have been measured using the outside-out configuration [94, 95]. In membrane patches of *Xenopus* oocytes, outside-out currents of VRACs could be measured without pre-swelling of the oocytes by exploiting the increased basal activity of C-terminally tagged LRRC8 subunits [80].

The by far most used configuration to study VRACs and their underlying signaling is the whole-cell configuration. To establish the whole-cell configuration, the

membrane patch in the pipette of a cell-attached configuration is ruptured by the application of abrupt suction. Rupture of the plasma membrane grants direct access to the cytosol, dialyzing it against the pipette solution. Thereby, the ionic composition of the cytosol can be controlled and adjusted according to the question at hand. In the whole-cell configuration the currents of all channels activated at that moment are recorded, in comparison to the small subset or even single-channels of the other configurations. A variation of the whole-cell configuration, to avoid dilution of proteins and signaling molecules, is the perforated-patch configuration [96]. To achieve perforation of the plasma membrane, pore-forming antibiotics are included in the pipette solution. Small ions as K^+, Na^+, and Cl^- can pass these pores, allowing control of their intracellular concentration, whereas bigger molecules as proteins or, e.g., ATP are retained in the cytosol. While the whole-cell configuration is used in virtually every publication dealing with the electrophysiology of VRACs, only a subset of them utilized the perforated-patch configuration [68, 97–99].

Electrophysiology revealed valuable information about the biophysics of VRACs and their regulation. As for every method, it has its limits and drawbacks as well that need to be considered. Investigation of VRACs in excised membrane patches (inside-out and outside-out configuration) allows detailed characterization of VRAC's biophysics, but always in the absence of the cellular signaling context. Theoretically, the addition of potential binding partners, or modifying enzymes to the bath or pipette solution could be used to identify those involved in VRAC activation. However, it is unsure whether they can fulfill their role in activation isolated from the cytosol and their direct identification without other upstream pathways is rather unlikely. In the cell-attached configuration, the cellular context is still available for the patch embedded channels. As mentioned, a successful measurement of VRAC currents in this configuration is hard to accomplish. Furthermore, the channels in the isolated patch seem to be influenced by their isolation, since currents in the cell-attached configuration can only be measured on pre-swollen cells, not on patches of cells that are swollen post patching [92]. Thereby, the effect of manipulations of the cellular signaling pathways can not be monitored directly. When using the whole-cell configuration, the formulation of the pipette solution, against which the cytosol is dialyzed, needs to be carefully adjusted to the channel type under investigation. For example, in most experiments dealing with VRACs, the pipette solution contains Cs^+ to block K^+ channels which might pollute the recorded currents. Recently, it was proposed that the addition of Cs^+ impairs isolation of anionic currents by Han and coworkers[1] [100]. Besides, the volume of the pipette solution is huge compared

[1] The paper of Han et al. is highly controversial. They state that the hypotonicity induced chloride currents in astrocytes are due to the Tweety-homolog family and not due to the LRRC8 family. Judging the implications and correctness of this finding is beyond the scope of this thesis.

to the cytosol, thereby the efflux of osmolytes through channels is nullified by the same osmolytes diffusing back into the cell through the ruptured membrane from the pipette solution. RVD is, therefore, heavily impaired, reflected in a highly increased volume gain of patched cells to unpatched cells in a hypotonic solution. Together with the blocked K^+ channels, the whole-cell configuration creates an artificial environment with unpredictable influences on cellular signaling events underlying the regulation of VRACs. The perforated-patch configuration can at least minimize the mentioned dilution effects of the whole-cell configuration but is seldom used.

A basic premise of electrophysiological measurements is that the osmolytes passing the channels under investigation are either positively or negatively charged. As introduced above (see section 1.2.3), VRACs can conduct uncharged osmolytes like taurine. At physiological pH of 7.4, taurine is uncharged and can, therefore, not be detected as current. It is generally possible to measure taurine as current by increasing the pH of the extracellular solution to a pH of 8 [85]. Those measurements were more valuable for investigation if taurine is released through the same channel as Cl^-, but are of limited value for analysis of cellular signaling since the pH change itself might influence it. So electrophysiological experiments can only detect the flow of charged species, even though it might be of functional importance that VRACs conduct uncharged species as well in the explored case. Detection of fluxes of specific osmolytes can, nevertheless, be accomplished by a different method.

1.3.2 Determination of osmolyte concentrations

An elegant approach to determine the efflux of a specific osmolyte is the loading of cells with radiotracer variants of that osmolyte and following measurement of radioactivity in the supernatant after stimuli application. Usually, either ^{3}H or ^{14}C labeled osmolytes, as D-$^3[H]$aspartate or $^{14}[C]$taurine, are used [30, 34, 35, 101]. Incubation of cells with labeled osmolytes for several hours leads to their uptake by cellular transport systems (reviewed in [102]). After their uptake, the release of labeled osmolytes can be measured, e.g., after hypotonic treatment, by scintillation counting and compared between different conditions. The detection efficiencies for ^{3}H exceed nowadays 68 % and for ^{14}C 98 %, rendering radiotracer efflux measurements very sensitive and enables detection of very small concentrations of osmolytes [103]. Radiotracer studies were useful to directly show that VRACs do conduct specific osmolytes [30, 104].

The content of amino acids of a cell (or their supernatant) can be measured independently of exogenously applied radiotracers with, e.g., high-performance liquid chromatography (HPLC) based seperation and detection. For intracellular amino acid content determination, cells incubated with and without hypotonic medium are

lysed, and the protein content denatured, leaving soluble amino acids for measurement. Using this technique, reduced levels of several amino acids and mainly taurine could be shown in cultured astrocytes challenged with hypotonicity [105]. Analysis of the supernatant of swollen cells can also yield information about osmolyte efflux. Again, an HPLC technique with sufficient sensitivity can be used to detect increases of extracellular amino acid contents [106]. Furthermore, readily buyable assay kits for glutamate level measurements were used to show VRAC dependent increased extracellular glutamate concentration after hypotonicity [35].

The assay used to identify the LRRC8 protein family to form VRACs exploits the quenching of a fluorophore by I^- influx into cells by channel opening [29, 30]. To perform this assay, a halide sensitive YFP mutant [107] is either stably [29, 30, 43] or transiently expressed in cells [108]. As described above, VRACs conducts halides in general and I^- to a bigger extent than Cl^-. Upon opening of VRACs, extracellular I^- can, therefore, enter the cells and quench the fluorescence of the halide-sensitive YFP. The intensity of YFP is then detected as an indicator of VRAC activity.

Nevertheless, these methods can not be used as a general tool to detect VRAC activity. Radiotracer approaches can only detect the osmolytes that were loaded to the cells before. VRACs are capable of conducting several osmolytes, and the regulation of which is released upon specific stimuli is still unknown. Furthermore, there are several transporters and channels for the species that VRAC can conduct as well, so tedious controls to determine which channel is responsible for the measured concentration change are needed. To validate, e.g., that results of the YFP quenching assay are due to the opening of VRACs, knock-down or knock-out models are required. Pharmacological manipulations, though, can only result in hints toward VRAC, for the named unspecificity.

1.3.3 Cell volume measurements

Since one of the roles of VRACs is the RVD after swelling, measurement of the cell volume is a seemingly straight forward approach to detect their action. Surprisingly, the exact determination of cell volume can be difficult, and various methods exist for cell volume measurements (reviewed in [109]). The gold standard of exact volume measurements is the electronic conductance (better known as coulter sizing) method that has been used for investigation of VRACs role in RVD [29, 110]. Here, two compartments, each containing an electrode, are separated by a small aperture. Cells in suspension pass through this aperture and increase, thereby, the resistance of the electrical circuit. The cell volume is a function of the voltage spike generated by this high resistance. Being very reliable, the only drawback of this method is the need for an according coulter sizer device.

Many groups used a calcein based method to determine volume changes semi-quantitatively [30, 111, 112]. Crowe et al. established calcein as a volume probe by merely exploiting the fact that the intensity of a fluorophore in a restricted plane of a cell is dependent on its concentration [113]. This approach was further refined to use the self-quenching of calcein at higher concentrations to obtain quick and low-noise measurements of cell water content [114]. However, the need for intracellular concentrations high enough for self-quenching to occur can lead to inconsistencies between cells and loading conditions and are, therefore, less accurate as coulter sizing. Volume estimations with calcein are usually semi-quantitatively, but most VRAC studies investigated the relative volume change between cells and did not rely on absolute volume values.

The least accurate method used to determine relative volume changes upon VRACs action is the so-called optical sectioning [115, 116]. Differential interference contrast (DIC) images of detached, therefore round, cells were used to measure the diameter of the cross-section and to calculate the cross-sectional area. The ratio of the cross-sectional area at two different time points is then used as an approximation for relative volume changes. To assure high accuracy of the determined cross-sectional area, the same plane of a cell needs to be measured every time. Acquisition of z-stacks for every time point is a rather slow process, not feasible for most applications, whereas selection of the plane by the experimenter inherits a human selection bias. It is possible to calculate the volume for adherent cells as well with the sectioning method, but this approach is rather cumbersome and time-consuming (discussed in [109]).

Taken together, cell volume measurements can be useful to assess the influence of VRACs on RVD, but for the redundancy of the RVD processes in cells the exact mechanism of VRAC's action need to be verified with other methods as well.

1.3.4 VRAC heterogeneity as a challenge

As introduced in section 1.2.3, LRRC8 subunit composition dictates channel properties, creating several problems concerning the established methods to investigate VRACs. In the decades before the identification of the LRRC8 protein family to form VRACs, all investigations were done with endogenous, mixed subunit populations. Not only do the expression levels vary between different tissues and potentially species, but it is also still unknown how channels composed of more than two different subunits combine the properties of their single members. Therefore, old data suffers from uncertainty if investigated effects were due to VRACs in general (caused by unspecific drugs) and if so, due to which composition. Knowledge of the channel composition is of importance to avoid contradictory findings. A striking example is

the opposite effect of oxidation on different subunits [117].

Having knock-out and knock-down approaches available, it is possible today to directly compare, e.g., electrophysiological results in the presence and absence of single or multiple LRRC8 proteins. Being undoubted of value, these approaches are inflexible and can not account for the potential interplay of differently composed VRACs over time (especially considering the invasiveness of electrophysiology).

1.4 The data maze of VRAC activation and regulation

Most of the work regarding the activation of VRACs presented here was done without knowing the molecular nature of VRACs. Therefore, misconceptions and contradictions had to occur due to the missing knowledge of the modular complexity behind these channels. Furthermore, it seems likely that a group of channels with tasks as diverse as VRACs are controlled by several different pathways, that might be dependent on tissue and even cell cycle state of a single cell. Following statements concerning VRAC regulation are, therefore, not as general as the formulation might implicate and shall give an overview of potential pathways worth of revisiting with new tools.

As their name suggests, VRACs are volume regulated and, therefore, activated in swollen cells. Since they can not directly sense changes of cellular volume, other parameters that are altered upon swelling and activate VRACs have to exist (reviewed in [118]). A controversial activation path involves the ionic strength of a cell. Cells swell due to a water influx, which dilutes the cytosolic ion content, reducing the ionic strength inside of a swollen cell. Several publications state that ionic strength directly activates VRACs in living cells [119, 120]. This notion is convincingly supported by the fact that single VRACs in lipid bilayer droplets are activated by reduced ionic strength but not by lowered osmolarity [79]. However, other studies could show that an isosmotic swelling, with constant ionic strength, by injecting fluids into cells leads to activation of VRACs as well [115, 121, 122]. The activating role of ionic strength for VRACs is, therefore, elusive yet.

Intracellular ATP levels were shown to regulate VRACs activation by hypotonicity induced swelling [123–126]. Interestingly, the substitution of intracellular ATP by non-hydrolyzable analogs did not prevent channel activation, leading many groups to conclude that phosphorylation events are not a crucial part in the underlying signaling of VRAC activation [86, 116, 123, 125]. Subsequent studies found that even though substitution by non-hydrolyzable ATP derivates does not impair VRAC activation, the kinase activity of protein tyrosine kinases (PTK) is critical for it [127].

This led to the conclusion that dialysis of cytosolic ATP and replacement with non-hydrolyzable derivates is not extensive enough to suppress all phosphorylation events in a cell. The theory of insufficient ATP depletion is supported by the low levels of ATP required for phosphorylation compared to needed concentrations for ATP-binding dependent processes (reviewed in [128]).

In compliance with the ambiguous role of phosphorylation events concluded from ATP experiments, the involvement of kinases and phosphatases is obscure. Pharmacological hints exist for a role of PTKs in dog cardiac myocytes, rat astrocytes, and bovine endothelial cells [129–131]. Surprisingly, inhibition of the counter enzyme family of protein tyrosine phosphatases (PTP) impaired VRAC activation in bovine chromaffin cells, and mouse fibroblasts [132, 133]. An equivalently confusing data situation is found for the regulation of VRACs by the protein kinase C (PKC) family. PKCs were found to be important for VRAC activation in astrocytes by pharmacological, and PKC depletion by small interfering RNA (siRNA) and mutation approaches [134, 135]. Other inhibitor-based studies identified either an activating or deactivating role of PKCs in various other cells [136–140].

Apart from the contradictory findings mentioned above, several other seemingly unrelated regulatory signaling molecules and messengers have been ascribed to VRAC's activation mechanism. Those include purinergic signaling, sphingosine-1-phosphate (S1P), phosphatidylinositol-3,4,5-triphosphate (PIP3), calcium concentration, G-proteins, G-protein-coupled receptors (GPCR), reactive oxygen species (ROS), and tumor necrosis factor-α (TNFα) (reviewed in [8, 9, 36]). For the sake of understandability, they shall not be discussed here in-depth, but rather complete the picture of the confusing data maze around the regulation of VRACs.

1.5 Assessing ion channel activity with fluorescence microscopy

Advances in the field of fluorescence microscopy have pushed the borders of resolution and sensitivity achievable today. Using super-resolution microscopy and techniques as Förster-resonance energy transfer (FRET), the underlying mechanisms of several ion channels could be investigated in fascinating new ways (reviewed in [141]). An example is the usage of FRET to determine the molecular events behind the slow-gating of the Cl^- channel ClC-0 [142]. The process of opening and closing of channels is referred to as gating, whereas ClC-0 is known to have two different modes of gating (slow and fast, reviewed in [143]). The molecular events behind the slow gating mode were elusive until FRET experiments could show a rearrangement of the C-termini of ClC-0 subunits to be involved [142]. Another example of

fluorescence microscopy being used to study the activity of channels is the AMPA receptor (AMPAR) [144]. Again exploiting FRET microscopy, it was shown that intracellular domains rearrange upon extracellular ligand binding.

Optical methods have several advantages compared to classical approaches to study VRACs. By knowing which subunits are labeled, optical experiments do not suffer from uncertainty which LRRC8 proteins are responsible for seen effects. Furthermore, it would offer spatio-temporal information about the channels and would be less invasive than electrophysiological approaches. Since the imaging of cells is a gentle measurement approach, longtime experiments of cells expressing fluorescently labeled LRRC8 proteins can be performed. Especially FRET microscopy is a versatile tool since sub-resolution information about the relative localization of two or more proteins to each other can be recovered from macroscopic fluorescence signals.

2 Aim of this work

Volume-regulated anion channels (VRACs) are a diverse class of channels conducting various osmolytes, including Cl^-, taurine and glutamate. Besides their crucial role for regulatory volume decrease, they have proposed roles in physiological processes like apoptosis, differentiation, insulin secretion, and auto/paracrine signaling. VRACs are composed of at least LRRC8A and another member of the LRRC8 family, leading to the characteristics of VRACs being dictated by their subunit composition.

A critical step in the preparation of this thesis was the realization of the imperfection of existing data concerning VRAC regulation. I do want to emphasize that most of the work was performed without knowing the molecular nature of VRACs and relied on unspecific inhibitors. Furthermore, have the existing methods for investigations of VRACs the drawbacks of being invasive (as in electrophysiological approaches) and the requirement for cumbersome pharmacological and protein depletion manipulations to distinguish effects caused by specific subunit compositions from either other plasma membrane channels or differently composed VRACs.

Therefore, I aim in this thesis to establish a new microscopy-based tool for investigations of VRACs. The new optical tool should be less invasive then electrophysiology, offer time-resolved information about channel activity, and pay respect to the different subunit compositions of these channels. With this optical tool, I aim to characterize the elusive activation mechanism of specifically composed VRACs by hypotonicity induced cell swelling with special emphasis on the role of ionic strength in living cells.

3 Results

3.1 Establishing a FRET sensor for optical monitoring of VRAC activity

3.1.1 Validation and characterization of FRET between LRRC8 subunits

FRET occurs between fluorophores that are in close proximity to each other and have the correct orientation. The Förster radius describes the distance between two fluorophores at which they transfer non-radiatively their energy with an efficieny of 50 % and depends on various factors and is different for given sets of FRET pairs, being 5 nm for the classic FRET pair of cyan-fluorescent protein/yellow-fluorescent protein (CFP/YFP). Many variables can be changed to successfully create fusion proteins with the fluorophores positioned for FRET, namely the exact position of the fluorophore in the protein sequence and the length, and rigidity of the linker sequence between the native protein and the tag. Tags at the N-terminus of LRRC8 subunits were shown to render VRACs inactive [30]. Therefore, I chose to insert either CFP or YFP tags at the extreme C-terminus with a short 12 amino acid long linker. LRRC8A tagged with either CFP or YFP (A-CFP, A-YFP) is expressed and transported to the plasma membrane in HeLa cells (Figure 3.1). LRRC8E tagged with CFP or YFP (E-CFP, E-YFP) is stuck in the ER when expressed alone (data not shown), but colocalizes with LRRC8A at the plasma membrane when co-expressed (Figure 3.1) [30].

To test if the fluorophores are positioned in a way for FRET to occur, I utilized acceptor photobleaching (APB). If CFP is close enough to YFP and correctly oriented, a specific percentage of CFP molecules will transfer their excitation energy radiation less to YFP. The CFP emission is thereby quenched by this percentage and can be unquenched by bleaching of YFP. So, FRET can be calculated by the increase of CFP emission after bleaching of YFP compared to the emission before bleaching. Usually APB is performed on confocal microscopes with fixed specimen. A small area of YFP is then bleached with its respective laser line and the CFP emission is measured before and after this process. But APB experiments can be

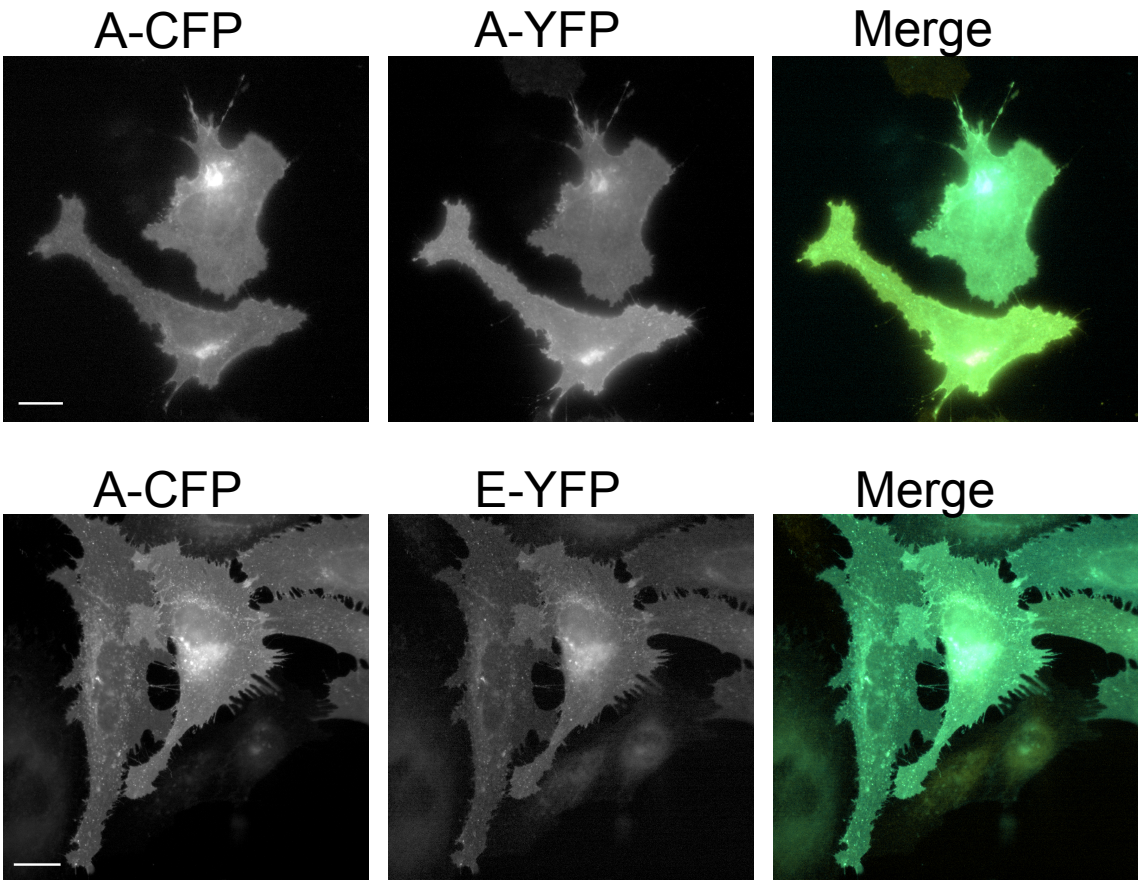

Figure 3.1: Expression and localization of FP labeled LRRC8A and E
Plasma membrane localization of fluorescently labeled LRRC8 subunits in HeLa cells 24 h after transfection with either A-CFP/A-YFP (top) or A-CFP/E-YFP (bottom). Scale bar= 20 μm

performed on widefield microscopes with living cells as well, with certain limitations to the accuracy of determined FRET (dFRET) values. Especially for samples with small FRET efficiencies, there is a need for careful control experiments, including seperate negative controls and negative controls in the same experiment. I bleached only a small portion of a field of view (FOV) by closing the field diaphragm to the size of one or two cells (Figure 3.2A). Thereby I can directly compare the increase in CFP intensity of bleached to unbleached cells as an intrinsic negative control. Indeed complexes formed by A-CFP/A-YFP show a significant increase of CFP intensity after bleaching of YFP compared to unbleached control cells (Figure 3.2B). This increase strongly hints towards the occurrence of FRET between the fluorescent proteins fused to the LRRDs of LRRC8A.

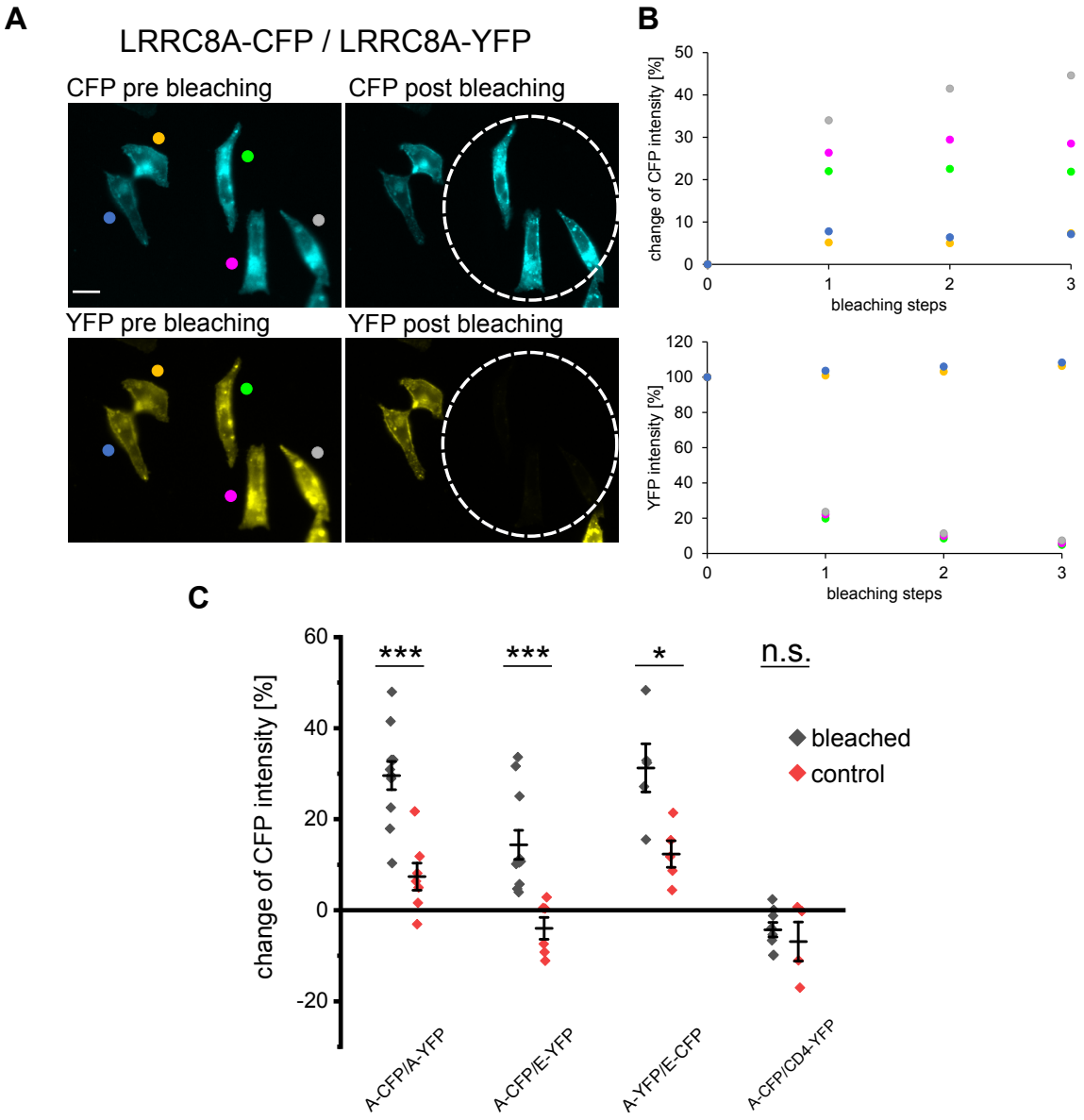

Figure 3.2: Acceptor photobleaching of CFP and YFP labeled VRACs
(**A**) Example images of an APB experiment with HeLa cells expressing A-CFP/A-YFP. Shown are the CFP channel (top row) and the YFP channel (bottom row), before (left panels) and after (right panels) bleaching. The region bleached with closed field diaphragm is indicated by white circles. Colored circles (next to the respective cell) added for identification in graphs shown in B. Scale bar, 20 μm. (**B**) Quantification of exemplary APB experiment shown in A. Individual cells are represented by the color code in A. Top graph represents the percentual CFP intensity change compared to t=0 of the respective cell. Bottom graph represents the percentual YFP intensity during the APB experiment. (**C**) Quantification of all APB experiments. Data points (diamonds) represent the percentual CFP intensity change of indicated subunit compositions. For each subunit pair, the CFP change of bleached (black diamonds), unbleached cells (red diamonds) and the mean ± s.e.m. is shown.

Homomers formed by LRRC8A alone might have the interesting potential to discover mechanisms intrinsic to all VRACs since this is the obligatory subunit needed, but they are believed to be of no biological relevance. Functional VRACs are rather formed by LRRC8A and at least one other member of the LRRC8 family. I, therefore, performed APB with complexes of A-CFP/E-YFP and A-YFP/E-CFP, which again both showed an increase in CFP intensity after bleaching as seen for A-CFP/A-YFP complexes (Figure 3.2C). Co-expression of A-CFP and the unrelated plasma membrane protein CD4 tagged with YFP did not lead to an increase in CFP after APB. Theoretically the FRET efficiency in dependence on the fraction of interacting donors can be recovered from the change in CFP intensity according to

$$dFRET = I^{DD}/I^{DD}_{AB}$$

Whereas, I^{DD} is the CFP intensity before bleaching and I^{DD}_{AB} the CFP intensity after bleaching. According to ABP experiments, A-CFP/E-YFP complexes have a mean dFRET of 14.4 ± 10.1 %, whereas switching the fluorescent proteins leads to a mean dFRET of 31.3 ± 12.3 % for A-YFP/E-CFP. The efficiency for A-CFP/A-YFP homomers is higher as well with 29.6 ± 7.3 %. Comparison of the dFRET values hints to a situation with a large fraction of non-interacting donors for A-CFP/E-YFP. This is consistent with the likely stoichiometry of VRACs formed by overexpressed A and E subunits, which was shown in *Xenopus* oocytes to be dependent on sheer abundance of subunits: Comparing the intensities of overexpressed A-CFP and A-YFP with E-CFP and E-YFP it is obvious that LRRC8A is more strongly expressed. This expression ratio leads to a shift in the distribution of likely channel compositions towards more A subunits per channel and even channels solely formed by A. In the case of A-CFP/E-YFP, not all donors can interact with an acceptor, decreasing the observable dFRET since those donors cannot show an increased intensity after ABP. The acceptor E-YFP is thereby the limiting factor for FRET, a notion supported by the higher dFRET seen for the A-YFP/E-CFP combination.

ABP is a reliable but destructive process, preventing the observation of FRET over time. To do so, one can utilize the most commonly used sensitized-emission FRET (seFRET) technique. Here FRET efficiency is recovered from the sensitized acceptor signal upon excitation of the donor. This is achieved with emission and excitation filters which as specifically as possible excite only donor molecules and let only the emission of the acceptor pass. The following nomenclature is used for the different channels used for seFRET experiments: the donor channel detects donor emission after donor excitation (I^{DD}), the acceptor channel detects acceptor emission after acceptor excitation (I^{AA}), and the FRET channel detects acceptor emission after

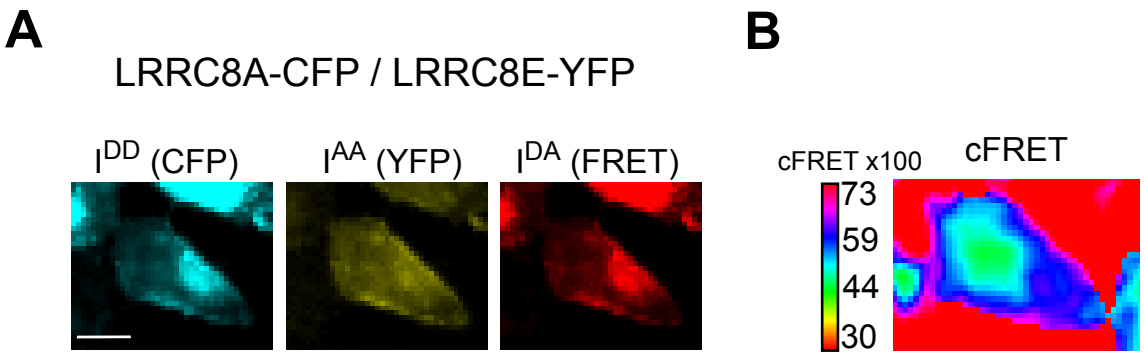

Figure 3.3: Measurement of FRET between LRRC8 subunits by seFRET
(**A**) Wide-field images of HeLa cells expressing A-CFP/E-YFP. Shown are the three channels needed for cFRET calculation: donor (I^{DD}), acceptor (I^{AA}), and FRET(I^{DA}). (**B**) The cFRET map calculated from the three channels shown in A with pixFRET plugin for ImageJ. Calibration bar left of cFRET map represents cFRET values and their respective color code in the LUT.

donor exciation (I^{DA}). Technical limitations and the broad excitation and emission spectra of fluorophores prohibit the detection of sensitized emission to be specificly pure FRET signals. I^{DA} contains as well signals from cross-excitation of acceptors in the donor channel and bleed-through of donor emission into the acceptor channel. To account for these errors seFRET experiments need correction factors for the given set up which can be recovered from samples expressing only donors or acceptors. To calculate seFRET from a sample with acceptors and donors, one detects three channels: I^{DD}, I^{AA}, and I^{DA} (Figure 3.3A). With the beforehand determined correction factors the erroneous contributions of the cross-talk to the IDA can be subtracted. The cFRET, purged of cross-talk, is now still dependent on fluorophore concentrations and cannot be compared to cFRET values generated on a different platform since filter sets and camera sensitivities influence it as well. There are several possible normalization variants to minimize these problems, namely normalizing to total acceptor concentration (aFRET), total donor concentration (dFRET) or the arithmetic or geometrical mean of both. For many applications one can gain information by the comparison of aFRET and dFRET, since a difference here shows the stoichiometry of the interaction. Higher aFRET values imply non-interacting donors and vice versa. The focus of this thesis is on VRACs formed by LRRC8A and -E due to their biological relevance compared to VRACs formed only by A. With YFP being brighter and having a higher quantum yield than CFP, I chose to work mainly with A-CFP/E-YFP to have the brighter fluorescent protein on the lesser expressed subunit. Having recorded I^{DD}, I^{AA}, and I^{DA} one can calculate a cFRET map, by removing cross-talk and normalize to one of the above-mentioned values for every pixel of the image (Figure 3.3B).

I acquired multiple of these seFRET sets from HeLa cells expressing A-CFP/E-

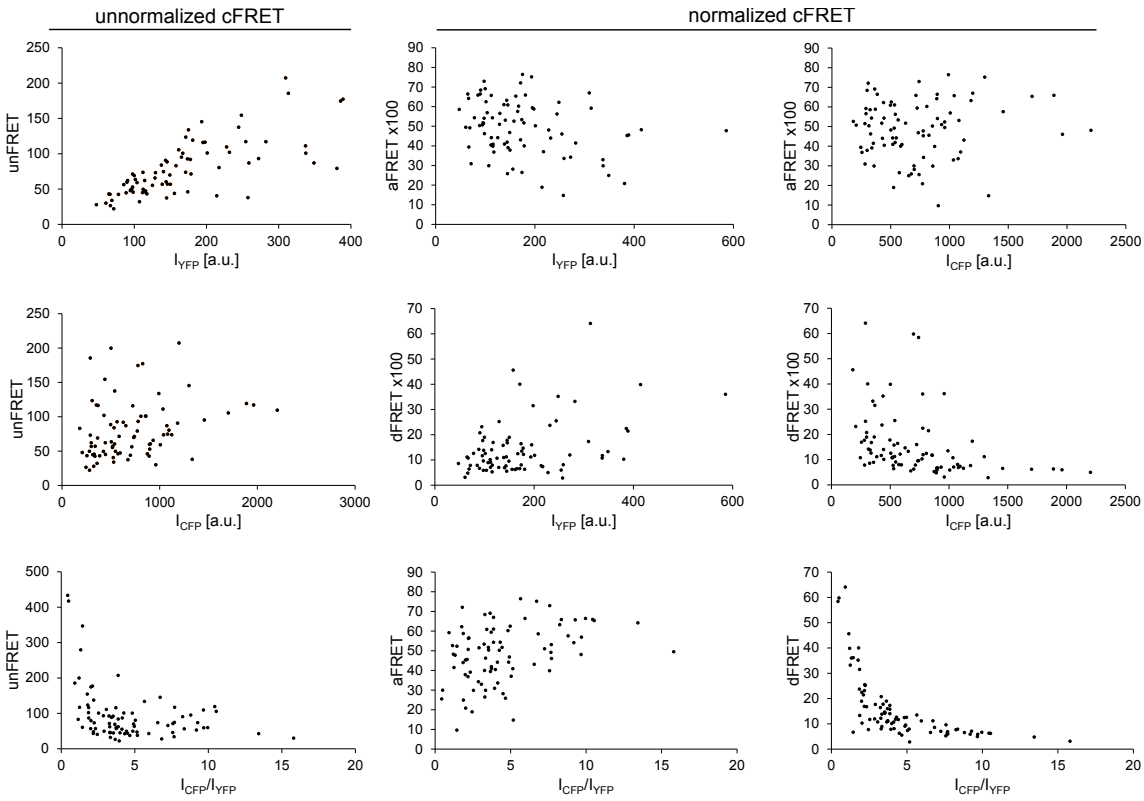

Figure 3.4: Comparison of normalization methods reveals aFRET to be superior
Distribution of different cFRET values depending on normalization in relation to CFP, YFP intensity and CFP/YFP ratio. Data points were acquired from 84 different HeLa cells expressing A-CFP/E-YFP, for which unFRET,aFRET, and dFRET maps were calculated and mean values of identical ROIs measured. CFP and YFP intensities of the same cells were measured in the same ROIs as used for FRET measurement.

YFP at varying ratios to compare unnormalized cFRET (unFRET), aFRET and dFRET (Figure 3.4). The expected dependency of FRET on the relative abundance of the subunits can be seen for unFRET levels of cells in relation to their expression profiles. With more E-YFP expressed, unFRET is linearly increasing, verifying it to be the limiting factor. A-CFP as the donor, on the other hand, is in such an excess, that even unFRET is not affected by changing expression levels. If the ratio of A-CFP to E-YFP becomes greater than one, unFRET is exponentially getting smaller. The seen linear dependency on E-YFP abundance vanishes by normalizing to the acceptor concentration, rendering aFRET independent of absolute abundance of either A-CFP or E-YFP and their ratio in an individual cell. Normalizing to the donor shows that dFRET suffers from clear concentration dependency with dFRET decreasing with increasing absolute A-CFP abundance and a clear exponential decrease with increasing ratio of A-CFP to E-YFP. Without searching for specific expression ratios, I could see higher A-CFP levels in most cells. This is reflected in aFRET being higher with a mean efficiency of 48.4 $\pm$ 14.5 % compared to dFRET

with 15.7 ± 12.6 %. This verifies the observation of APB experiments that LRRC8A is in excess and dFRET is very small due to non-interacting donors for A-CFP.

Taken together, FRET can be measured between C-terminally labelled LRRC8 subunits and aFRET is the beneficial normalization method for A-CFP/E-YFP experiments, with it being independent on expression ratios and approximating absolute cFRET values best due a high probability of all acceptors (E-YFP) interacting with donors and no free acceptors, since LRRC8E is not able to form homomers that reach the plasma membrane. For clarity aFRET and cFRET will be used synonymously throughout this thesis.

3.1.2 FRET changes upon activation of VRAC and can be used as optical activity sensor

After establishing seFRET measurements of fluorescently labeled VRAC subunits I next asked whether this can be used to monitor VRAC activity in living cells. HeLa cells expressing A-CFP/E-YFP show a decrease in cFRET when the bath solution of the cells was switched from isotonic (340 mOsm) to hypotonic buffer (250 mOsm; Figure 3.5A,E). The same effect was observed in NRK (data not shown) and HEK293 cells (Figure 3.5E). Reduction of cFRET was reversible and repeatable. The absolute cFRET values differ highly between individual cells. Interestingly, when normalized to their respective cFRET in isotonic buffer, the percentual reduction was robustly by 5 to 10 % (Figure 3.5E). VRAC homomers formed by LRRC8A are usually considered to be conducting no measurable currents (reviewed in [74]). Nevertheless, I could detect the same reduction of cFRET upon hypotonicity in HeLa cells expressing A-CFP/A-YFP (Figure 3.5B,E). Interestingly, there seem to be two distinct populations of cFRET reduction for LRRC8A homomers, but the used sample size here is too small for a clear statement. FRET occurs between molecules that are correctly oriented and in close proximity to each other, which creates the risk for overexpressed proteins to statistically enter the Förster radius of each other by simple diffusion. Membrane proteins do suffer even more from this crowding effect due to the limited space of the 2D plasma membrane compared to the 3D space of the cytosol.

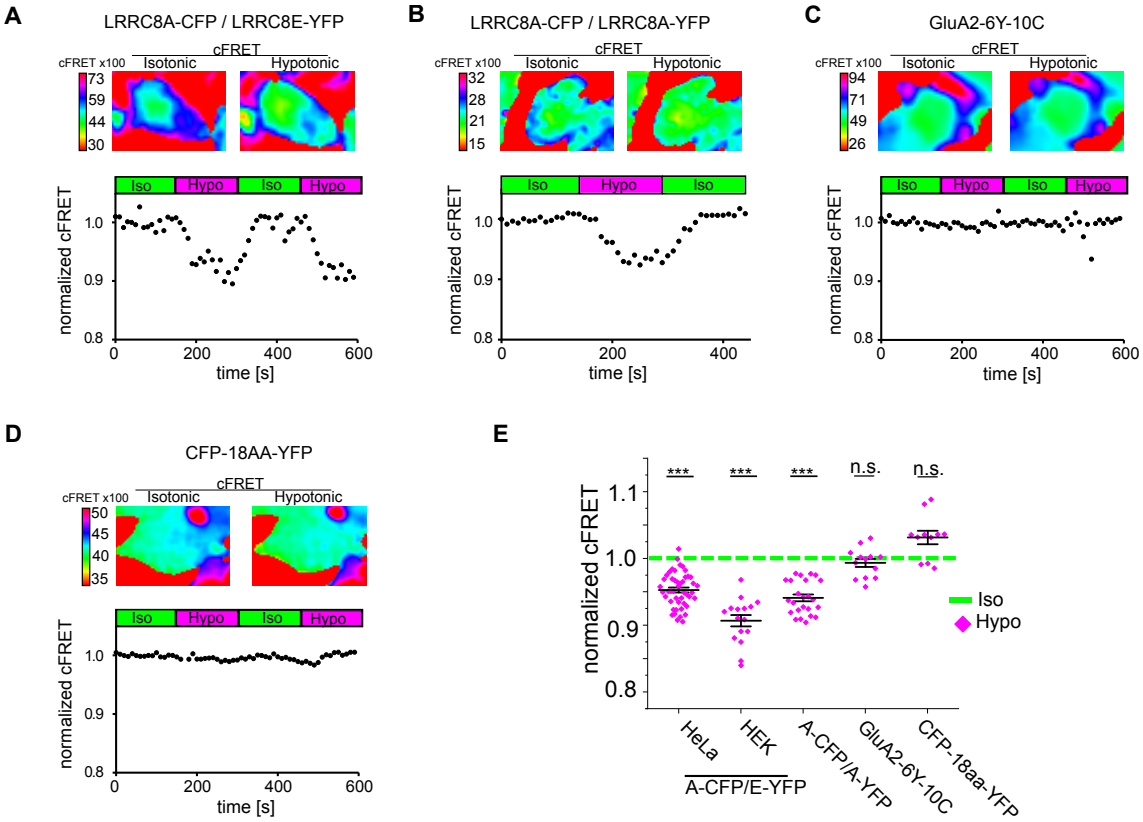

Figure 3.5: VRAC activation by hypotonicity is reflected by cFRET changes (**A, B, C, D**) Top panels: cFRET maps of cells expressing FRET constructs in isotonic and hypotonic buffer. Calibration bar left of cFRET map represents cFRET values and their respective color code in the look-up table (LUT). Bottom graph: cFRET normalized to isotonic conditions of the cell shown in top panels over time in different buffers. (**A**) HeLa cell expressing A-CFP/E-YFP. (**B**) HeLa cell expressing A-CFP/A-YFP. (**C**) HEK293 cell expressing GluA2-6Y-10C. (**D**) Hela cell expressing CFP-18AA-YFP. (**E**) Quantification of normalized cFRET of cells expressing A-CFP/E-YFP (n = 9 dishes with 47 HeLa cells; n = 8 with 29 HEK293 cells), A-CFP/A-YFP (n = 8, 24 HeLa cells), glutamate receptor GluA2-6Y-10C (n = 4, 13 HEK293 cells) and CFP-18AA-YFP (n = 4, 11 HeLa cells). Data represent mean of last five time points in hypotonic buffer of individual cells (magenta diamonds), and mean of all cells ± s.e.m. Baseline cFRET in isotonic buffer indicated by green dashed line. Statistics: *p<0.05; ***p<0.0005; n.s., not significant, Student's t-test comparing isotonic to hypotonic.

FRET signals arising from crowding would, therefore, be susceptible to volume changes by either reducing the chance of fluorophores entering each other's Förster radii in swollen cells or increasing it in shrunken. I utilized two negative controls to rule out the contribution of crowding on the detected decrease of cFRET upon cell swelling caused by hypotonicity. Neither GluA2-6Y-10C, an intra-receptor FRET sensor of the AMPAR subunit GluA2 localized at the plasma membrane [144], nor the cytosolic fusion construct CFP-18AA-YFP [145] showed reduced cFRET when expressing cells were challenged with hypotonicity (Figure 3.5C,D,E). Especially the GluA2-6Y-10C construct is comparable to VRACs by being a plasma membrane protein forming homotetramers, which could, therefore, suffer from the same

crowding effects as VRACs, that would change by cell volume changes. To further validate that the observed FRET change is due to channel gating I performed patch-clamp fluorometry together with Yuchen Hao from the AG Plested, FMP Berlin. All beforehand shown experiments were performed on HeLa and HEK293 cells with unaltered genetic background, having all five LRRC8 genes intact and normally expressed.

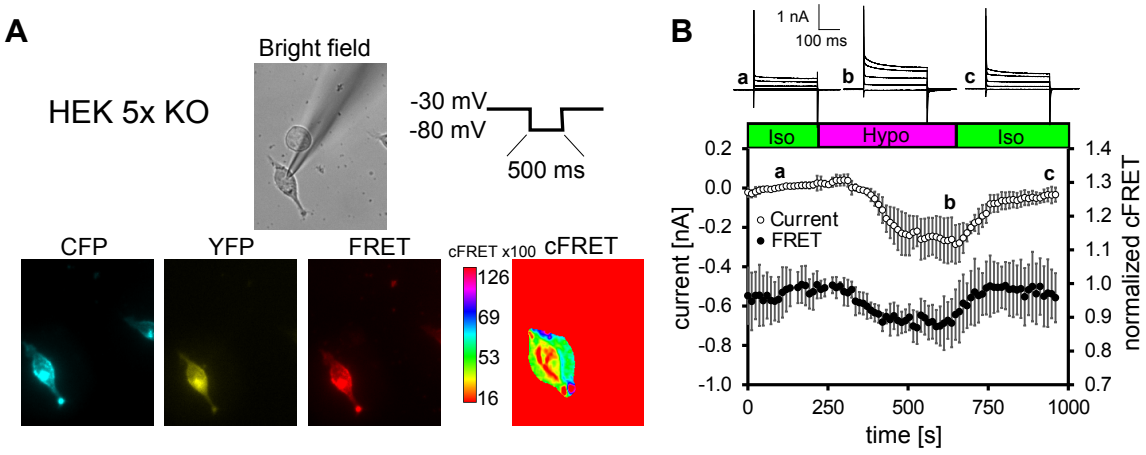

Figure 3.6: FRET changes reflect channel gating
(**A**) Representation of a patch-clamp fluorometry experiment. Images of a HEK 5xKO cell transfected with A-CFP/E-YFP. Voltage step protocol for assessing VRAC current over time shown on top right. Bottom row: I^{DD}, I^{AA},I^{DA}, and cFRET maps of the cell shown in bright field picture (top).Calibration bar left of cFRET map represents cFRET values and their respective color code in the look-up table (LUT). (**B**) Simultaneous measurements of whole-cell current at -80 mV (open circles) and normalized cFRET values (solid circles) during buffer exchange experiment with A-CFP/E-YFP-expressing HEK 5xKO cells. Data represent mean of 4 cells ± s.d. Above, representative current traces from voltage-step protocols at the indicated time points (a, b, c).

Hence channels might be formed with mixtures of fluorescently labeled subunits and endogenous unlabeled ones. This mixture does not interfere with monitoring VRAC activity by FRET since all signals of the sensitized emission can only arise from channels with at least a donor and an acceptor molecule. For whole-cell voltage-clamp measurements it would mean that there is no way to discriminate currents of expressed subunits and endogenous VRACs. We, therefore, used HEK cells deficient of all 5 LRRC8 genes (5x KO). These were transfected with A-CFP/E-YFP and patch-clamped after 24 to 48 h for simultaneous recording of current and FRET responses to hypotonicity in the same cell (Figure 3.6A). As is described for untagged VRACs [30], we detected currents developing over a timescale of minutes, which were outwardly rectifying and inactivating at positive potentials (Figure 3.6B). Current and cFRET correlated very well and changed concurrently upon osmolarity changes, with a slow opening and a faster closing process. Concludingly, the reduction of cFRET indeed seems to reflect VRAC activation.

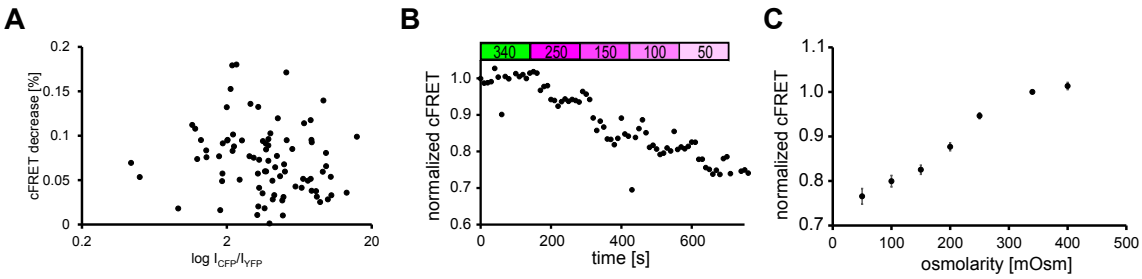

Figure 3.7: FRET changes with channel activity irrespective of expression ratio
(**A**) Relationship between the relative cFRET change (isotonic to hypotonic buffer) and the expression ratio of A-CFP/E-YFP represented by the ratio of their measured fluorescence intensities [a.u.] for 84 cells HeLa cells. (**B**) Normalized cFRET of a titration of single HeLa cell expressing A-CFP/E-YFP with gradual decreasing osmolarities.(**C**) Quantification of osmolarity titration experiments from 50 to 400 mOsm. In total, 68 cells were measured for the titration curve, n = 7-21 depending on osmolarity.

Since the stoichiometry of VRACs formed by expressed subunits depends on sheer abundance, as shown in *Xenopus* oocytes [80], it might influence the amplitude of cFRET changes when the ratio of acceptors and donors is different in individual cells. A comparison of cFRET changes upon activation and the expression ratio of A-CFP/E-YFP of individual cells showed no correlation (Figure 3.7A), minimizing the selection bias for cells as theoretically all cells that do express the fluorescently tagged subunits in a detectable amount can be used for seFRET experiments. Next, I tested whether the magnitude of activation can also be monitored with this sensor. Indeed, cFRET reduced further, the smaller the osmolarity of the bath solution got (Figure 3.7B). This change could be monitored in a single cell, opening possible applications for cells with varying VRAC activity over time. The percentual decrease of cFRET between cells was consistent and robust, with a sigmoid relation of cFRET change and osmolarity (Figure 3.7C).

Having seen the sensitivity of the FRET sensor towards the magnitude of activation of VRACs, I next wanted to corroborate the overall applicability of it by reproducing results of previously published electrophysiological experiments. It was shown that the current amplitude is dependent on the cholesterol content of the plasma membrane, with less cholesterol leading to larger currents [146]. To deplete the plasma membrane of HeLa cells of cholesterol, I utilized methyl-β-cyclodextrin (MbCD). The decrease of cholesterol levels was verified by staining treated and untreated cells with filipin, a fluorescent dye specifically binding to cholesterol (Figure 3.8A). Depletion of cholesterol did not alter the mean cFRET, but the cells showed a significantly stronger decrease of cFRET between A-CFP/E-YFP upon hypotonicity, compared to untreated cells (Figure 3.8B). This reflects a higher activity of VRAC, ultimately leading to bigger currents, and is further proof that the FRET sensor is not only indeed showing the activity of VRAC but can as well monitor the

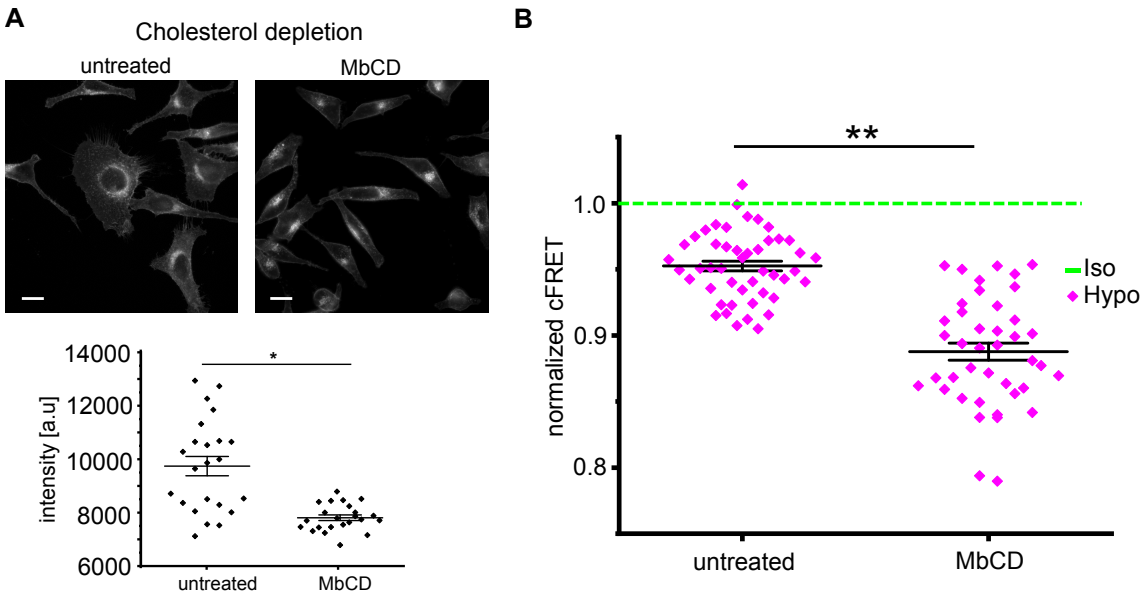

Figure 3.8: Depletion of cholesterol enhances VRAC activity
(**A**) Top panel: wide-field images of untreated, and MbCD treated, fixed Hela cells stained with filipin. Scale bar, 20 μm. Bottom graph: Quantification of filipin fluorescence (n=5, over 300 cells per condition). (**B**) Quantification of untreated and MbCD treated HeLa cells expressing A-CFP/E-YFP challenged with hypotonicity (n=10 dishes with 46 cells). The isotonic baseline is indicated by green dashed line. Data represent individual cells (magenta diamonds) and mean ± s.e.m. Statistics: *p<0.05; **p<0.005; n.s., not significant, Student's t-test.

magnitude of channel activation.

Taken together cFRET of fluorescently tagged LRRC8 subunits can be used to monitor VRAC activity in living cells. Being less invasive than voltage-clamping in whole-cell configuration, this new technique enables tracking of VRAC activity in new contexts.

3.2 Ionic strength changes do not activate VRACs on endomembranes

Having FRET established as an optical sensor for VRAC activity, I next wanted to explore the activation mechanism of these channels. The variety and seemingly contradictive nature of published data concerning the activation mechanism of VRACs encouraged the use of this new tool that hopefully circumvents biases introduced by older methods. A study of VRACs in an artificial lipid bilayer environment could show that these channels can be activated by iso-osmotic reduction of ionic strength [79]. The underlying mechanism is believed to depend on electrostatic interactions between the LRRDs of neighboring subunits in an individual channel [69–71]. Since this would be a very elegant mechanism for VRAC activation but was only shown

in an artificial *in vitro* environment, I investigated the influence of ionic strength in living cells.

The ionic strength in living cells can be monitored with the FRET based "RD-sensor" [147]. It consists of CFP and YFP connected by two α-helices (Figure 3.9 A). An arginine in the one and an aspartic acid in the other helix create an electrostatic attraction which locates the two fluorophores in proximity close enough for FRET to occur. The distance between the fluorophores relies thereby on the attraction of the charged amino acids, which are influenced by surrounding ions. More ions, and therefore higher ionic strength, weaken the interaction between the two helices and lead to the fluorophores moving apart and the FRET between them to decrease. Fewer ions, on the other hand, lead to less interference of the electrostatic attraction, moving the fluorophores closer together and therefore increase FRET. Cells challenged by hypotonicity face a water influx created by the osmotic pressure of their cytosolic osmolytes. With no net ion flux, the ionic strength in a swollen cell will, therefore, decrease, which again is believed to activate VRAC. Indeed I saw a robust decrease of ionic strength in HeLa cells expressing the RD-sensor upon hypotonicity (Figure 3.9B). As expected, the ionic strength returns to its baseline level when changing back to isotonic conditions. This change was homogenous over the whole cell (Figure 3.9C). In most cells there was an accumulation of the RD-sensor in the nucleus, making it discernable from the cytosol. With a mean FRET ratio of 1.27 $\pm$ 0.06 the ionic strength in the nucleus of a cell is smaller compared to the cytosol with a ratio of 1.26 $\pm$ 0.06. Nevertheless, the relative changes of the FRET ratio upon hypotonic treatment were nearly identical, with a 7.9 % increase in the cytosol and 7.6 % in the nucleus. Changes of ionic strength affect, therefore, the whole cell and not only the plasma membrane. Concludingly, I tested the activation of VRACs by hypotonicity on endomembranes since the ionic strength is reduced there as well and should activate them if the hypothesis of ionic strength solely activating VRACs is right. Firstly, I trapped expressed VRACs in the endoplasmic reticulum (ER) by application of brefeldin-A (BFA). HeLa cells treated with BFA during transfection with fluorescently labeled VRAC subunits show clear retention of the expressed proteins in the ER meshwork compared to the plasma membrane localized untreated cells (Figure 3.9D). The exact mechanism and location of VRAC formation by different subunits is not well understood. To verify that VRACs are already assembled in the ER, I tested for the occurrence of intra-complex FRET of A-CFP/E-YFP expressing cells treated with BFA by acceptor photobleaching. CFP intensity of A-CFP/E-YFP complexes trapped in the ER did increase significantly compared to unbleached cells (Figure 3.9E) leading to a mean dFRET of 14.1 $\pm$ 8.8 %, which fits the dFRET of plasma membrane localized channels. Cells expressing A-CFP/CD4-YFP and treated with BFA did not show this

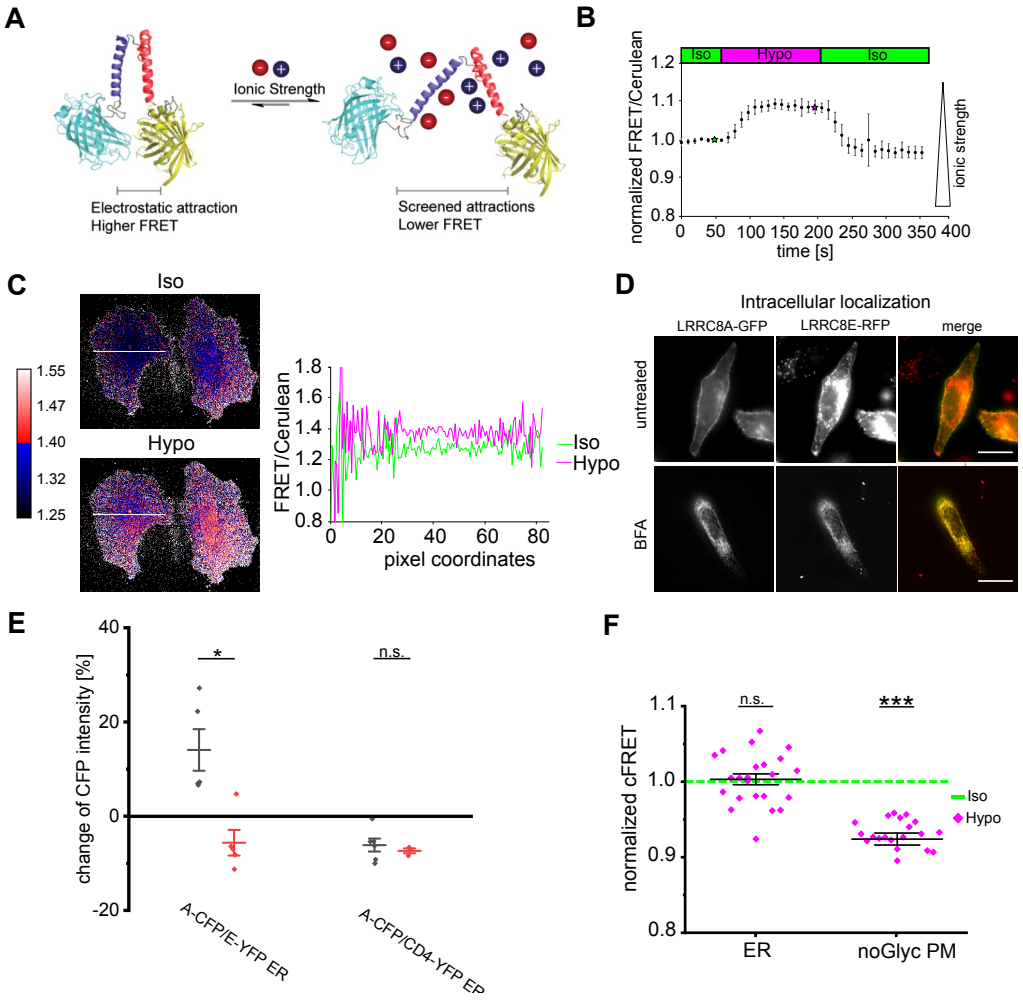

Figure 3.9: Ionic strength reduction is not sufficient for VRAC activation in the ER

(**A**) Scheme of the RD-ionic strength sensor. Increased ionic strength leads to reduced FRET. Modified from [147]. (**B**) Changes of ionic strength measured in HeLa cells expressing the ratiometric RD sensor during hypotonic treatment. FRET intensity was divided by Cerulean intensity and normalized to basal values, with increasing values corresponding to decreasing ionic strength. Data represent mean of 10 cells ± s.d. (**C**) Ratio maps of two representative cells in isotonic (green star in panel B) and hypotonic (magenta star in panel B) buffer. Calibration bar left of ratio maps represents FRET/Cerulean ratios and their respective color code in the LUT. Right: intensity profile along the white line shown in the ratio maps. (**D**) Epifluorescence images of A-GFP and E-RFP in live cells without (top row) and with (bottom row) 5 μg/ml brefeldin-A (BFA) treatment. Images of BFA-treated cells were background-subtracted by rolling-ball algorithm (radius = 50 pixels) and contrast increased by an unsharp mask (sigma = 3, weight = 0.7). Scale bar, 20 µm. (**E**) Quantification of APB experiments of HeLa cells expressing A-CFP/E-YFP or A-CFP/CD4-YFP treated with 5 μg/ml BFA. Data points (diamonds) represent the percentual CFP intensity change of indicated subunit compositions in individuel cells. For each subunit pair, the CFP change of bleached (black diamonds), unbleached cells (red diamonds) and the mean ± s.e.m. is shown. Statistics: *p<0.05; ***p<0.0005; n.s., not significant, Student's t-test.

CFP intensity increase due to bleaching, ruling out crowding effects as the reason for the observed dFRET of A-CFP/E-YFP complexes. So, I could show, that VRACs are already formed by their subunits in the ER and that the ionic strength of a cell changes over the whole cell volume upon extracellular hypotonicity. Challenging BFA-treated cells with hypotonicity did not decrease cFRET however (Figure 3.9F). During the maturation of a protein it can be post-translationally modified for example by glycosylation. LRRC8A was shown to be glycosylated at N66 and N83 [30]. The collapse of the Golgi due to BFA treatment prohibits the modification of glycosylations and might lead to the observed absence of cFRET change upon hypotonicity. To rule this out I tagged a non-glycosylatable mutant of LRRC8A (noGlyc) with CFP, having both glycosylation sites mutated to alanine [30]. Cells co-expressing noGlyc-CFP/E-YFP showed the expected decrease of cFRET due to hypotonic treatment, even though the glycosylation is missing on the LRRC8A subunits of the complexes.

VRACs trapped in the ER by BFA cannot be activated by hypotonicity, but BFA itself does influence the signaling and overall health of cells and might, therefore, be the reason for this inactivity. So, I next aimed to exploit the reverse dimerization system to follow VRAC through the sectretory pathway [148]. This system relies on the self-dimerizing domains of the FK506-binding protein (FM). These dimerize with high affinity and lead to aggregation of fusion proteins, which are retained in the ER. The interaction of FM domains can be substituted with the small molecule "D/D-solubilizer", releasing fusion proteins out of the aggregates. Released proteins will then travel in bulk from the ER to the Golgi complex and finally to the plasma membrane (Figure 3.10A). First I tested a fusion protein of green-fluorescent protein (GFP) and four FM domains (GFP-FM_4), that contains the signal sequence of human growth hormone for ER import [149]. When expressed, GFP-FM_4 is retained in the ER as clearly visible aggregates (Figure 3.12B). Upon addition of D/D-solubilizer the aggregates disassemble and GFP-FM4 spreads over the ER meshwork. After 53 minutes the proteins traveled to a juxtanuclear region, the Golgi apparatus. From there they were excreted to the extracellular space within 89 minutes after D/D-solubilizer addition. The release by D/D-solubilizer was carried out at room temperature and worked in all cells observed. To transfer this system to VRAC I chose to fuse the FM tag to LRRC8A, being the obligatory subunit and therefore contained in every channel formed. I inserted two FM domains in the second extracellular loop of LRRC8A since other studies used this position as well to insert for example HA-tags [30]. Expression of this construct though led to CFP signal spread homogeneously over the ER volume, rather than spot like aggregates as seen for GFP-FM4. The two inserted FM domains seem to have prohibited proper protein folding, with the misfolded outcome being retained

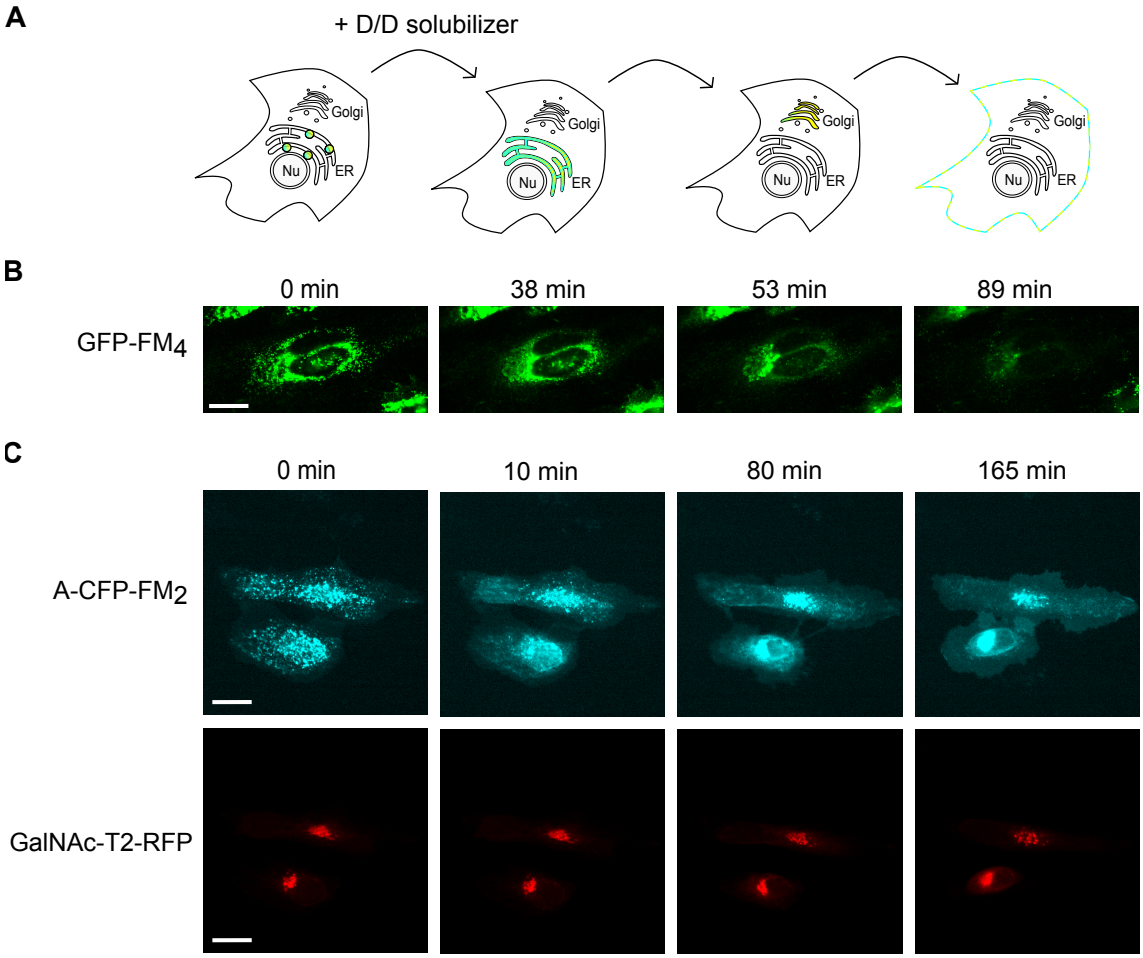

Figure 3.10: Fluorescent fusion proteins can be tracked through the secretory pathway by the reverse-dimerization system
(**A**) Scheme of the reverse-dimerization system. Proteins fused with FM tags multimerize to aggregates that are retained in the ER. Upon D/D-solubilizer addition, the FM multimers dissociate and traffick through the ER to the Golgi network and finally to the plasma membrane. (**B**) A HeLa cell expressing GFP-FM_4 at the indicated time points after D/D-solubilizer addition. Scale bar, 20 μm. (**C**) Two HeLa cells expressing A-CFP-FM_2 and the Golgi marker protein GalNAc-T2-RFP at the indicated time points after D/D-solubilizer addition. Scale bar, 20 μm.

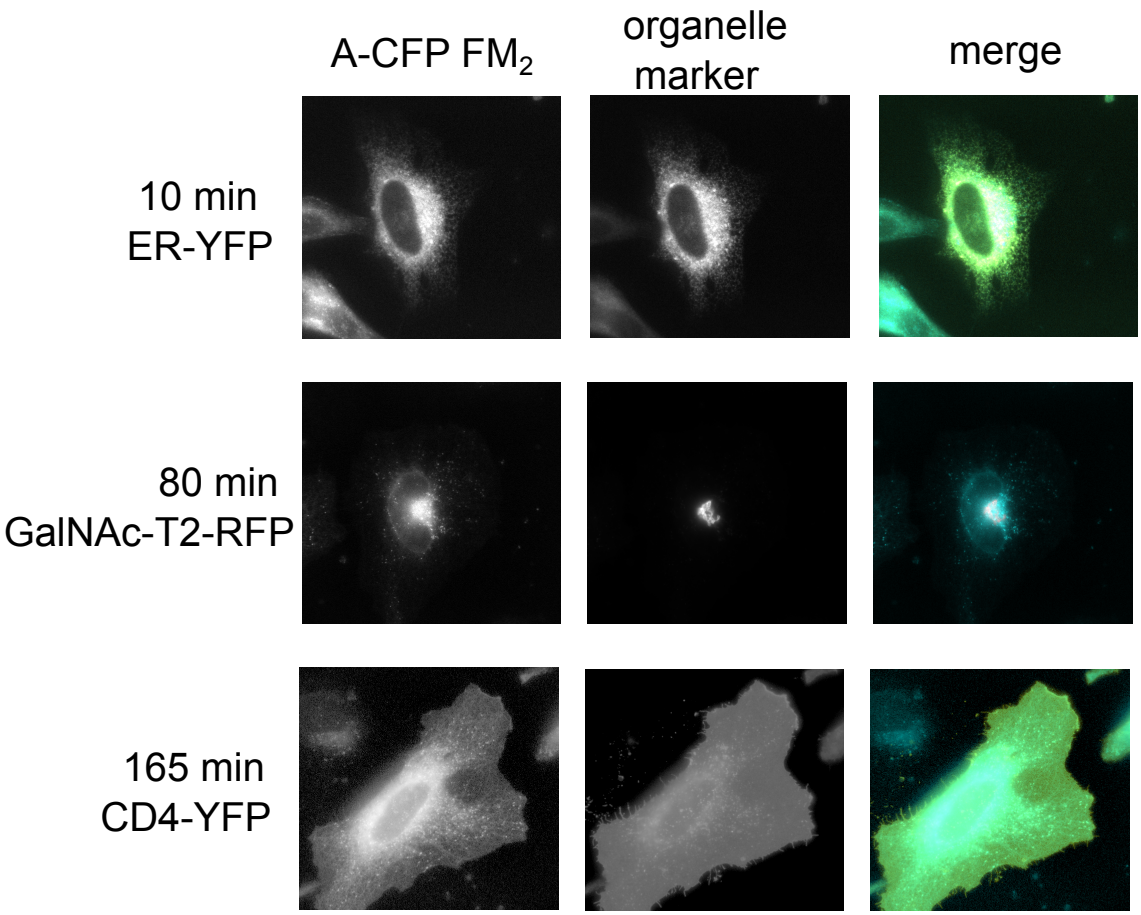

Figure 3.11: Dissociated A-CFP-FM$_2$ complexes colocalize with organelle markers
Representative fluorescence images of HeLa cells co-expressing LRRC8A-CFP-FM2 (left, cyan in merge) and organelle markers (middle) ER-YFP (top, yellow in merge), GalNAcT2-RFP (middle, red in merge) and CD4-YFP (bottom, yellow in merge) at indicated time points after addition of D/D solubilizer.

in the ER. So I next tried to fuse two FM domains to the C-terminus of the CFP tag of LRRC8A (A-CFP-FM$_2$). Expression of A-CFP-FM$_2$ finally led to the expected spot-like aggregates in the ER (Figure 3.10C).

Attempts to release VRACs out of the aggregates with D/D-solubilizer failed at room temperature, with cells either dying, no change of aggregates or incubation times of hours before release (data not shown). Incubation at 37 °C, however, led to homogeneously spread A-CFP-FM$_2$ signal in the ER meshwork after 10 minutes and bulk travel of the channels to the Golgi after 80 minutes. 165 minutes after addition of D/D-solubilizer channels were inserted in the plasma membrane (Figure 3.10C). To validate the subcellular localization at the respective time points I co-expressed A-CFP-FM$_2$ with organelle markers for ER, Golgi and plasma membrane. Indeed, A-CFP-FM$_2$ showed good co-localization with the respective organelle markers at the respective time points after D/D-solubilizer addition (Figure 3.11). Co-expression of A-CFP-FM$_2$ with E-YFP resulted in spot like aggregates as well, with

co-localizing CFP and YFP signal (data not shown). The time course for the release of A-CFP-FM_2/E-YFP complexes was identical to that of A-CFP-FM_2 homomers, enabling the activity measurement of VRAC with FRET in different organelles. Unfortunately, it was not possible to measure all organelles in the same cell, since they died either before or after the Golgi measurement. A possible reason might be the combined cytotoxicity of the D/D-solubilizer treatment and light exposure during seFRET measurement. So, I tested individual cells at the determined time points after release. Again cFRET did not decrease upon hypotonicity for ER-localized channels; neither did it for those that reached the Golgi apparatus (Figure 3.12). As soon as VRACs were transported to the plasma membrane, cFRET did decrease when cells were treated with hypotonic buffer, showing on the one hand the general functionality of CFP-FM_2 tagged subunits and on the other hand that the plasma membrane localization is required for VRAC activation. However, the decrease of intracellular ionic strength was not able to activate VRACs on endomembranes.

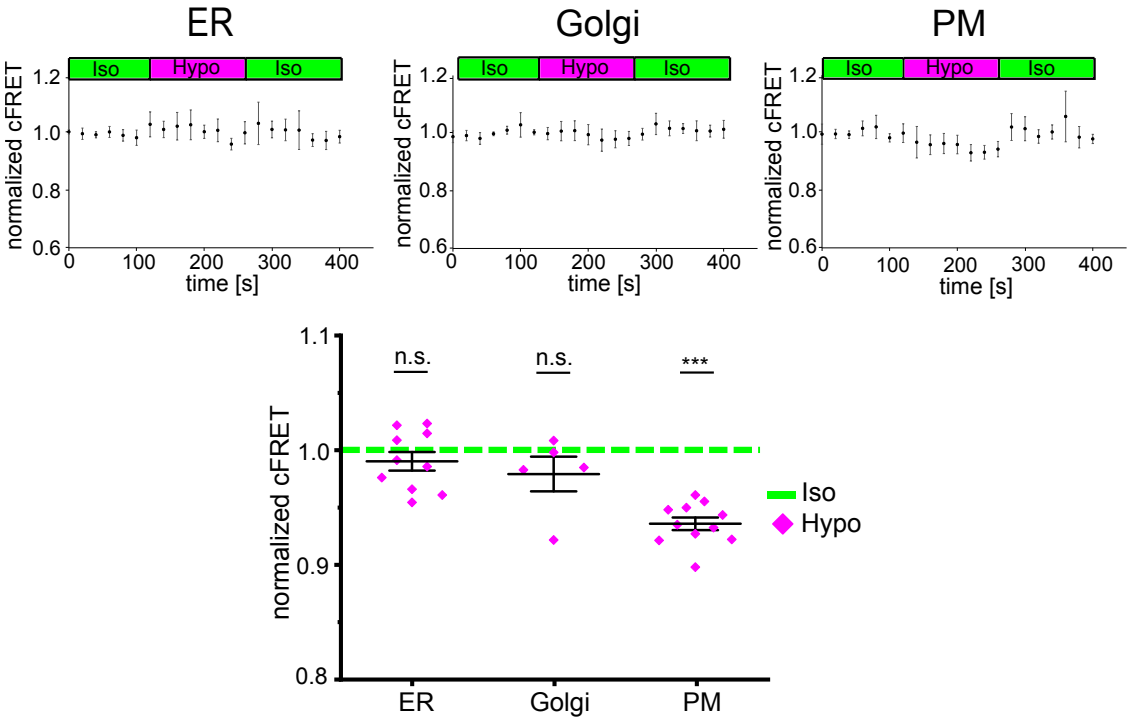

Figure 3.12: A-CFP/E-YFP formed channels are not activated by hypotonicity on endomembranes
Top panels: cFRET measured in HeLa cells expressing A-CFP-FM_2/E-YFP. VRACs localizing to the ER (n = 4, 10 cells), Golgi (n = 5, 26 cells) and plasma membrane (PM; n = 5, 11 cells) were measured at 10, 80 and 165 min after addition of D/D solubilizer. Data in time traces represent mean ± s.d. Bottom graph: average normalized cFRET in of the first seven-time points in isotonic and last three time points in hypotonic buffer. Data represent individual cells (ER, PM) or FOVs (Golgi) and mean ± s.e.m. Statistics: ***$p<0.0005$; n.s., not significant, Student's t-test, comparing hypotonic with isotonic.

3.3 VRAC activation by PMA can be shown with FRET but is impeded by whole-cell voltage clamp

The established FRET sensor could already show that ionic strength is likely not the activating stimulus of VRAC in living cells, so I next aimed at several signaling pathways that were published to either activate or inactivate VRAC. During the last decades, numerous workgroups published a plethora of different signaling molecules and mechanisms that are supposed to be involved in VRAC activity, for some pathways having publications that claim them to be activating while others state the opposite (reviewed in [9, 36]). Most of the acquired data suffer from the lack of knowledge which protein family forms VRACs, thereby having no good negative controls to discriminate detected osmolyte fluxes from other channels. Furthermore it is now known that VRACs have different biophysical properties depending on subunit composition and even varying activation mechanisms [30, 79, 117]. So, I started to decipher the signaling pathway with the new subunit-specific tool.

With the reverse dimerization system, I could show that the plasma membrane localization is needed to activate VRACs by hypotonicity in living cells. One factor present there is the actin cytoskeleton, with ambiguous data concerning VRAC regulation [146, 150–152]. To assess the involvement of the actin cytoskeleton for VRAC activation, I exploited the toxin latrunculin B (LatB), which prevents F-actin assembly and leads to depolymerization of microfilaments. Treating HeLa cells for one hour with LatB led to complete depolymerization of actin filaments (Figure 3.13A). Nevertheless did cFRET of A-CFP/E-YFP complexes decrease upon hypotonicity similarly to untreated samples, ruling out a general necessity of the actin cytoskeleton for VRAC activation (Figure 3.13B). There still might be a modulating role of actin for VRAC activity (for many publications hint towards its involvement in VRAC regulation, discussed in [153]), but I wanted to focus on the key regulatory pathway.

Another potential activation pathway involves PKCs, again with publications proposing a stimulating or inhibiting effect [134–140]. The protein kinase C family consists of several paralogs with different tasks that they fulfill by phosphorylating their specific substrates on a serine or threonine residue. PKCs are activated and recruited to the plasma membrane by diacylglycerol (DAG), which is the product of phospholipase C catalyzing the cleavage of phosphatidylinositol-4,5-bisphosphate (PIP2) to DAG and inositol-1,4,5-triphosphate (IP3). Activation of PKCs is experimentally accomplished by the addition of phorbol esters, which serve as DAG analogs, for example phorbol-12-myristate-13-acetate (PMA) or 1-oleoyl-2-acetyl-sn-glycerol (OAG). First I tried to reproduce findings that suggested activation of VRAC by PKC by application of OAG [140]. Pilot experiments were in agree-

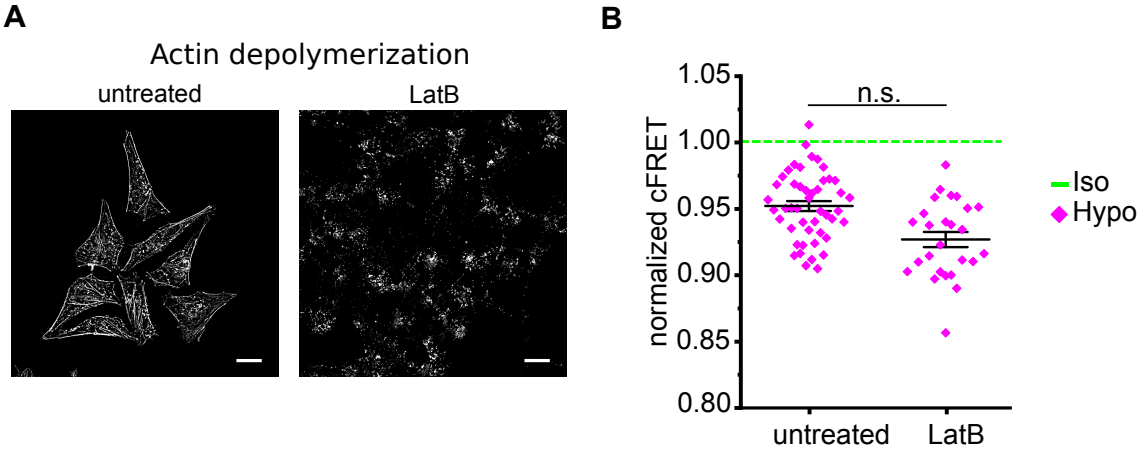

Figure 3.13: VRAC activation is independent of the actin cytoskeleton
(**A**) Representative fluorescence images of control HeLa cells treated with 2 μM latrunculin B (LatB) or not (untreated) that were fixed and stained with Alexa Fluor 546-phalloidin. Image of untreated cells was deconvolved using the blind-algorithm package of LAS X. Scale bar, 20 μm. (**B**) Quantification of normalized cFRET of HeLa cells expressing A-CFP/E-YFP, treated with LatB and untreated challenged with hypotonicity (n=8 dishes with 26 cells). Data represent individual cells (magenta diamonds) and mean ±s.e.m. Statistics: n.s., not significant, Student's t-test, comparing hypotonic with isotonic.

ment with this by showing decreasing cFRET upon application of OAG (data not shown). The consecutive experiments suffered from varying quality of OAG batches, with batches causing no cFRET change and some with a highly variable degree of cFRET changes. So, I decided to test the effect of PMA, since both chemicals are supposed to activate PKCs. Addition of 1 μM PMA led to a reproducible and robust decrease of cFRET for A-CFP/A-YFP homomers and A-CFP/E-YFP heteromers (Figure 3.14A). For homo- and heteromers cFRET decreased by up to 10 %. Cells expressing CFP-18AA-YFP did not show any change of cFRET upon PMA addition (Figure 3.14B). I want to emphasize that VRACs formed solely by LRRC8A subunits can be activated by PMA, hinting towards a general mechanism that might be true for all VRACs irrespective of their subunit composition. For yet unknown reasons, isosmotically activated VRACs were previously shown in many situations to be closing when the bath solution is switched to hypertonic buffer [44, 154]. After activation of A-CFP/E-YFP in HeLa cells by PMA there was no change of cFRET when I applied 400 mOsm hypertonic buffer (data not shown), but application of 500 mOsm led to cFRET recovering to the initial value in isotonic buffer before PMA addition (Figure 3.14C). The effect is therefore likely due to a real conformational change of the channel subunits and not due to photophysical alterations of CFP or YFP creating a false-positive result.

To validate that the cFRET decrease by PMA reflects the opening of VRACs and that they conduct osmolytes, we performed patch-clamp fluorometry. Surprisingly, PMA did neither evoke currents nor did cFRET of A-CFP/E-YFP complexes

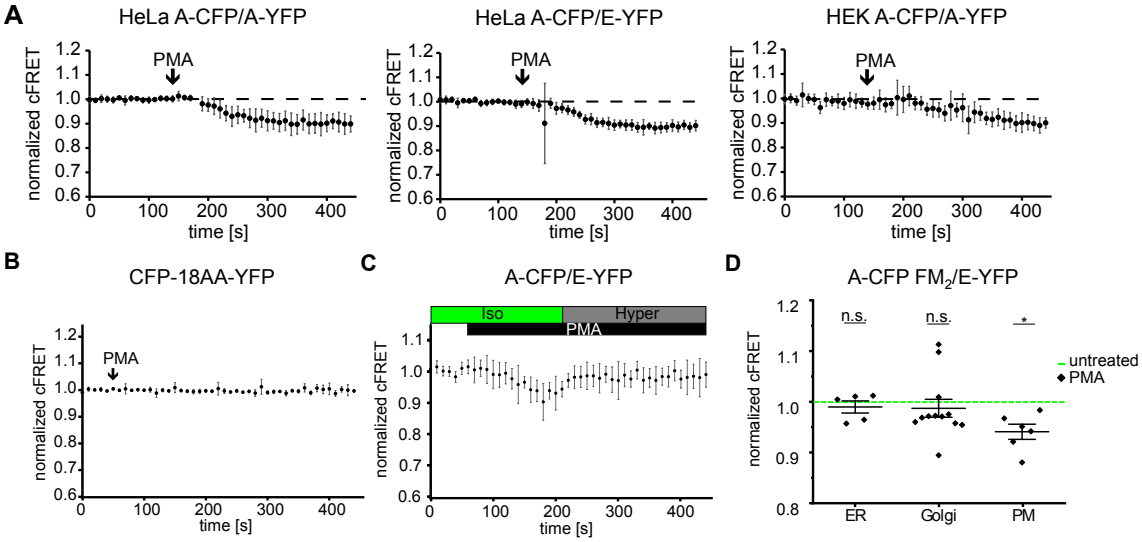

Figure 3.14: VRACs in the plasma membrane are activated by the DAG analog PMA

(**A**) Normalized cFRET of HeLa cells expressing A-CFP/A-YFP (11 cells), A-CFP/E-YFP (12 cells), and HEK293 cells expressing A-CFP/A-YFP (12 cells). 1 μm PMA was added at the time point indicated by black arrows. Data represent mean ± s.d. (**B**) Normalized cFRET of HeLa cells expressing CFP-18AA-YFP (21 cells).1 μm PMA was added at the time point indicated by black arrow. Data represent mean ± s.d. (**C**) Normalized cFRET of HeLa cells expressing A-CFP/E-YFP (9 cells). After addition of PMA, VRACs were inactivated with hypertonic solution (500 mOsm). Data represent mean ± s.d. (**D**) Quantification of a reverse-dimerization experiment in HeLa cells expressing A-CFP-FM_2/E-YFP. At 10 min (ER; n = 4 dishes with 5 cells), 80 min (Golgi; n = 5, 12 cells) or 165 min (PM; n = 5, 6 cells) after addition of D/D solubilizer, when VRACs have reached the respective compartments, cFRET was measured before (untreated) and after addition of 1 μM PMA. Data represent individual cells (diamonds) and mean ± s.e.m. Statistics: *p<0.05; n.s., not significant, Student's t-test, comparing before and after PMA application.

decrease in the whole-cell configuration (Figure 3.15A). Patch-clamp fluorometry experiments had to be performed in KO cells with all 5 LRRC8 genes depleted (HEK 5x KO), as already discussed. A possible explanation for this contradiction of activation by PMA in wildtype HEK293 and HEK 5x KO cells could be the different genetic background of the clonal expanded KO cell line compared to the more heterogenous wildtype one. As well could the FRET sensor show artifacts that do not relate to actual channel gating, but the artificial cFRET decrease should be reproducible. I suspected rather the whole-cell configuration to impair cell signaling and masking thereby the activating effect of PMA. In the previous experiments, cells were dialyzed with the pipette solution for at least 10 minutes, diluting cellular osmolytes including signaling molecules. Therefore, we tested the currents of cells pre-incubated with PMA before membrane breakthrough and establishment of whole-cell voltage clamp. With this method we measured a mean current of -406 ± 306 pA in HEK 5x KO cells expressing A-CFP/E-YFP after PMA incubation,

whereas untreated cells resulted in -148 ± 94 pA (Figure 3.15B left panel). To assess the influence of background currents, created by measuring directly after membrane breakthrough without time to test persisting gigaseal, we measured untransfected HEK 5x KO cells treated with PMA as well, resulting in a mean current of -166 ± 66 pA (3.15B left panel). The measured currents showed a high variability for several reasons. VRAC currents shown before were corrected for basal currents in isotonic buffer by subtracting the mean current measured in isotonic buffer for all timepoints. Furthermore, we waited after membrane breakthrough that the baseline, reflecting stable giga seal and possible background currents, did not shift anymore. Lastly it is a general recommendation for whole-cell voltage-clamp to wait up to five minutes before the measurement to dialyze the cytosol against the pipette solution, an incubation skipped here on purpose due to it likely causing the seen false-negative result. Besides the recording of currents at -80 mV, we recorded voltage step traces. For untreated and PMA treated cells they showed the outward rectification and inactivation at positive potentials characteristic for VRACs and were not present in untransfected HEK 5x KO cells. Activation of VRAC by PMA is obvious by the increase of currents at positive potentials. The observed current increase of A-CFP/E-YFP channels by PMA contradicts the before acquired results in whole-cell configuration, whereas it corroborates the predicted opening by cFRET experiments.

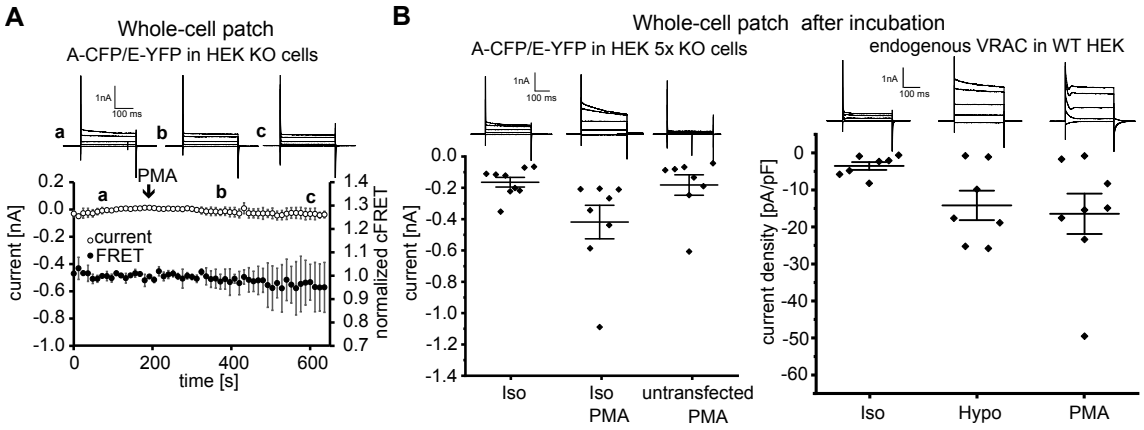

Figure 3.15: Whole-cell configuration impedes PMA activation of VRACs
(**A**) Simultaneous measurements of whole-cell current at -80 mV (open circles) and normalized cFRET values (solid circles) in A-CFP/E-YFP-expressing HEK5x KO cells with addition of 1 μM PMA (indicated by arrow). Data represent mean of 3 cells ± s.d. Above, representative current traces from voltage-step protocols at the depicted time points (a, b, c).(**B**) Whole-cell currents at -80 mV of A-CFP/E-YFP-expressing (and untransfected as control, n = 8 cells) HEK 5xKO cells (left) and current densities of wild-type HEK293 cells (right) with whole-cell configuration established after pre-incubation with indicated buffers: isotonic buffer without (n = 9) or with 1 μM PMA (n = 8) (left), isotonic (n = 7) and hypotonic (n = 7) buffers without and isotonic buffer with 1 µM PMA (n = 8) (right). Data represent individual cells (diamonds) and mean ± s.e.m. Above, representative current traces from voltage-step protocols for each condition.

The subunits used for FRET experiments have to be tagged with a fluorescent protein at their C-termini. Even though we and others previously [30, 80] could show that they still conduct currents when cells are challenged by hypotonicity, the FP tags still might influence the underlying signaling. So, we next measured endogenous VRAC currents in wildtype HEK293 cells with the whole-cell patch after incubation method. As for A-CFP/E-YFP complexes in KO cells, endogenous VRACs of HEK293 cells open upon PMA application and have a mean current density of -16.6 ± 15.4 pA/pF compared to the current density provoked by hypotonic treatment of -14.4 ± 10.5 pA/pF (Figure 3.15B right panel). The activation is observable in negative, as well as positive clamp voltages compared to cells incubated in isotonic buffer.

These experiments demonstrate the involvement of DAG in the signaling events activating VRACs. Its analog PMA can evoke currents of A/A homomers, A/E heteromers and of endogenous VRACs in HEK293 cells. We could also show that the whole-cell configuration, used for decades to investigate VRAC characteristics, can adulterate findings concerning the underlying signaling pathway.

3.4 DAG mediates activation of VRAC by PKD rather than PKC

I could show that the DAG analog PMA activates VRACs isosmotically. PMA is a known PKC activator [155, 156], so I next aimed at manipulating PKCs to see the effect on VRAC activity. The PKC family consists of several members and their physiological activation depends on the specific isozyme, with cofactors as Ca^{2+} for the conventional subclass of PKCs, having in common the activation and localization by plasma membranous DAG. I used the inhibitor Gö6983 for its ability to affect a broad spectrum of the PKC family, according to the suppliers, excluding only the isoform PKCμ (better known as PKD).

Addition of Gö6983 to HeLa cells expressing A-CFP/E-YFP led to an unexpected increase of cFRET in isotonic and hypotonic buffers (Figure 3.16A). Since a decrease of cFRET reflects channel opening, increasing cFRET likely resembles a deactivation of already open VRACs. The steady increase even under isotonic conditions might be caused by the increased basal activity seen for fluorescently labeled LRRC8 subunits in *Xenopus* oocytes [80]. Photophysical artifacts created by Gö6983 leading to the observed increase of cFRET can be excluded due to it not influencing cFRET of CFP-18AA-YFP (Figure 3.16B). Furthermore, I observed the same ominous increase for staurosporine and tamoxifen, drugs known to inhibit PKCs as well (data not shown). To further investigate the effect of inhibiting PKCs on current and

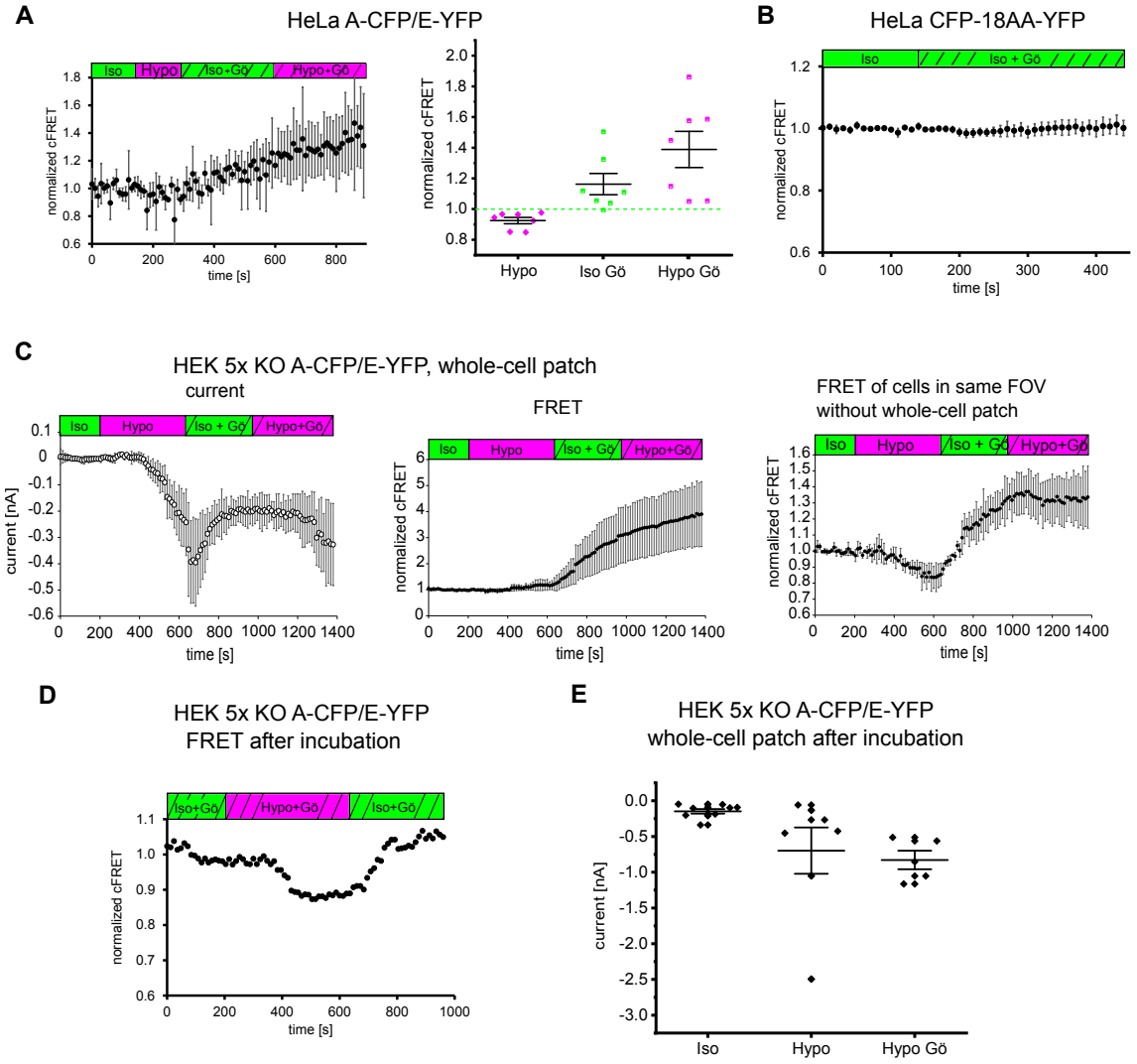

Figure 3.16: PKC signaling is dispensable for FP labeled VRAC activation by hypotonicity

(**A**) Time traces (left) and quantification (right) of HeLa cells expressing A-CFP/E-YFP, treated with 1 μM Gö6983 and buffer switching to hypotonicity (7 cells). Left: data represents mean ± s.d. Right: data represents mean of individual cells (squares) and mean ± s.e.m (**B**) Time trace of HeLa cells expressing CFP-18AA-YFP treated with 1 μM Gö6983. Data represent mean ± s.d. (**C**) Simultaneous measurements of whole-cell currents (left) and normalized cFRET values (middle) during a buffer exchange experiment with A-CFP/E-YFP-expressing HEK 5x KO cells. Isotonic and hypotonic buffers without and with 1 μM Gö6983, as indicated above. Right: normalized cFRET values of an unclamped HEK 5xKO cell expressing A-CFP/E-YFP in the same FOV. Data represent mean of 3 cells ± s.d. (**D**) Normalized cFRET of a representative HEK 5xKO cell expressing A-CFP/E-YFP pre-incubated with 1 μM Gö6983 for 20 minutes and then challenged with hypotonicity. (**E**) Whole-cell currents at -80 mV of HEK 5xKO cells expressing A-CFP/E-YFP. Whole-cell configuration was established after at least 15 minutes incubation in isotonic (n=9), hypotonic (n=7), and hypotonic buffer containing 1 μM Gö6983 (n=5). Data represent individual cells (diamonds) and mean ± s.e.m.

FRET of VRACs we performed patch-clamp fluorometry. Surprisingly, and seemingly contradicting the FRET experiments, channels in Gö6983 treated cells still opened upon hypotonic treatment and were seemingly impaired in closing again in isotonic buffer (Figure 3.16C). The FRET signal of patched cells again increased after inhibitor addition, but to unexplainable high values. This effect was again caused by the whole-cell configuration, as unpatched cells in the same field of view showed the same FRET response as HeLa cells expressing A-CFP/E-YFP. When switching from Gö6983 containing isotonic medium to Gö6983 containing hypotonic medium there was a small decrease of cFRET detectable in unpatched cells (Figure 3.16C right panel). Differences in the perfusion system of the setups used for sole microscopy or patch-clamp fluorometry experiments led to longer incubation times for the latter. I suspected this time difference to be responsible for the observed decrease in HEK 5x KO cells compared to HeLa cells. To test this we incubated HEK 5x KO cells expressing A-CFP/E-YFP with Gö6983 for 20 minutes before application of hypotonic buffer and indeed those cells showed the expected decrease of cFRET upon hypotonic treatment, concludingly the signaling is unaffected by PKC inhibition (Figure 3.16D). The influence of whole-cell configuration seen for PMA and Gö6983 led to us testing the PKC inhibitor with the whole-cell after incubation method again. Detected currents after membrane breakthrough were unaffected by Gö6983 compared to hypotonic pre-incubation (Figure 3.16E).

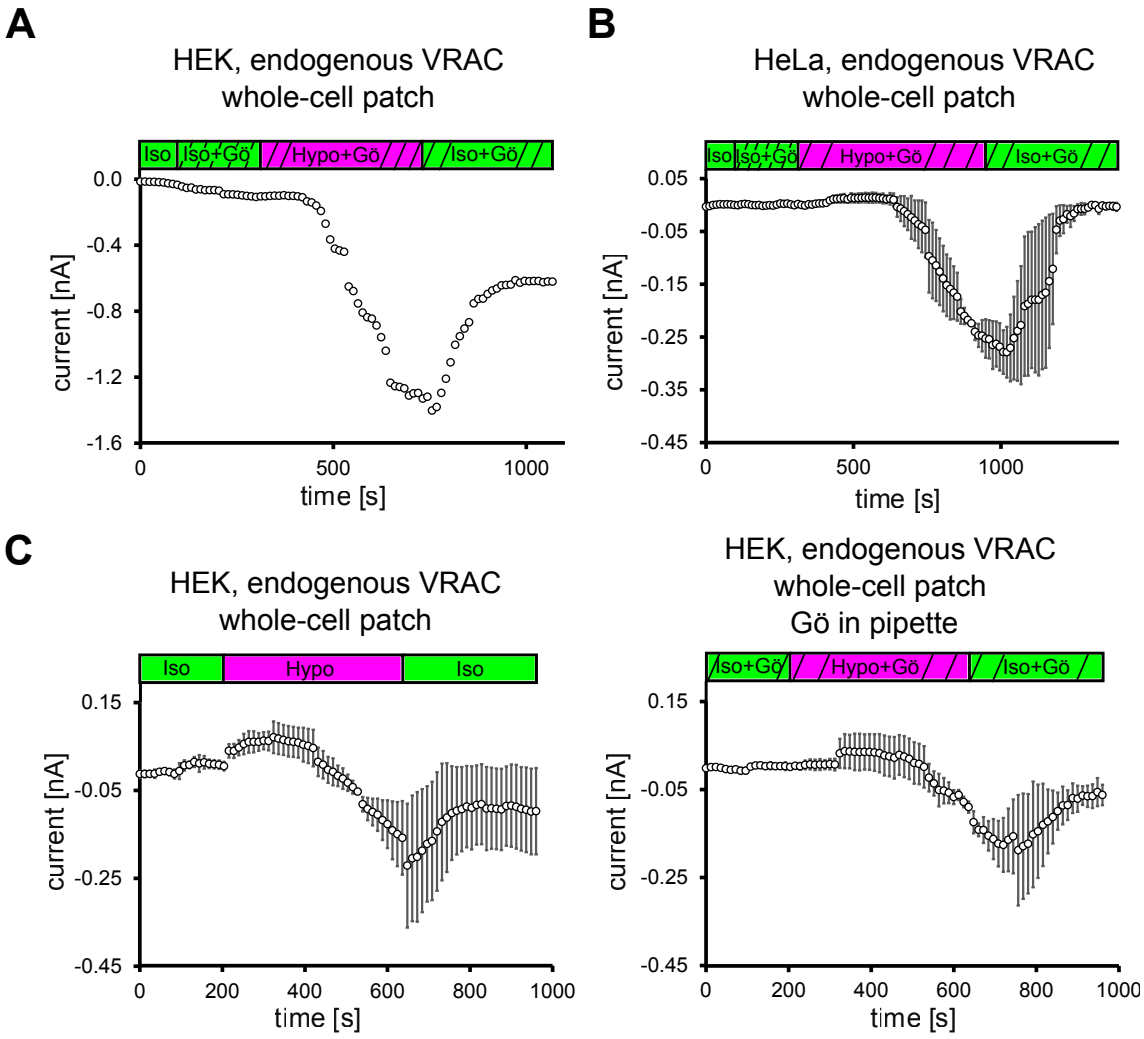

Figure 3.17: PKC signalling is dispensable for endogenous VRACs in HEK293 and HeLa cells
Whole-cell currents of endogenous VRACs measured at -80 mV (**A,B,C**) (**A**) Representative time trace of a HEK293 cell challenged with isotonic and hypotonic buffer containing 1 μM Gö6983.(**B**) Time trace of HeLa cells challenged with isotonic and hypotonic buffer containing 1 μM Gö6983 (n=2). Data represents mean ± s.d. (**C**) Time traces of HEK293 cells either untreated (left;n=2) or treated with 1 μM Gö6983 (right;n=2) challenged with hypotonic buffer. Pipette solution of 1 μM Gö6983 treated cells contained as well 1 μM Gö6983. Data represents mean ± s.d.

Since the increasing effect of Gö6983 on the FRET of fluorescently tagged VRACs at short inbuation times seems to be unrelated to simultaneously recorded currents, we validated the influence of Gö6983 with untagged endogenous VRACs as well. Currents of untranfected HEK293 and HeLa cells could be measured by whole-cell voltage clamp upon hypotonicity in the presence of Gö6983 (Figure 3.17A,B). To rule out time-dependent inhibition of PKCs by the drug, we compared untreated and HEK293 cells pre-incubated with Gö6983 for 20 minutes. Current traces upon hypotonicity are indistinguishable between those cells (Figure 3.17C). Taken together the broad spectrum PKC inhibitor Gö6983 did not prevent the activation of VRACs

formed by A-CFP/E-YFP or untagged endogenous ones upon hypotonicity, ruling out a general necessity of PKC signaling for VRAC activation in the used model.

According to the shown data, PMA is activating VRAC via a different protein family. Even though PMA is sold and used as a PKC activator, it is recruiting and potentially activating every protein to the plasma membrane that contains a C1 domain (discussed in [157], note the title: "Eyes wide shut: protein kinase C isozymes are not the only receptors for the phorbol ester tumor promoters."). This domain is an "unzipped" beta sheet that is coordinating the binding of C1-containing proteins with DAG or its phorbol ester analogs [158]. Besides being present in conventional and novel PKC family members, C1 domains can be found in the protein kinase D family (PKD). There are several members of the PKD family, namely PKD1,2 and 3. Interestingly PKD1 was initially defined as a member of the PKC family and named PKCμ, already showing that this class of protein kinases was confused for PKCs before. I want to emphasize that "PKCμ" is the PKC isoform excluded by vendors to be targeted by Gö6983. So, even though there is some pharmacological cross-talk between PKDs and PKCs, the observed effects of Gö6983 are most likely only due to PKC inhibition. Since PKDs are recruited to the plasma membrane by PMA as well, we investigated the effect of the PKD inhibitor CRT 0066101 with patch-clamp fluorometry. After a 15 minutes pre-incubation with CRT 0066101 the current of HEK 5x KO cells expressing A-CFP/E-YFP was strongly reduced, and cFRET did not decrease upon hypotonicity (Figure 3.18A). Instead, a mild increase was observed. In contrast to the strong increase caused by Gö6983 and the hypotonicity induced decrease of cFRET after 20 minutes of incubation, in CRT 0066101 treated cells no cFRET decrease was observable after this incubation time. Again, we wanted to rule out possible artificial effects of the whole-cell configuration and compared cells with membrane breakthrough after incubation in hypotonic buffer with or without CRT 0066101. Indeed, we could detect reduced currents here as well (Figure 3.18B). The pharmacological evidence hints towards VRAC activation by hypotonic induced increase of DAG levels, which then recruits PKD.

3.5 Membrane localized VRACs are activated by DAG but not ionic strength

With the new optical FRET sensor, I was able to show that ionic strength does not affect VRACs on endomembranes. Furthermore, VRACs are affected by pharmacological manipulation of DAG and PKD signaling. To further validate that ionic strength is not the activating factor in living cells and further strengthen the role of

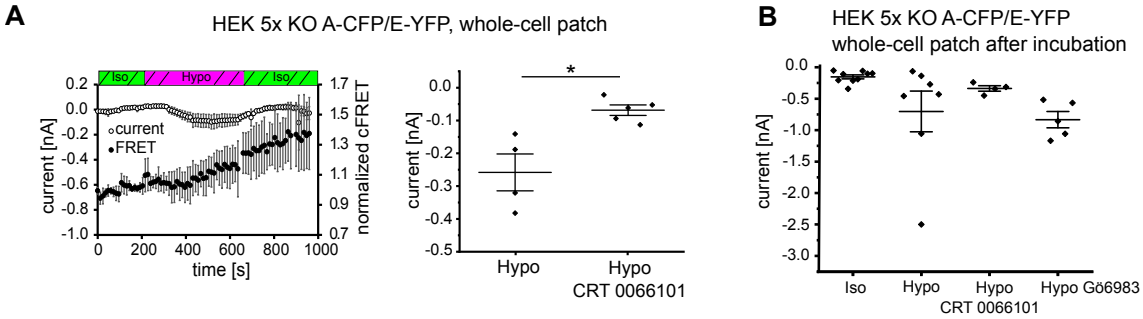

Figure 3.18: Inhibition of PKDs impairs VRAC currents and cFRET change upon hypotonicity
Left: simultaneous measurements of whole-cell current at -80 mV (open circles) and normalized cFRET values (solid circles) during buffer exchange experiment with A-CFP/E-YFP-expressing HEK 5xKO cells, after 15 min pre-incubation with 5 μM CRT 0066101 in the presence of CRT 0066101. Data represent the mean of 5 cells ± s.d. Right: average currents of the last five time points in hypotonicity with (data from left panel) and without (data from Figure 3.7B) CRT 0066101; data represent individual cells (diamonds) and mean ± s.e.m. (**B**) Whole-cell currents of HEK 5xKO cells expressing A-CFP/E-YFP clamped at -80 mV after pre-incubation with indicated buffers: isotonic buffer (n = 9), hypotonic buffer (n = 7), hypotonic buffer with 5 μM CRT 0066101 (n = 4) or 1 μM Gö6983 (n = 5). Data represent individual cells (diamonds) and mean ± s.e.m. Statistics: *p<0.05; Student's t-test.

DAG, I aimed at manipulating the DAG recycling after activation (scheme of underlying hypothesis shown in Figure 3.19). Hypotonicity leads via an unknown mechanism to an increase in DAG levels at the plasma membrane by activating PLCs. There, DAG is recruiting and activating PKDs which again lead to the activation of VRACs. Changing the medium back to isotonic conditions creates the need for cells to reduce the concentration of the activating DAG in the plasma membrane. This reduction is achieved by phosphorylation of DAG by DAGK, generating phosphatic acid (PA) which cannot bind to C1-domains, ending the recruiting of PKDs.

To show that this pathway indeed controls VRAC activity in living cells, I used the DAGK inhibitor dioctanoylglycol (DOG). HEK 5x KO cells expressing A-CFP/E-YFP showed unaltered currents due to hypotonicity when treated with DOG compared to untreated cells (not shown), but did not recover to baseline values as did control cells (Figure 3.20B left panel). Endogenous VRACs of untransfected HEK293 cells could be kept open in isotonic conditions after activation in the same way (Figure 3.20B right panel). The cFRET of A-CFP/E-YFP expressing HeLa cells did, in accordance with electrophysiology, not recover after activation when incubated with DOG (Figure 3.20C left panel). With these experiments confirming again the importance of DAG signaling for VRAC activity, I next looked at the ionic strength of DOG treated HeLa cells with the RD-sensor. I could show that the ionic strength is unaltered by DOG (Figure 3.20C right panel). It needs to be noted that DOG, being a DAG analog as well, was shown to interact with the C1 twin domains

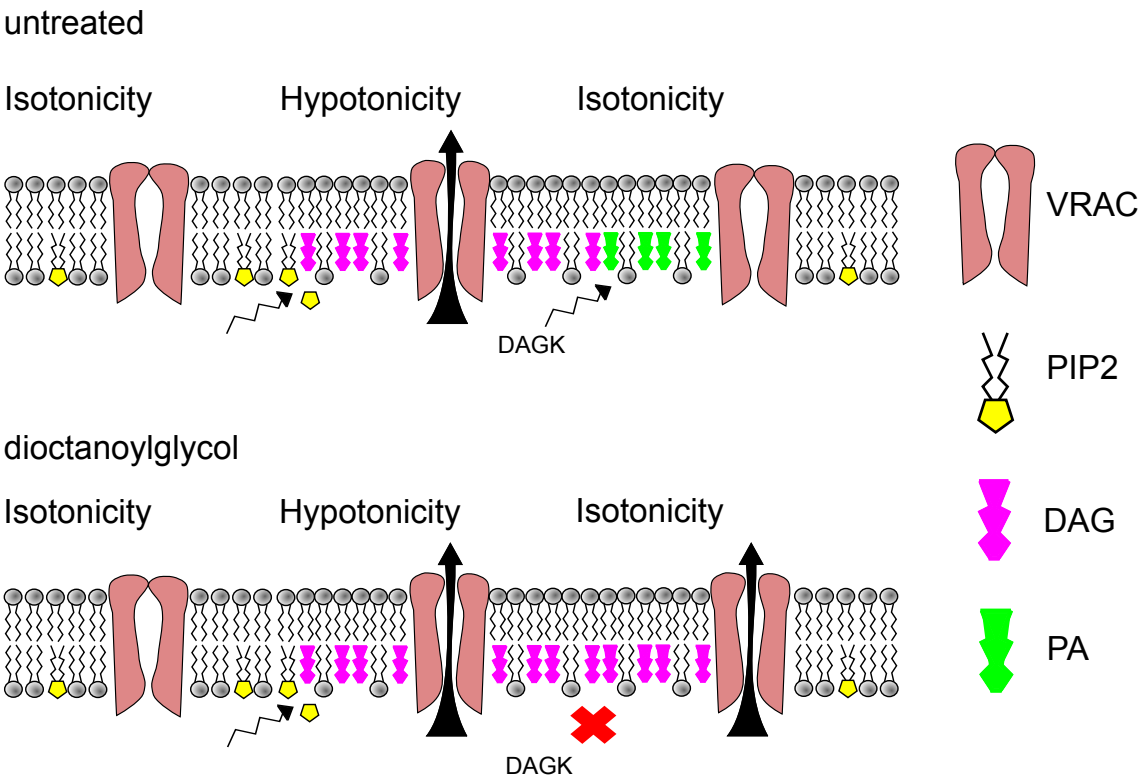

Figure 3.19: Scheme of the action of dioctanoylglycol
Scheme of persisting VRAC activity with inhibited DAGK by DOG. Top: in an untreated cell, hypotonicity leads to DAG production that activates VRAC. Returning to isotonic conditions stimulates DAGK to phosphorylate DAG to PA, ending the activating stimulus for VRAC. Bottom: in DOG treated cells, DAGK is inhibited, so that after production of DAG by hypotonicity it is not phosphorylated to PA, leading to a persisting activation stimulus in isotonic conditions.

of PKDs [159]. The affinities of recombinant C1 twin domains towards DOG were dependent on the PKD isozyme they were derived from. The domain of PKD3 had the highest affinity compared to those of PKD1 (4-fold) or PKD2(8-fold). Application of DOG in isotonic buffer led only to a mild, not significant decrease of cFRET (Figure 3.20A). If DOG recruited involved PKD isoforms in the used conditions, I would expect it to cause the same reduction of cFRET as did PMA. The effect of DOG to render activated VRACs still open in isotonic conditions is therefore likely due to it inhibiting DAGK and not recruiting e.g. PKD3. Concludingly DOG treatment leads to activated VRACs at the plasma membrane under isotonic conditions regardless of ionic strength changes evoked by osmolarity. The activation of VRACs in living cells is, therefore, independent of ionic strength and is rather controlled by DAG signaling.

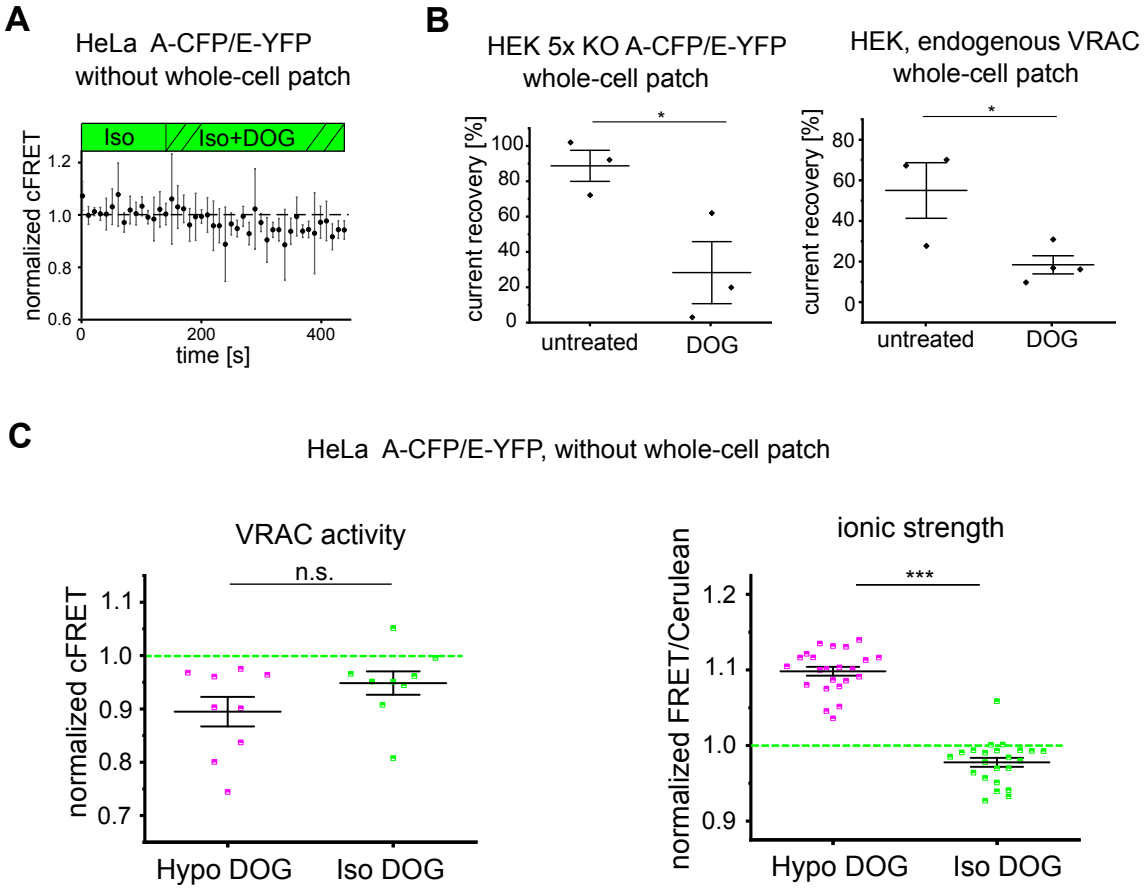

Figure 3.20: DAG regulates VRAC activity rather than ionic strength
(**A**) Time traces of HeLa cells expressing A-CFP/E-YFP treated with DOG in isotonic buffer. Data represent mean ± s.e.m. (**B**) Recovery of whole-cell currents in HEK 5x KO cells expressing A-CFP/E-YFP (left) and wild-type HEK293 (right) at -80 mV to basal levels after switching from extracellular hypotonicity to isotonicity in the absence or presence of the DAG kinase inhibitor dioctanoylglycol (100 μM DOG). In HEK 5x KO, n = 3 for untreated (from measurements in Figure 3.7B) and n = 3 for DOG-treated; in wild-type HEK293, n = 3 for untreated and n = 4 for DOG-treated. Data represent individual cells (diamonds) and mean ± s.e.m. (**C**) cFRET was measured for HeLa cells expressing either VRACs containing A-CFP/E-YFP (left, n = 7 dishes with 9 cells) or the RD sensor for ionic strength (right, n = 6, 23 cells) consecutively in isotonic buffer, hypotonic buffer supplemented with 100 μM DOG and isotonic buffer with DOG. Data represent average cFRET of the last five time points per condition of individual cells and mean ± s.e.m. Statistics: *p<0.05; ***p<0.0005; n.s., not significant, Student's t-test.)

4 Discussion

4.1 FRET as an optical sensor for VRAC activity in living cells

In this thesis, I managed to establish LRRC8 subunits fluorescently tagged at their C-termini as a FRET sensor for VRAC activity. Decades of research on ion and osmolyte transport by VRACs created a data landscape as diverse as it is contradictory and confusing. This situation was mostly caused by the missing identification of the protein class forming VRACs, so researchers relied mostly on pharmacological and biophysical characteristics to discriminate effects of VRACs from other channels. Over the last years more and more of the supposed specific inhibitors used for these pharmacological identifications were shown to affect several targets, not seldom other channels [52, 112, 160]. The diverse nature of possible activation mechanisms and functions of VRACs became explainable by the identification of the LRRC8 protein family as the subunits forming VRACs. Different stoichiometries of these subunits lead to channels with differing biophysical characteristics, for example, inactivation kinetics and conducting preferences, and even different signaling pathways leading to their activation [30, 43, 117]. The unawareness of the fact that there is probably not the one VRAC but rather different VRACs depending on subunit composition and unspecificity of used drugs renders the conclusions of existing data at least questionable. Whole-cell voltage-clamp experiments have been the gold standard for research on VRACs, with an opening of the channel being detectable as current produced by the flow of charged species. For the subunit dependence, electrophysiological experiments are either cumbersome in preparation, requiring knock-out cell lines to study a specific subunit composition or suffer from uncertainty which species is responsible for the seen effects. All this initially led to the idea of a new method that overcomes these drawbacks of the established ones. Monitoring the FRET between subunits with CFP and YFP tags at their C-termini is a promising new approach.

I could show, that fluorescent proteins fused to the C-termini of LRRC8 proteins are in FRET distance by acceptor photobleaching. Intracomplex-FRET could be reliably detected using sensitized emission FRET (FRET) microscopy. Further-

more, activation of VRACs by either hypotonicity or the DAG analog PMA led to a significant change of cFRET. Showing a high variability in absolute cFRET values, the changes normalized to basal FRET levels were similar between cells with varying cFRET. During the preparation of this thesis, four groups published independently of each other cryo-EM structures of LRRC8A VRAC homomers [69–72]. Even though there is some debate concerning the overall channel symmetry (discussed in [161]), all structures have in common that the leucine-rich repeat domains (LRRDs) are facing towards the pore axis with their C-termini. The occurrence of FRET between fluorophores at that position is thereby in accordance with the proposed position of the LRRDs by cryo-EM. FRET measurements in biological systems only generate apparent FRET values, whereas the approximation of the distance between these fluorophores necessitates tedious calibrations and need to fulfill certain criteria as random orientation and homogeneous distance between the fluorophores [162]. Non-interacting donors and acceptors are problematic as well, with even more intense work needed to estimate the fractions of each carefully [163]. The complex nature of VRAC's subunit stoichiometry renders it therefore impossible to estimate the mean distance between the fluorophores at the C-termini of the subunits in the used system. I can neither predict which fluorophores in a hexamer could interact, creating a situation where the position of a given subunit in the hexamer and their neighbors influences potential FRET to occur, nor is it possible to exactly determine non-interacting LRRC8A subunits, since they can form homomers with no FRET partner at all. The varying absolute cFRET values determined for A-CFP/E-YFP channels underline this mentioned complexity. Accordingly, I focused on the relative FRET changes of VRACs formed by CFP/YFP fused LRRC8 proteins and how to exploit that, rather than concentrating on analysis of absolute cFRET values.

Of the four groups having solved the cryo-EM structure of VRAC, two groups discussed a subpopulation of particles with an overall expanded channel architecture, hypothesizing this to be an intermediate state to open channels [70, 72]. The LRRDs are further apart in this subpopulation as well, increasing the distance between their C-termini. It is tempting to hypothesize that our data is proving exactly that, with cFRET of channels with activating stimuli applied decreasing, which could mean that the distance between CFP and YFP is increased, whereas closing of channels brings them back to their original distance and thereby to the same cFRET as before. However, the FRET between fluorophores does not only rely on the distance but as well on the orientation of their dipole moments. It is, therefore, possible that the decreased cFRET I detected upon activation is not due to a loosening of the overall architecture of the channel but rather an angular change of the flexible LRRDs. As for the absolute cFRET values, the question if changes occur due to distance or angle may be adressed in interesting future studies but are not of importance for

the here discussed general use as an activity sensor.

I initially detected the decrease of cFRET upon channel activation by lowering the extracellular osmolarity. I want to discuss why this indeed reflects channel gating. A major concern was that the volume change of the cells upon hypotonicity leads to a decrease of cFRET by reducing membrane crowding. APB experiments of cells expressing A-CFP homomers and the unrelated plasma membrane protein CD4-YFP hinted at no occurrence of crowding effects at expression levels used in this thesis, but do not completely rule it out. Hypotonic treatment of cells expressing the intra-complex FRET construct GluA2-6Y-10C did not lead to a decrease of cFRET, even though these proteins form channels at the plasma membrane as well and are therefore a suitable control that variations of the plasma membrane surface caused by volume changes do not influence the FRET between proteins in the same complex. Furthermore, I would expect a similar effect for cell shrinkage, if there was a volume impact on FRET of LRRC8 subunits, but hypertonicity did not increase cFRET. Another striking finding is the co-occurrence of gradual cFRET decrease with current increase determined by patch-clamp fluorometry supporting that cFRET changes reflect channel gating.

Application of hypotonic medium leads to a change of several variables in the cell, for example concentration of ions and even pH fluctuations [164]. In this thesis I used YFP as the acceptor of the FRET pair, even though it is known for its sensitivity towards pH and halides [165]. Since VRAC conducts Cl^-, this flux might quench YFP residing at the LRRDs. For patch-clamp fluorometry I fused the brighter and stable mutants mVenus and mCerluean3 to LRRC8A and E. Even though mVenus is still sensitive to the named factors, it is affected to a lesser extent than native YFP [166]. If the changes caused by hypoosmolarity would be responsible for the cFRET decrease by effecting YFP, this should manifest itself in a smaller effect for mVenus tagged constructs, but the cFRET decrease is indistinguishable between YFP or mVenus paired VRACs. Lastly, I could activate VRACs isosmotically by manipulating cellular signaling molecules in two different ways. The first is the activation of VRACs under isotonic conditions by application of PMA, shown by cFRET decrease and by patch-clamp experiments (discussed in section 4.5) and the second the persisting activity of activated VRACs in isotonic medium with inhibited recycling of DAG by DOG (discussed in section 4.3). Those experiments show the sensitivity of the FRET sensor towards VRAC activity and not to biophysical alterations of the fluorophores that could lead to false-positive results.

Even though the expression of different subunits varied highly between individual cells, there was a clear trend towards a higher expression of LRRC8A compared to LRRC8E. For aFRET being a good approximation to absolute cFRET if the donor is in excess with no free acceptor, I chose LRRC8E to be tagged with the acceptor

YFP for most experiments. In this case, the normalized decrease of cFRET between cells was independent of the expression ratio of A-CFP/E-YFP. This enables an unbiased choice of cells to measure since there is no need to sort for specific subunit ratios. In addition this shows a major advantage of the FRET sensor over conventional methods: the specificity for subunits that are detected in potential heterogeneous populations. For both fluorophore combinations of A/E complexes (A-CFP/E-YFP and A-YFP/E-CFP), higher intensities in the channel detecting LRRC8A were regularly observed. LRRC8A was, therefore, abundant at higher levels than LRRC8E in the used conditions. Even though A-CFP is expressed at a higher rate and will thereby form A-CFP homomers with no interacting acceptor, they will not influence the cFRET of heteromeric channels and can be neglected. The same is true for non-fluorescent endogenous channel populations. With the FRET sensor, one can only detect channels that contain both A-CFP and E-YFP, or any other tagged LRRC8 protein, and do not suffer from the influence of their relative ratios to each other. Expecting no feedback between different subunit stoichiometries, fluorescently labeled LRRC8 proteins can be readily expressed along with endogenous species of the model system in use and still report only activity of the specifically labeled VRACs.

Among the confusing results around VRACs is the finding that their overexpression does not lead to currents increased above wild type levels [30]. In a seeming contradiction to that, I found that the relative decrease of cFRET upon hypotonicity is not dependent on the absolute expression levels of A-CFP/E-YFP. Therefore it seems that always the same percentage of channels open irrespective of how many were expressed. In all experiments performed in this thesis, I found A-CFP to be expressed at higher levels than E-YFP, even though they were cloned in the same plasmid and are thereby under the control of the same promoter. It was shown that overexpression of LRRC8A reduces currents of endogenous VRACs [29, 30]. Furthermore, the ratio of expressed LRRC8A to another subunit influences current amplitude as well, with more A subunits leading to decreased currents and less to increased ones [28]. Experiments concluding that more channels do not lead to increased currents didn't check for the ratio of expressed subunits. Therefore, more VRAC heteromers may lead to increased currents, but there were only small numbers of them in those experiments.

Another explanation could be that it is not possible to express VRACs over a certain limit. The beforehand discussed variations of the expression ratio of A-CFP/E-YFP are mostly due to varying A-CFP levels. Whereas 94 % of analyzed cells had E-YFP intensities evenly distributed from 1 to 450 a.u., the same percentage of cells were distributed between 1 and 1400 a.u. for A-CFP. There seems to be only a small window for E-YFP expression, hinting towards the regulation of their

absolute levels. Cells might tightly regulate VRAC numbers post-transcriptionally, what could explain that LRRC8 B and D are hard to express in the same cells expressing, for example, A and E. Another possibility is that cells simply die if too many functional VRACs reach the plasma membrane, leaving those cells for observation that have a low expression by chance. This theory is supported by high cell death of HeLa cells with released A-CFP-FM2/E-YFP complexes that did not occur for solely A-CFP-FM2 expressing cells. In this conditions, high numbers of A-CFP/E-YFP channels could reach the plasma membrane that would have either been suppressed by cellular control mechanisms or would have gone unnoticed by me due to the cells dying when expressed without trapping the channels in the ER. More evidence is needed to conclude what is the reason for the not increasing current for seemingly more expressed VRACs. I can, however, see for the FRET sensor system that in the small range of possible LRRC8E levels the percentage of opening upon hypotonicity is not related to the overall expression. This would lead to increased currents since more channels are open at the same time.

The FRET sensor is for the discussed reasons a reliable tool for VRAC activity. Nevertheless, as for any method, experiments with fluorescently tagged LRRC8 proteins need the correct controls to account for possible false-negative or false-positive results. A good example was my attempt to reproduce experiments that investigate the effect of oxidation on different VRAC subunits [117]. It was shown that currents of A/E complexes could be strongly potentiated by application of the oxidative reagent chloramine-T. Pilot experiments with A-CFP/E-YFP expressing cells seemed to confirm this by showing strongly reduced cFRET upon chloramine-T addition (data not shown). Control experiments with the FRET constructs CFP-18AA-YFP and GluA2-6Y-10C showed the same effect, due to YFP being sensitive to oxidation and therefore affirm results of A-CFP/E-YFP complexes to be false-positive. By carefully ruling out FRET changes due to photophysical alterations, the FRET sensor can show in a sensitive and subunit-specific way the activity of VRACs in living cells.

4.2 Possible modulation but not activation of VRAC by ionic strength

The understanding of cellular mechanisms for volume sensing was once described as “frustratingly incomplete” [22]. It is still under debate whether VRACs themselves can sense volume changes by the accompanying intrinsic property alterations or if there is a signaling cascade leading to activation of VRACs. Some researchers of the VRAC field argue that ionic strength can directly activate VRACs, rendering them

the sensor for volume increase by hypotonicity (reviewed in [167]). In this model the volume increase is not sensed since it is an extensive thermodynamic parameter, but rather the ionic strength as an intensive one. Especially experiments showing that single VRACs in lipid droplet bilayer systems can be activated by isosmotically lowered ionic strength hinted towards this model. On the other hand, there are arguments against this theory, including activation of VRACs by injecting isosmotic buffers into cells leading them to swell with unchanged ionic strength (reviewed in [9]). In this theory, ionic strength is a modulating factor for VRAC activity, controlling its volume set point and which osmolytes pass through.

With the new FRET sensor, I could provide evidence, that ionic strength is not directly activating VRACs in living cells. This was shown in two different ways. Firstly, I showed that VRACs could not be activated by reduced ionic strength when they are trapped intracellularly. Since the ionic strength is reduced over the whole cell volume, as shown by the RD-sensor, VRACs would be affected by that reduction regardless of their localization. Strikingly, APB experiments hint towards a completed channel formation in the ER, a general prerequisite for the assumption that VRACs can be activated in the ER or Golgi. Neither did cFRET of A-CFP/E-YFP complexes change upon hypotonicity when they were trapped in the ER by BFA, nor in the ER or Golgi when using the reverse dimerization system. Both methods together rule out possible negative influences of the other one, strengthening the conclusion that ionic strength does not open VRACs directly. Especially the reverse dimerization system is a very elegant approach since it directly proves that complexes of A-CFP-FM2/E-YFP can only be activated when they are delivered to the plasma membrane. I hypothesize that this is due to mandatory interaction partners that are localized at the plasma membrane. It could be argued that especially in the ER the protein maturation might not be finished yet, with for example correct glycosylation missing or still ongoing glycosylation in the Golgi. Experiments with a non-glycosylatable mutant of LRRC8A showed that this subunit is still forming activatable channels at the plasma membrane together with LRRC8E. The latter subunit contains two predicted glycosylation sites as well, one in every extracellular loop. Eventhough glycosylation of LRRC8A is not needed for activatable channels, my data does not rule out a genral requirement for correct trimming of glycosylation of at least a subset of subunits within a complex, since noGlyc-CFP/E-YFP complexes could still be correctly glycosylated on LRRC8E. For further validating that the missing trimming of glycosylations in the Golgi is not the cause for complexes trapped there are not activatable, studies with a non-glycosylatble mutant of LRRC8E co-expresswed with the non-glycosylatable LRRC8A mutant are needed. A strong argument against the interpretation that intracellular trapped channels are not activatable by ionic strength is that there is another unknown factor in the mat-

uration process that is only taking place directly before or at the plasma membrane, rendering trapped VRACs insensitive to activating stimuli. Another argument is the different lipid composition of endomembranes compared to the plasma membrane, implying a specific composition that is needed for proper channel function (reviewed in [168]). The reverse dimerization system opens up interesting possibilities for future experiments, with potential interaction candidates that are believed to activate VRACs at the plasma membrane being verifiable by their ability to activate VRACs intracellularly as well.

The second line of evidence for ionic strength not directly activating VRACs is the persisting activity of already activated channels with inhibited DAG recycling in isotonic buffer. With the RD-sensor, I could show that the ionic strength reduction and recovery by osmolarity changes are unaffected by the DAGK inhibitor DOG. Whereas the ionic strength decreases upon hypotonicity and increases again in isotonic buffer, VRAC stays active after the activation. This clearly shows that the activity is not coupled to the variations in ionic strength in a cellular context.

A seemingly striking argument against the theory that ionic strength does not activate VRACs directly but that they rather need a plasma membrane related co-factor is the fact that they were activatable in lipid bilayers and reconstituted liposomes [70, 72, 79]. I was also reported that VRAC currents could be evoked in not swollen cells with reduced intracellular ionic strength [115, 169]. All of the mentioned experiments have in common that there was an immense change of ionic strength necessary to evoke currents (reviewed in [9]). So even though it is possible to open VRACs without a cellular signaling context, the conditions needed for that are not comparable to physiological ones. The fact that VRACs in artificial lipid layers without co-factors can produce currents when the ionic strength is highly reduced could be explained in several ways. The solved structures of LRRC8A homomers led to the hypothesis that there might be interactions between charged amino acids in the LRRDs of the subunits within one complex and that this interaction is transmitting the ionic strength of the cytosol to the rest of the channel [69–71]. The overall stability of proteins is highly affected by the properties of the surrounding medium, for example, the ion content [170]. A drastic change of the ionic strength might impair the natural flexibility of the LRRDs by supporting the named interactions between the LRRDs of neighboring subunits, leading to a steric conformation that reflects the open state under natural conditions. This steric rearrangement could potentially be similar to that initiated by physiological interaction partners or modifications of LRRC8 proteins *in vivo* upon activation, which concludingly might involve fixation of the LRRDs in a defined position.

4.3 Combining old and new- Revisiting signaling of VRAC activation with the FRET sensor

A plethora of different signaling pathways and molecules have been proposed to be involved in VRAC activation over the last decades (reviewed in [9, 36, 82]). With the new FRET sensor, I revisited old hypotheses and explored from there the underlying signaling of VRAC for A/E complexes in HeLa and HEK293 cells. I could show that VRAC is activated by plasma membranous DAG, which leads to PKD activation and ultimately to the opening of VRACs. This can be brought into accordance with existing old data, forming a promising hypothesis for VRAC activation.

Apart from other suspected roles for VRAC in vivo, it does play a role in RVD [29, 30]. This process takes place when cells swell due to an osmotic pressure-driven water influx, caused by either an extracellular reduction of osmolarity or an intracellular increase. It is unknown how cells determine their volume to react accordingly, but influences of macromolecular crowding, the concentration of ions and mechanochemical alterations of the plasma membrane are involved in different ways (excessively reviewed in [8]). Which of those lead to activation of VRAC though is a matter of debate until today. I could show in this work that VRACs can be activated isosmotically by the DAG analog PMA. Isosmotic activation was observed for heteromers formed by A-CFP/E-YFP, but as well for homomers of A-CFP/A-YFP. The role of DAG for VRAC activation is further strengthened by the observation that manipulation of DAGK affected VRAC under isotonic conditions when they were activated by hypotonicity before. Especially the activation of A-CFP/A-YFP homomers hints towards a general role of DAG, since at least the A subunit of every heteromeric complex would probably be affected as well. The DAG dependent activation mechanism proposed in this thesis can explain old data sets and is confirmed by others. Production of DAG in living cells is usually accomplished by the phosphoinositide pathway. Here, the phospholipid phosphatidylinositol 4,5-bisphosphate (PIP2) is hydrolyzed by activated phospholipase C (PLC) to inositol 1,4,5-triphosphate (IP3) and diacylglycerol (DAG). Both products of the PLC reaction then further act as second messengers. It was shown that membrane stretch, which is a result of cell swelling, leads to PLC activation via an unknown mechanism [171–174]. VRACs are known to be insensitive to membrane stretch, so they are not the volume sensitive entity in respect of membrane stretch. Nevertheless, in ventricular cells, it could be shown as well that membrane stretch leads to a Cl^- current with VRAC characteristics [175]. Inhibition of PLC by a specific inhibitor, on the other hand, led to reduced currents in hypotonic buffer [140]. Concordantly to increased PLC activity, stretch and hypotonicity were shown to lead to increased cellular IP3 levels, eventhough the DAG levels were not measured directly their in-

crease by the shown PLC activity appears logic [176]. The role of PLC is, therefore, a verified part of VRAC activation by hypotonicity and it is safe to assume that the DAG, which I show to be the next downstream partner in VRAC activation, is produced by this enzyme class. DAG levels are in this scheme coupled to cell swelling by indirect activation of PLC by membrane stretch.

Many experimental findings that suggest a regulative influence of compounds or messenger molecules can be linked to this part of the activation mechanism of VRACs. One example is the activation of VRACs by reactive oxygen species [44, 117, 177, 178]. ROS were shown to activate PLCs in different tissues and cells [179–182]. Further on it was shown that hypotonicity leads to elevated ROS production in various cell types [183–185]. A fascinating finding was that PLC preferentially hydrolyzes oxidized lipids [181]. Consequently, existing data points towards the production of ROS by hypotonicity, which then activate PLCs to hydrolyze finally PIP2 and leading to the activation of VRACs. So how can one explain the seemingly contradictory finding that A/C and A/D heteromers are inhibited by oxidation, whereas A/E heteromers are potentiated [117]? Two possible scenarios can be concluded from my data and the existing ones. Firstly, A/E and A/A complexes are controlled by the here proposed signaling pathway of DAG activating PKD but A/C and A/D are activated differently. Since I did not test the activation of, e.g., A/D complexes by PMA, I cannot rule out that a different pathway controls them. So, the ROS supported action of PLC by hypotonicity would only lead to VRACs opening that contain A and E subunits. It is necessary to emphasize that it is not known how channels composed of more than two different subunits are regulated by oxidation, even though they are believed to be physiologically relevant [35, 80]. Secondly, and which I believe to be more likely, are all different stoichiometries of VRAC activatable by PLC mediated DAG activation of PKD. The elegant sorting mechanism of cells to decide which VRAC population, dependent on subunit stoichiometry, is activated would then be a feedback of the upstream activation stimuli. ROS, for example, could be produced by cells due to hypotonicity and would, if the same stimulus activates PLC, theoretically lead to activation of all VRACs, irrespective of their subunit composition. The initially upstream signaling event of ROS would now influence the downstream decision of which channel composition is needed, by impairing currents of A/C and A/D channels [117], leaving A/E and potentially A/B heteromers to be opened. In both cases, it would be mysterious, how currents can be measured of either A/D or A/C expressing cells deficient in all five LRRC8 genes when they are challenged with hypotonic medium [30]. Since hypotonicity leads to increased ROS levels, one could have expected low or no currents due to the inhibiting effect of ROS on A/D and A/C channels. Only A/D rescue experiments led to decreased maximum currents compared to wildtype, whereas A/C

currents were unaltered [30]. As discussed in section 4.6, more work in consistent cell models are needed to fully understand the subunit dependence of the activation mechanism in this and various other respects.

Apart from the PLC family, the protein class of G-proteins can be brought into accordance with DAG mediated VRAC activation. Several groups found evidence for an involvement of this group of proteins for VRAC activation [131, 186–188]. The group of G-proteins contains the heterotrimeric and the small monomeric G-protein families. These are divided into different subclasses, with for example a plethora of different α subunits for heterotrimeric G-proteins (reviewed in [189]). As diverse as the nature of G-proteins is the data concerning their involvement in VRAC activation. It is tempting to hypothesize a possible role of G-proteins for VRAC since for example G(q/11)-coupled receptors are believed to be sensors for mechanical membrane stretch und would therefore logically appeal as upstream activators of VRAC [190, 191]. Especially since they were shown to lead to PLC activation (reviewed in [192]). Another hint at a possible role for G-proteins in VRAC activation is that they were shown to be involved in organic osmolyte flux upon hypotonicity [193]. Since alone the PLC-β family comprises four isozymes that are differently regulated by the Gq family, that again comprises several members, the exact meshwork which isozyme acts when is beyond the scope of the discussion of this thesis. Physiological activation of PLC isozymes by G-proteins is likely to be even more complex, suggested by the fact that there is some evidence that not heterotrimeric G-proteins activate VRAC, but rather the small GTPase Rho, which again activates the PLC-ϵ subgroup [187, 188, 192]. Activation of VRAC was also reported by S1P [194]. S1P can activate a group of G-protein coupled receptors, the sphingosine-1-phosphate signaling-receptor (S1PR) family (reviewed in [195]). Of the S1PR family, the members S1PR2,3 and 4 were shown to activate PLCs, again converging at the here proposed signaling pathway. Nevertheless, Burow et al. [194] proposed S1PR1 to be responsible for VRAC mediated ATP release in RAW macrophages. This family member was shown to be coupled to the α subunit Gi that activates the tyrosine kinase Src, which again can activate PLC [196]. If the discrepancies which G-protein exactly activates VRAC between different publications is due to technical limitations of used methods or due to different cell models will hopefully be shown in future work. The FRET sensor presented here enables this new, subunit-specific measurement of VRAC activity and opens new possibilities to revisit older experiments concerning the role of G-proteins in VRAC activation (as discussed in section 4.6).

The activation of PLC by several means striving towards VRAC is thereby backed up with numerous pieces of evidence, supporting the here presented hypothesis that VRAC activation is carried by the second messenger DAG. Excitingly, I can report

here for the first time, to my knowledge, that in relation to VRAC activation DAG is not the upstream signal for PKC, but rather for the PKD family. Using the broad spectrum PKD inhibitor CRT 0066101, I could show that both the currents and the FRET change are impaired upon PKD inhibition. The PKD family consists of the three members PDK1, PKD2, and PKD3. When PKD1 was discovered, it was firstly confused for another PKC isoform since it shares a homologous C1 domain with them [197]. Shortly after their discovery, the catalytic domain of PKD1 was found to share a higher homology with the Ca^{2+}/calmodulin-dependent protein kinase (CAMK) group than with the PKA, PKG and PKC group and were therefore classified as an own kinase family [198] (reviewed in [199]). As for PKCs, the activation of PKD involves the binding towards plasma membranous DAG by their C1-domain. This binding is believed to unfold the catalytic domain, rendering two serine residues available for phosphorylation that is carried out by PKCs, that are recruited to the plasma membrane as well. The phosphorylation by PKCs is not a general necessity though, and the complete activation mechanism is not understood yet [200]. A new idea is that PKDs contain a self-dimerizing ubiquitin-like domain at their N-termini, leading to autophosphorylation of the catalytic domains by DAG bound and dimerized PKDs at the plasma membrane [201]. Being fully activated, PKDs than phosphorylate their substrates either on the plasma membrane or dissociate from DAG to further operate in the cytosol. I discussed already the interwoven findings towards stimuli detected upon hypotonicity and PLC activation, intriguingly for most of them exists data that they lead to PKD activation as well. A good example is activation of PKDs by ROS [202–204]. Especially the studies by Waldron et al. [202, 203] hint towards a potential meshwork of mechanisms around VRAC activation by DAG mediated PKD recruitment. They could show that treatment of different cells with H_2O_2 lead to autophosphorylation of essential serine residues and phosphorylation of the added PKD substrate syntide-2. This was mediated via PLC and Src, the latter kinase already mentioned in the potential activation of VRACs by S1P signaling and the S1PR1, which lead to PLC stimulation by Src through Gi. It was shown that ROS triggers S1PR1 sensitization and enhances S1P signaling in bovine aortic endothelial cells, pointing towards a potential mechanism of ROS mediated VRAC activation involving S1PR1 ultimately leading to PLC activation and PKD recruitment by the PLC product DAG [205]. The Src-mediated PKD activation relies on PKCs phosphorylating essential PKD serine residues. Concludingly if this is indeed a potential activation mechanism for VRACs, it is not the one underlying VRAC activation by hypotonicity in HeLa and HEK293 cells. This is demonstrated very clearly by a study using the same PKC inhibitor Gö6983, resulting in abolished PKD activation by ROS [202], that I used in this thesis to show unaltered currents and FRET reduction upon hypotonicity. If this is due to cell

type-specific signaling pathways or different activation pathways for specific subunit compositions fulfilling diverse tasks remains to be shown.

As discussed in section 4.5, the role of PKCs for VRAC activation in the used system of HeLa and HEK293 cells is not fully clear, but they are dispensable for general activation of VRACs by hypotonicity. The activation of PKD without upstream PKC is supported by the mentioned new theory of self-dimerizing and trans-autophosphorylating DAG bound PKDs [201]. Further on, it was shown that PKDs can be activated in a PKC-independent manner, by the Gq family member Gα q by GPCR signaling [206]. There are thousands of different GPCRs, which again can bind to several isoforms of α, β and γ subunits (reviewed in [189]). I already discussed the potential role of Gα q as a subunit known to be bound to GPCRs suspected to sense mechanical deformation of the plasma membrane [190, 191]. Just like VRACs, these G-proteins are ubiquitously expressed and would, therefore, be available as a fundamental activation pathway. Together with the findings that those lead to PLC and ultimately to PKC-independent PKD activation, which was shown by me to activate VRAC, this might be a worth path to test for VRAC activation.

A very recent finding of our group now impressively links my finding of PKD activating VRACs to a before known physiological role of both. Chen et al. [207] could show that knock-down or inhibition of VRACs leads to impaired mouse myoblast differentiation. An earlier study already presented the same effect with knocked down PKD2 [208]. For the here presented data, it seems possible that impaired differentiation of mouse myoblasts by PKD2 knock-down is caused by the missing activation of VRACs at early stages of differentiation. The PKD2 isoform was activatable by S1P [208], again strengthening the here made assumptions of a role for S1PRs in VRAC activation through PKD. Nevertheless, did the same study show a role for PKCs, with the absence of PKD2 activation by application of Gö6983 [208]. As before, future experiments will show if the PKC dependency is linked to PKD phosphorylation in a pathway-dependent manner.

Having discussed multiple ways leading to the DAG-PKD mediated activation of VRACs, I want to shorty discuss as well the found mechanism of deactivation by DAGK. I demonstrated that VRACs could be rendered active in isotonic conditions after hypotonic treatment by application of the DAGK inhibitor DOG. Recovery to basal levels after switching from hypotonic to isotonic buffer was impaired for currents measured by whole-cell patch-clamp for A-CFP/E-YFP and endogenous VRACs in HEK293 cells and FRET in HeLa cells. Thereby I could show that the conversion of DAG, which recruits PKD to the plasma membrane, by DAGK to PA is likely a deactivating mechanism for osmolarity change-induced VRAC opening. As for the other above-mentioned enzymes, there exist several isoforms of DAGK, with different stimuli leading to their activation and needed cofactors (reviewed

in [209]). Some of the isoforms are expressed in a tissue-specific manner, whereas others, e.g. DAGKα and ζ, were found in all examined tissues [209]. So, as for the activation, the deactivation of VRACs by consumption of DAG could adapt to various stimuli and tasks by different DAGK isoforms. It is known, that VRACs can be deactivated by application of extracellular hypertonicity [44, 154]. This phenomenon was until now, if at all, explainable with the theory that ionic strength directly activates VRACs by influencing their LRRDs. Supposed that lowered ionic strength leads to a steric rearrangement that opens the channel, increased ionic strength should then theoretically close it again. Now it is possible to explain this with molecular signaling, by hypertonicity leading to activation of DAGK which removes the activating stimuli DAG. Indeed could be shown for DAGKη that this isoform is recruited to the plasma membrane by hyperosmolarity [210]. It will be interesting to see, whether distinct DAGK isoforms serve as off switches for VRACs, depending on the specific task and tissue.

4.4 LRRC8 proteins as potential PKD targets

The identification of PKDs as an essential part of the signaling leading to VRAC activation naturally leads to the question of the substrate of this group of kinases. Apart from known signaling cascades, that could further regulate VRAC localization, expression, and sensitivity, the LRRC8 family forming VRACs could potentially be directly phosphorylated by PKDs. It is still under debate whether or not phosphorylation events are generally needed for VRAC activation (reviewed in [9]). Nevertheless, LRRC8 A,B,C, and D were found in phospho-proteome screens with only LRRC8 E having neither a predicted nor a shown phosphorylation according to Uniprot [211–215]. Strikingly, all these sites are located in Il1 (see Figure 4.1). Il1 could be shown to have a crucial role for trafficking and probably activation as well, by chimeras of LRRC8A IL1 with D,C and E [216]. The chimeras of D, C, and E with A IL1 were transported to the plasma membrane as homomers [216], whereas native homomers apart from LRRC8A formed ones are known to be stuck in the ER [30]. Different lengths of the IL1 domain inserted, showed that only LRRC8C chimeras containing two residues of LRRC8A that were identified in phospho-proteome screens, T200 and S202, trafficed to the plasma membrane and conducted currents comparable to A/C heteromers. If this effect is due to phosphorylation or, e.g. protein-protein interactions at that loop remains to be shown.

Threonine 200 and Serine 202 of LRRC8A might, therefore, play a crucial role by being phosphorylated, but they do not have a PKD consensus sequence. Comparing found substrates of PKD1 and 2, the consensus sequence for these kinases turned out to be L/V/I-X-R/K-X-X-S/T [217, 218]. To my knowledge, there is not yet a

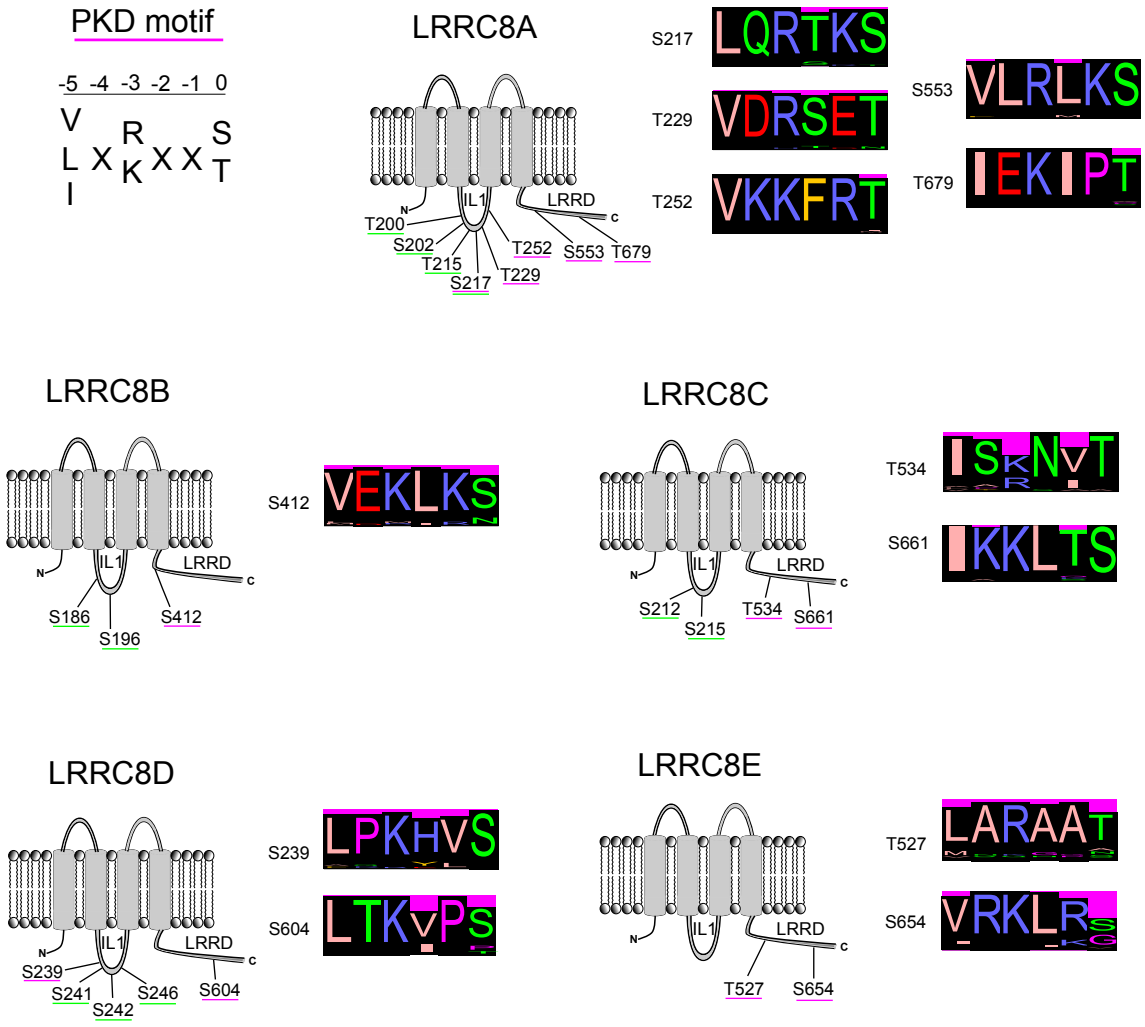

Figure 4.1: Conservation of PKD motifs in the LRRC8 family
Upper left corner: PKD consensus motif. Rest: Schematic representation of LRRC8 subunits. Position numbers of amino acids refer to their position in human LRRC8 variants. Phosphorylation sites found in phosphoproteome screens (underlined in green) and PKD motifs (underlined in magenta) are indicated below each structure scheme with the respective amino acid and its position shown (one-letter code). Right of every structure scheme are the consensus histograms of all found PKD motifs of that subunit. Black bars represent percentual conservation of that position in the sequence, magenta bars behind black bars represent 100 % conservation . Size of letters reflects their percentual occurrence. The number of species analyzed per subunit was: A 34, B 29, C 31,D 27, and E 25 depending on identification of these genes in the chosen species. S217 of LRRC8A is the only residue having a PKD motif, and that was found in phosphoproteome screens.

consensus sequence found for PKD3, due to low numbers of known substrates. I used the web-tool ScanProsite to search all five human LRRC8 members for the consensus sequence of PKD1 and 2 [219]. Indeed there are serine and threonine residues within PKD motifs in all five LRRC8 proteins (Figure 4.1). Interestingly, most of them are located in the LRRD of the respective protein. Combining this possibility with the hypothesis of ionic strength, that was thought to alter attraction forces between neighboring subunits, it is tempting to hypothesize that phosphorylation of neighboring subunits could lead to the same effect. Apart from the LRRD localized consensus sequences, serine 217 of LRRC8A has the PKD motif as well. This amino acid did not only show up in general phospho-proteome screens [211, 212, 215], but it was also detected in a PKD1 specific screen in HEK293 cells [220]. I want to emphasize, that even though chimeras of LRRC8C with parts of IL1 of LRRC8A not containing S217 were transported to the plasma membrane and conducted ions, only the homomeric C-IL1 chimera with a long stretch of IL1 containing S217 produced currents larger than heteromeric A/C complexes [216].

The PKD motif is rather short and variable and could thereby be found by chance, with ScanProsite predicting to find it in "100 000 proteins around 138 000 times". A good way to further strengthen or weaken the possible role of the found amino acids as phosphorylatable residues is to determine their conservation between different species. Especially since I want to identify potential residues that are phosphorylated to activate VRACs. Potential regulative phosphorylations might evolve differently between species, but crucial ones for activation usually do not. I compared LRRC8A-E from up to 34 species, throughout the subphylum of vertebrates (see Material and Methods for details), to determine the conservation of the potential phosphorylation sites found by ScanProsite (Figure 4.1). Of all analyzed motifs, only two are perfectly conserved in all inspected species, being S217 in LRRC8A and S661 in LRRC8C (note that the only mutation in LRRC8A S217 is a homologous S217 to T217 in *Felis catus*). Combining the facts that LRRC8A S217 already showed up in a PKD1 phospho-proteome screen, its inclusion in chimeras leading to higher peak currents and the high conservation between various species renders this residue a good potential candidate for future mutagenesis experiments to validate its role in activation by phosphorylation by PKD (see section 4.6). Another well-conserved PKD motif is at S239 in LRRC8D, with the serine and lysine or arginine at position -3 being conserved in all species an only leucine at position -5 missing in 7 % of them. This residue again is in the IL1, so regardless of several motifs found in human LRRC8 LRRDs, they are not well conserved and are therefore probably not involved in activation by PKD mediated phosphorylation. If there is a dependency on phosphorylation, A/E complexes might be an interesting tool, since LRRC8E has neither been identified in phospho-proteome screens nor could I find a

conserved PKD motif. Activation by phosphorylation would thereby rely solely on LRRC8A, assuming no other controlling mechanisms of LRRC8E.

Direct phosphorylation of VRACs for activation is a comprehensible model since various other channels have been shown to be activated or deactivated by direct phosphorylation or dephosphorylation (reviewed in [221–223]). Several voltage-gated sodium channels,e.g., are phosphorylated at their intracellular loops for activation and deactivation [221]. Another example of a Cl^- channel being regulated by phosphorylation is the cystic fibrosis transmembrane conductance regulator (CFTR) channel (reviewed in [224]). CFTR has a regulatory domain (being formed by a long intracellular loop) that is phosphorylated several times in order to activate the channel [225, 226]. It will be exciting to see wether future work shows VRACs to be part of this group of channels regulated by direct phosphorylation.

4.5 The whole-cell voltage-clamp bias and the mysterious role of PKC

A striking finding of this thesis was the bias introduced by whole-cell voltage-clamp configuration regarding VRAC activation by the phorbol ester PMA. Neither could currents nor FRET changes be detected upon PMA addition with established whole-cell configuration. Only by measuring the currents of cells incubated prior to established whole-cell configuration with PMA a increase of ion flux compared to untreated cells could be detected. After gigaseal formation, the plasma membrane of a patched cell is ruptured by, e.g. strong suction, to access the cytosol and dialyze it with the pipette solution. This enables tight control of variables per experiment, by either adding or omitting compounds to the pipette solution and thereby the cytosol. As well is the ion content of the cell under the control of the experimenter, which allows for the investigation of the influence of specific ions to the overall population of a certain channel type in a cell. The drawback of this method is created by its advantage at the same time: the dilution of cytosolic contents. Cytosolic molecules can be diluted this way by factors of thousands to millions, with published methods trying to minimize this effect [227]. Dialysis of the cytosol can happen in seconds to minutes, depending on cell size and pipette diameter [228, 229]. A dramatic dilution of signaling molecules can, but does not necessarily have to, impair the signaling pathway containing this molecule. Since the whole cytosolic content is diluted with the whole-cell configuration, all signaling pathways are influenced to a not predictable extent this way. In the scenario presented by me in this thesis, the activation of VRAC by recruiting PKDs to the plasma membrane by PMA was completely abolished by the whole-cell configuration. Without the FRET sensor,

one could have concluded that C1-domain-containing proteins are not involved in the activation of VRACs. Exactly that has already happened in a publication, stating that VRAC is activated in a PKC independent manner by measuring currents in the whole-cell configuration with added PMA [140]. As mentioned above, PMA is often confused (and advertised by suppliers) as a pure PKC activator. Interestingly, another phorbol ester, recruiting C1-domain-containing proteins to the plasma membrane [230], OAG did evoke currents under isotonic conditions and established whole-cell configuration [140]. This leads to the question whether OAG and PMA, apart from recruiting C1-domain-containing proteins, have different secondary effects that bring about the activation of VRAC with whole-cell configuration for one but not the other compound. A mere concentration-dependent effect is comprehensible as well, with OAG being used with a concentration of 100 μM, whereas PMA was used by Zholos et al. with 100 nM [140]. It is not predictable which compounds, and experiments suffer from the same false-negative (and potentially false-positive as well) effect of the whole-cell configuration, and I could clearly show its influence for at least PMA and Gö6983. Therefore, all performed experiments of the past utilizing this method need to be revisited to rule out biases potentially beyond the effects for those two drugs.

That establishing the whole-cell configuration abolishes the activating effect of PMA on VRAC observed by FRET can be easily explained by the dilution of crucial factors for the DAG-PKD signaling pathway. A less clear situation is found for the PKC inhibitor Gö6983. FRET of unpatched cells increased upon Gö6983 addition. An initial hypothesis was that this rise is due to the closing of channels constitutively opened by being fluorescently tagged at their C-termini, as was shown in *Xenopus* oocytes [80]. Longer incubation with Gö6983 though led to an overall increased cFRET value that nevertheless was similarly reduced upon hypotonicity to untreated cells. Further on could we detect channel opening as current flow regardless of Gö6983 treatment. Since the baseline current in isotonic buffer was not decreased upon Gö6983 addition, the rise is not due to closing of opened channels. A general photophysical alteration as seen for chloramine-T (discussed in section 4.1), leading to this increase of cFRET, can be excluded by unaffected other FRET constructs, as CFP-18AA-YFP. The effect is, therefore, VRAC specific and not related to channel gating. Whereas the increase in unpatched cells was of an explainable degree, with more acceptor and donor pairs in a more efficient orientation and distance, the increase of cells in the whole-cell configuration was altered again in comparison to unpatched cells, by being magnitudes higher. The dilution of the cytosol thereby enhances the effect of Gö6983, that leads to increased cFRET. In my experiments, I sacrificed spatial resolution for temporal resolution and sensitivity, rendering visual inspection of cells treated with Gö6983 to no avail. It might be enlightening to see

whether the PKC inhibitor leads to an altered distribution of VRACs at the plasma membrane that could result in clustering and therefore increased crowding FRET.

I could show that VRAC still conducts ions by electrophysiology and that A-CFP/E-YFP complexes show reduced cFRET independent of Gö6983 treatment. Concludingly PKCs are dispensable for VRAC activation in HeLa and HEK293 cells by hypotonicity for at least this VRAC subunit combination. Still, several publications state a role of PKCs for VRAC activation. Unfortunately, they suffer from several potential sources of error. For example, some used the PKC inhibitor Gö6976, which was shown to inhibit PKDs as well [134, 135, 195]. Others used phorbol esters, for example phorbol 12,13-dibutyrate (PDBu) or the already discussed OAG to claim an activating effect of PKCs on VRAC, even though PKDs are affected by the same compounds [140, 231]. So apart from the discussed bias introduced by the whole-cell configuration, that leads to the conclusion that PKC does not activate VRAC since PMA is unable to evoke currents, a general specificity problem of pharmacological approaches further complicates the interpretation of old data sets. I want to emphasize the part of the work of Hermoso et al. [135] that went beyond a drug-based approach since they also used HeLa cells and are thereby easier to compare to my experiments than the plethora of data gathered in various other model systems. They created stable HeLa cell lines expressing kinase-dead variants of PKCα and ζ and compared their volume decrease after hypotonic swelling [135]. Indeed did the cell line with the kinase-dead PKCα show impaired RVD compared to control cells. Besides noting that the effect of Gö6976 was higher than that of kinase-dead PKCα, there are several explanations for this discovery in compliance with my data. On the one hand, it would be plausible that subunit composition influences the activation mechanism. HeLa cells were shown to express LRRC8D to several magnitudes higher extend than LRRC8E [232]. The impairment of hypotonicity induced cFRET change and current by inhibited PKDs, presented in this thesis, was shown for A-CFP/E-YFP complexes. With wildtype HeLa cells expressing LRRC8D most, the reduced RVD for HeLa cells lacking a functional PKCα could be due to VRACs containing the D subunits to be either directly activated by PKCs or rely on PKD variants that require phosphorylation by PKCs to be active. On the other hand it is known that long-term changes of one PKC isozyme level can lead to an accumulation of other isozymes of this family [233]. Intervening in the phospho-proteome homeostasis of cells may, therefore, cause up- and downregulation of signaling pathways in general, that ultimately interfere with VRAC activation, but do not necessarily suggest a causal role of PKCα.

Another layer of complexity, apart from functional diversity derived from subunit stoichiometries, is added by the fact that VRACs do not only conduct ions (with chloride being the most prominent). They were shown to conduct other organic os-

molytes as well, as excitatory amino acids and taurine in a subunit dependent manner. In rat astrocytes, it was shown, that PDBu affects potential VRAC mediated aspartate release, but not swelling-activated chloride currents [231]. Concludingly there might be different pathways for varying channel compositions or conducted species. I can therefore not rule out a role for PKCs in some of the possible combinations of species, tissue, subunit composition, and activating stimuli. Nevertheless, the presented data of A/E and A/A channels, activated in HeLa and HEK293 cells by the supposed DAG-PKD signaling pathway due to hypotonicity, creates a framework for future understanding of more complex and defined models and the potential involvement of PKCs in them.

4.6 Perspective and conclusion

The FRET sensor approach to detect VRAC activity is a very versatile tool, enabling fascinating new experiments that were not possible before and can complement the established field of electrophysiology and labeled osmolyte flux experiments. Since one of the biggest advantages of my FRET method is the subunit specificity, it will be of worth to label and test all other LRRC8 subunits together with LRRC8A. First pilot experiments performed by me with A-CFP/D-YFP complexes were very promising, with A-CFP/D-YFP formed VRACs showing the same drop as A-CFP/A-YFP and A-CFP/E-YFP ones (data not shown). For yet unknown reasons, LRRC8D is hardly expressed in HeLa, and other, cells [30]. This led me to firstly concentrate on LRRC8E for this thesis, nevertheless, expressing cells can be found and this issue should be addressed in the future. All combinations of A and another LRRC8 paralog are known to conduct current upon activation by hypotonicity. I expect therefore to see the same FRET drop as seen for A/A, A/D and A/E for the other combinations as well in HeLa cells. The repetition of here shown experiments with Gö6983, PMA and CRT 0066101 could than answer, if all subunit combinations are indeed controlled by the same signaling pathway in HeLa cells, or if for example, A/D complexes are activated by PKC instead. If the same mechanism controls all subunits, there is likely a stimulus and cell type dependence for VRAC activation. The FRET sensor could then be used in the discussed rat astrocytes (see section 4.5) to test again for general or subunit dependent activation pathways.

Another major advantage of the FRET sensor is its ability to monitor VRAC activity in living cells over a long period of time. I measured FRET in cells for up to four hours (data not shown), and in this time frame FRET was stable over the whole period of measurement, and I expect no big differences in longer experiments, provided that there is no substantial change of VRAC activity. The aforementioned results of our group that VRAC is necessary for myogenic differentiation could be

further verified and narrowed down to the exact time point of VRAC engagement in differentiation with the FRET sensor. For this and all other cells to be examined for VRAC functions, one could consider a knock-in approach as well. As a start, subunits should be labeled with CFP and YFP that were shown to be highly expressed in that type of cell. Later experiments could then focus on the other remaining subunits as well, highlighting again that the FRET sensor will always only report the activity of channels containing the labeled subunits without interfering with the others. Genetic engineering of endogenous LRRC8 proteins would lead to a less artificial accumulation of specific subunits created by transient transfection but might make high detection sensitivity of the camera in use necessary. Furthermore, potential artifacts created by the increased activity of fluorescently labeled LRRC8 subunits in stable knock-in cell lines need to be explored.

As discussed for the varying effect of oxidation on A/C, A/D and A/E heteromers, it is not known how channels formed by more than two subunits would combine the effects seen for only two subunits containing channels. This question is hard to address with classical methods, so again, the FRET sensor might be a useful tool to answer it. With LRRC8A being the obligatory subunit for VRACs, expression of LRRC8A together with two other subunits labeled with either CFP or YFP would lead to channels that would only show FRET if all three subunits are combined in one single channel. Without LRRC8A, potential VRACs formed by the other two could not reach the plasma membrane [30]. Channels containing only A and either the CFP or YFP labeled subunit would not contribute to FRET and are neglectable. Detection of FRET would only be possible from channels containing all three subunits, enabling specific assessment of the activity of this complex class of VRACs. If this approach is feasible, another step might be the establishment of a three-color FRET system. These comprise two donors and an acceptor, with the excitation and emission spectra of donor one and donor two matching for FRET to occur, so that finally donor two can excite the acceptor as well [234, 235]. The seemingly close orientation of the LRRDs in a single VRAC tempt me to think that a three-component FRET cascade could work here. An exemplary fluorophore combination that was shown to be efficiently transferring energy two the last acceptor, given a correct protein orientation, is Turquiose2, YPet and Cherry [236]. Expressing unlabeled LRRC8A together with three other subunits labeled with these fluorescent proteins could enable detection of channels composed specifically by these four subunits. If three color-FRET works with transiently transfected cells, this would enable the exciting possibility to generate knock-in cells with three different subunits, apart from LRRC8A, labeled with e.g. Turquiose2, YPet and Cherry to monitor nearly all possible channel compositions. This approach would require a lot of work and sophisticated imaging hardware, but I do believe that the potential laying in cell

lines with trackable VRACs justifies that.

In section 4.4, I discussed LRRC8 proteins as potential targets of PKDs. Considering the troubling side effects of used drugs by me and others concerning PKC,PKD, and DAG signaling, all results relying solely on pharmacological data have to be verified more thoroughly to be certain about signaling pathways involved. The here proposed PKD dependency of VRAC activation falls into this as well and should be considered as a hint for future experiments. Especially considering the existence of at least three different PKD isoforms with yet an only beginning understanding of mechanisms of action and targets. As discussed, stable knock-down or knock-out of PKC can have severe side effects, mimicking a direct involvement of PKCs, whereas their absence impeded proper phospho-proteome homeostasis. Nevertheless, it would be a good first step to see if HeLa cells lacking specific PKD isozymes still show the characteristic cFRET reduction upon hypotonicity. The next step proposed by me could be the usage of the affinity-directed protein missile system (AdPROM) [237, 238]. Cloning of AdPROM into an inducible vector system resulted in a reduction of target proteins already after two hours and a clear depletion after six hours of induction [237]. This time frame is crucially shorter than knock-out approaches and commonly used knock-down ones using siRNA, the first taking weeks to produce stable cell lines and the latter at least 24 hours up to 48 hours [239]. Protein depletion in two to four hours would be a vast improvement in time the cells suffer from depleted PKD signaling before assessing the influence of them on VRAC activation.

Another future approach should address the discussed direct phosphorylation of LRRC8 subunits by PKDs, complementing the aforementioned methods. The most promising potential PKD target is S217 in LRRC8A (see section 4.4). Mutating this residue to alanine would then result in a loss-of-function mutation if it is needed for activation. Since the FRET sensor method can detect activation of VRAC homomers solely formed by LRRC8A subunits, compared to the very little if at all detectable currents in electrophysiology, a LRRC8A^{S217A} mutant tagged with either CFP or YFP and following co-expression could be readily tested in HeLa cells. Challenging LRRC8A^{S217A}-CFP/LRRC8A^{S217A}-YFP expressing cells with hypotonicity will then reveal if VRACs lacking this motif are still active. Since LRRC8E has no conserved PKD motifs, nor was it ever detected in a phosphor-proteome screen, the next choice would logically be to co-express A^{S217A}-CFP/E-YFP and test again for activation by cell swelling. If the hetero- and homomers are still activatable one could consider mutating S553 in LRRC8A together with S217, since this residue is a likely candidate as well. Successful silencing of channel activity by substitution of serine to alanine could then be further verified by the typical mutation of the phosphorylatable residue to glutamic acid or aspartic acid, which in some cases can mimic phosphoserines.

If the discussed residues are phosphorylated to activate VRACs, mutation of them to glutamic or aspartic acid could render the channel constitutively open. Here a drawback of the FRET sensor can be seen, since until now it is only able to detect channel activity as a relative change from a before measured baseline cFRET value. Constitutively open channels can thereby not be distinguished from closed ones since the internal reference of the closed state is missing. But if these channels would be shown with electrophysiology to be constitutively opened, a FRET analysis still would be of benefit. Until now it is not sure, whether opening of a channel leads to the FPs at the LRRDs to move completely out of FRET distance or just into a position with less efficient FRET. In the first case, overall detected cFRET would be a mixture of closed channels still producing cFRET and opened channels not contributing to this value anymore. Constitutively open channels should then lead to very low or now cFRET at all. In the second case I expect a mildly reduced cFRET over the cell population. This knowledge might prove useful for understanding the structure-function relationship of VRACs and its detection by FRET.

To further investigate the potential phosphorylation of LRRC8 proteins by PKDs I propose to perform peptide spot arrays of all paralogs, incubated with the different recombinant PKD isozymes. Thereby either primary structure motifs that are involved in interactions with PKDs or even phosphorylated residues, by incubation of recombinant PKDs with radioactively labeled ATP, of the respective LRRC8 protein family member could be revealed. Newfound motifs could then be further analyzed by mutagenesis and conservation analysis.

All of the discussed future experiments deal with the downstream events after PLC mediated DAG production. It is still not known how cells sense their volume or accompanying intrinsic changes, especially since I could show that ionic strength, which was a likely explanation for VRAC activation by cell swelling, is not directly activating VRACs. So even more work needs to be done to identify the mechanisms upstream of PLC activation. I already discussed many hints, that could be dealt with in section 4.3. Emphasis should be paid towards G-proteins, especially G-protein coupled receptors, as this diverse group of plasma membrane proteins prominently converged in one or the other way on PLC and therefore possibly VRAC. A summary of the potential activating and deactivating stimuli concluded from my data and previously published ones is illustrated in figure 4.2

In conclusion, I managed to establish a useful new tool for exploring VRAC activation mechanisms and its functions in living cells and organisms. The here shown system did work robustly and reproducible with A/A homomers and A/E heteromers. I am confident that the other subunits will prove as promising as the already tested combinations did. Furthermore, I was able to directly show, combining electrophysiology and FRET microscopy, that the controversially discussed ionic

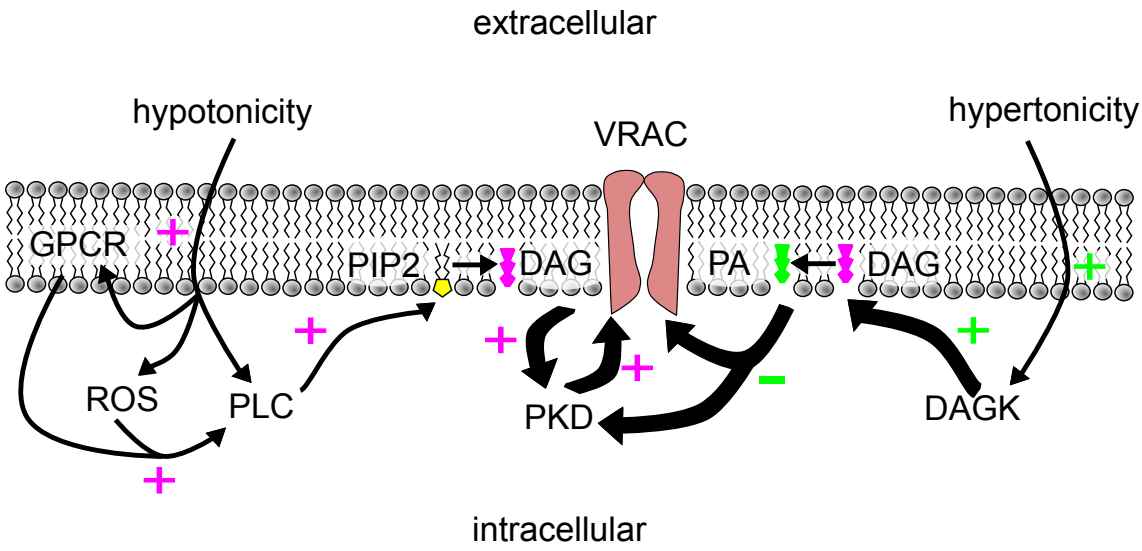

Figure 4.2: Hypothetical scheme of VRAC activation
Illustrated is the combination of published regulations (thin arrows) and regulating pathways shown in this thesis (fat arrows). Involved molecules are G-protein coupled receptors (GPCR), reactive oxygen species (ROS), phospolipase C (PLC), phosphatidylinositol 4,5-bisphosphate (PIP2), diacylglycerol (DAG), protein kinase D (PKD), phosphatic acid (PA), and diacylglycerol kinase (DAGK). Activating effects are marked with a plus sign and deactivating effects with a minus sign. The color of plus and minus refers to the osmolarity which triggers the pathway (green for hypertonic, magenta for hypotonic). Hypotonicity leads to the stimulation of PLC by several potential pathways including GPCRs and ROS. PLC hydrolyzes PIP2 to DAG (and IP3, the role of which in VRAC regulation is unclear) which recruits and activates PKD. PKD acts either on VRACs themselves or on different proteins leading to the opening of VRACs. Switching the extracellular solution from a hypotonic to a isotonic buffer (which is therefore hypertonic compared to the hypotonic buffer) stimulates DAGK, which is then converting DAG to PA. This ends the recruitment and stimulation of PKD and leads to the deactivation of VRACs.

strength is not directly activating VRACs in living cells and. Rather is DAG mediated PKD activation a key regulator for A/E heteromers and it will be exciting to see if this holds true for other subunit combinations as well. My work suggests that the localization in the plasma membrane is needed for VRAC activation, following investigations could, therefore, aim at the identification of the plasma membrane specific co-factors leading to VRAC activation. The here presented work provides completely new ways of accessing VRACs role in living cells that have not been possible to this extent until now.

5 Materials and Methods

5.1 Materials

Chemicals

All chemicals used in this thesis were purchased from Sigma-Aldrich, Merck or Roth, if not stated otherwise.

Cell lines

Table 5.1: Cell lines

Name	Source/Reference	Additional information
HeLa	RRID: CVCL_0030	Obtained from Leibniz Forschungsinstitut DSMZ
HEK293	RRID: CVCL_0045	Obtained from Leibniz-Forschungsinstitut DSMZ
HEK 5x KO	[35] (PMID:28193731)	Gift from T.J. Jentsch (MDC and FMP, Berlin, Germany)

Primers

Table 5.2: Primers

Name	Sequence
Q58A forward	ATCACTAGTAGCGGCCGCGACTCTAGA
Q58A reverse	ATCTCTAGACTTGTACAGCTCGTCCATGCC
GFP forward	TATAACCGGTCGCCACCATGGTGAGCAAGGGCGAG
GFP reverse	TATAGCGGCCGCTTTACTTGTACAGCTCGTCCATGCC

Drugs and chemicals

Table 5.3: Drugs and chemicals

Name	Supplier	Product number
Brefeldin-A (BFA)	Sigma-Aldrich	B5936
D/D-solubilizer	Clontech,TaKaRa	635054
Latrunculin B (LatB)	Sigma-Aldrich	428020
Alexa Fluor 546-phalloidin	Thermo Fisher Scientific	A22283
Methyl-β-cyclodextrin (MbCD)	Sigma-Aldrich	C4555
Filipin	Sigma-Aldrich	SAE0088
Phorbol-12-myristate-13-acetate (PMA)	Tocris, Bio-Techne	1201/1
Gö6983	Abcam	ab144414
CRT 0066101	Tocris,Bio-Techne	4975/10
Dioctanoylglycol (DOG)	Tocris, Bio-Techne	0484

Identifiers of LRRC8 homologs

Table 5.4: UniProt IDs of LRRC8 subunits from different species used for homology analysis

	UniProt IDs				
Species	**LRRC8A**	**LRRC8B**	**LRRC8C**	**LRRC8D**	**LRRC8E**
Xenopus laevis	Q6NU09	A0A1L8GMZ1	A0A1L8GMY5	A0A1L8GMW1	Q6NU09
Ornithorhynchus anatinus	F7E9Z4	F7E7Y7	F6QUQ7	-	-
Gopherus agassizii	A0A452IMR6	-	-	A0A452IF87	-
Monodelphis domestica	F7F2H1	F7G4V3	F7G4Z3	-	F7CGX2
Myotis lucifugus	G1PHG5	G1PZP4	G1PKY6	G1Q2B8	G1PNC3
Bos taurus	A5PK13	E1BDX2	A5PK13	A4IFE5	F6PRJ0
Ovis aries	W5PH89	W5Q1V8	W5Q1X3	W5PKY0	W5NY27
Eschrichtius robustus	A0A2F0AUK3	A0A2F0BNQ8	A0A2F0BJ07	-	A0A2F0B4N3
Dasypus novemcinctus	C1FXV0	-	-	-	-
Loxodonta africana	G3TL97	G5E711	G3T1R0	G3TTR1	G3TW15
Rattus norvegicus	Q4V8I7	D4A758	Q498T9	Q5U308	Q3KRC6

Table 5.4: continued

	UniProt IDs				
Species	**LRRC8A**	**LRRC8B**	**LRRC8C**	**LRRC8D**	**LRRC8E**
Mus musculus	Q80WG5	Q5DU41	Q8R502	Q8BGR2	Q66JT1
Erinaceus europaeus	A0A1S2ZZQ4	A0A1S3WDC4	A0A1S2ZUF3	A0A1S2ZUF7	A0A1S3ACI3
Homo sapiens	Q8IWT6	Q6P9F7	Q8TDW0	Q7L1W4	Q6NSJ5
Equus caballus	F7BJ71	A0A3Q2H0I2	F7BE34	F6Z951	F7C6Z4
Felis catus	M3W4V0	A0A337SKR1	M3X422	M3X2H7	M3WLN1
Iconisemion striatum	A0A1A7X3D9	-	-	-	A0A1A7YMV4
Danio rerio	E9QIH3	-	E7F333	Q08BM6	-
Salmo salar	A0A1S3M3U0	A0A1S3KLJ4	A0A1S3L6H5	C0H928	-
Canis lupus familiaris	E2RQD5	E2R9Z8	E2R9Z9	E2RA00	E2RNX3
Sus scrofa	F1RR61	A0A287B5M3	F1S4E4	A0A286ZWM5	F1SA81
Anolis carolinensis	H9G7Z5	G1KZ23	G1K985	G1KUQ0	G1KJG8
Ailuropoda melanoleuca	D2H153	D2HJK7	D2HJK8	D2HJK9	D2HI92
Cavia porcellus	H0V2C2	H0V7N0	A0A286XG73	H0VC12	H0V1Y0
Taeniopygia guttata	H0Z1B2	H0Z746	H0Z741	H0Z736	-
Ictidomys tridecemlineatus	I3LZR5	-	I3MF01	I3M5K2	I3NB98
Chlorocebus sabaeus	A0A0D9RPP4	A0A0D9S6T1	A0A0D9S6T0	A0A0D9SAE9	A0A0D9R756
Ficedula albicollis	U3JFD0	U3JG25	U3JG26	U3KKM5	-
Mustela putorius furo	M3YNJ3	M3Y036	M3Y030	M3Y018	M3Y9F8
Pan paniscus	A0A2R9CN78	A0A2R8ZS38	A0A2R9B1I8	-	A0A2R9BKS4
Macaca mulatta	F7E1A8	A0A1D5QGF5	F7HLE0	F6TCH4	F7GRN6
Meleagris gallopavo	G1MZK8	G1N8Q7	G1N8Q4	G1NR00	-
Mandrillus leucophaeus	A0A2K5YFP4	A0A2K5YLW9	A0A2K5Y2I2	-	A0A2K6A9Q8
Pongo abelii	A0A2J8UJR0	H2N6T9	H2N6T8	A0A2J8R3A9	A0A2J8RD66

Buffers for imaging and patch-clamping

All imaging buffers were prepared with sterile filtered stock solutions. Isotonic imaging buffer (340 mOsm) contained (in mM): 150 NaCl, 6 KCl, 1 $MgCl_2$, 1.5 $CaCl_2$, 10 glucose,10 HEPES, pH 7.4 (adjusted with NaOH). For osmolarity titration experiments, the concentration of NaCl was adjusted to (in mM): 105 (250 mOsm), 80 (200 mOsm), 55 (150 mOsm), 30 (100 mOsm), and 5 (50 mOsm). The buffer with 250 mOsm was the standard hypotonic buffer used in all other experiments. Hypertonic buffers were as isotonic buffer supplemented with 60 mM (for 400 mOsm) or 160 mM (for 500 mOsm) mannitol.

Patch-clamp experiments were performed with an isotonic bath solution (320 mOsm) containing (in mM): 150 NaCl, 6 KCl, 1 $MgCl_2$, 1.5 $CaCl_2$, 10 glucose, and 10 HEPES, pH 7.4 (adjusted with NaOH). The pipette solution (290 mOsm), against which the cytosol is dialyzed, contained (in mM):40 CsCl, 100 Cs-methanesulfonate, 1 $MgCl_2$, 1.9 $CaCl_2$, 5 EGTA, 4 Na_2ATP, and 10 HEPES, pH 7.2 (adjusted with CsOH). After preparation, the pipette solution was stored at -20 °C, and was thawed and kept in ice for usage. Hypotonic bath solution (240 mOsm) contained (in mM): 105 NaCl, 6 CsCl, 1 $MgCl_2$, 1.5 $CaCl_2$, 10 glucose, 10 HEPES, pH 7.4 (adjusted with NaOH). All solutions for patch-clamp experiments were sterile filtered after preparation and their osmolarities were measured with a vapor pressure osmometer (VAPRO 5600, Elitech).

Throughout this thesis, isotonic/hypotonic imaging buffer and isotonic/hypotonic bath solutions for patch-clamp experiments are named isotonic and hypotonic buffer.

Plasmids

Table 5.5: Plasmids

Name	Source/Reference	Additional information
LRRC8A-GFP (A-GFP)	[30] (PMID: 24790029)	Gift from T.J. Jentsch (MDC and FMP, Berlin, Germany)
LRRC8A-CFP (A-CFP)	This thesis	
LRRC8A-CFP-FM_2 (A-CFP-FM_2)	This thesis	
LRRC8A^{N66A,N83A}-CFP (noGlyc-CFP)	This thesis	LRRC8A-coding sequence subcloned from A^{N66A,N83A}-GFP ([30]; gift from T.J. Jentsch, MDC and FMP, Berlin, Germany)
LRRC8A-Cerulean (A-CFP)	This thesis	
LRRC8A-YFP (A-YFP)	This thesis	
LRRC8E-CFP (E-CFP)	This thesis	
LRRC8E-YFP (E-YFP)	This thesis	
LRRC8E-Venus (E-YFP)	This thesis	
LRRC8E-RFP (E-RFP)	This thesis	
CFP-18AA-YFP	[145] (PMCID: PMC2706461)	Gift from C.F. Kaminski (University of Cambridge, UK)
GluA2-6Y-10C	[144] (PMID:27313205)	
ionic strength sensor (RD sensor)	[147] (PMID: 28853549)	Gift from B. Poolman and A.J. Boersma (University of Groningen, The Netherlands)
pEYFP-ER (ER-YFP)	Clontech, TaKaRa	Catalog no. 6906-1
GalNAc-T2-RFP	This thesis	
CD4-YFP	This thesis	
GFP-FM_4	[148] (PMID:10852943)	

Cell culture media and solutions

Table 5.6: Cell culture media and solutions

Name	Supplier	Product number
DMEM (supplemented with glucose, L-glutamine and $NaHCO_3$)	PAN-Biotech	P04-03550
FBS	PAN-Biotech	P30-1506
DPBS w/o calcium and magnesium	PAN-Biotech	P04-36500
Accutase, cell detachment solution	PAN-Biotech	P10-21100
FuGENE 6	Promega	E2691
Opti-MEM	Gibco	31985070

5.2 Methods

5.2.1 Bacterial transformation and cloning

Heat-shock transformation and plasmid purification

Plasmids were transformed in chemically competent DH5α cells with a maximal total mass of 100 ng in 1-5 μl. Bacteria aliquots were thawed on ice before usage for 15 minutes. After addition of plasmids, DNA-bacteria mixtures were incubated for 30 minutes on ice. Heat shock was performed by incubation of bacteria at 42 °C for 45 seconds, and a following incubation for two minutes on ice. Then one ml of pre-warmed LB medium was added, and cells incubated for one hour at 37 °C before plating on either ampicillin or kanamycin containing LB-agar plates. Grown colonies were picked and incubated in LB medium before DNA purification (NucleoSpin Plasmid QuickPure, Macherey-Nagel). To control for the correct insert sequence, plasmids were Sanger-sequenced (Microsynth Seqlab GmbH).

Cloning of CFP,YFP, and RFP fusion constructs

The coding sequences of human LRRC8A, LRRC8A^{N66A,N83A} and LRRC8E were excised from LRRC8A-GFP, LRRC8A^{N66A,N83A}-GFP, and LRRC8E-GFP constructs [30] by a double digest with EcoRI and KpnI (New England Biolabs). The vectors pECFP-N1 and pEYFP-N1 were digested as well with EcoRI and KpnI. Vector backbones and inserts were gel-purified (NucleoSpin Gel and PCR clean-up, Macherey Nagel) after separation in a TAE based agarose gel prepared from UltraPure agarose (Invitrogen). Purified inserts were ligated with vector backbones at a ratio of 3:1

with T4-Ligase (New England Biolabs) for 10 minutes at room temperature. FRET constructs had 12 amino acid long linker (LVPRARDPPVAT for LRRC8A and $A^{N66A,N83A}$, and WVPRARDPPVAT for LRRC8E) between the respective LRRC8 protein and the fluorescent protein.

CD4-YFP was created from CD4-GFP [240] by excising the coding sequence of CD4 with EcoRI and SalI and cloning it into pEYFP-N3 using the same enzymes. For expression of GalNAcT2-RFP, the stalk region of N-acetylgalactosaminyltransferase 2 (GalNAcT2) was subcloned from pGalNAcT2-GFP [241] into pmRFP-N1. Purification and ligation were performed as described above.

The generation of A-CFP-FM_2 was done by inserting the restriction sites for XbaI-EcoRV-SpeI with the Q5 mutagenesis kit (New England Biolabs) 3' of the above described A-CFP construct. Mutagenesis was performed with Q58A forward and Q58A reverse primers (see table 5.2) and the PCR program shown below according to the suppliers manual. Two fused FM domains [148] were excised with XbaI and SpeI and cloned into the restricted sites of the mutagenesis product. Purification and ligation were performed as described above.

PCR program for Q5 mutagenesis

Temperature [°C]	Time	Number of cycles
98	30 sec	1
98	10 sec	25
69	20 sec	
72	3 min 30 sec	
72	2 min	1

Cloning of mCerulean3 and Venus constructs

To replace CFP and YFP in LRRC8X-XFP expression constructs by its improved derivatives mCerulean3 and Venus [242, 243], coding sequences of mCerluean3 and Venus were amplified from the GluA2-6Y-10C construct (see table 5.5) using GFP forward and GFP reverse primers (see table 5.2) and the PCR program shown below. PCR amplicons had 5' AgeI and 3' NotI restriction sites inserted. CFP or YFP were excised from LRRC8X-XFP expression constructs with AgeI and NotI to be replaced by either mCerluean3 or Venus amplicons digested with the same enzymes. Purification and ligation were performed as described above.

PCR program for FP replacement

Temperature [°C]	Time	Number of cycles
98	30 sec	1
98	15 sec	25
69	30 sec	
72	1 min	
72	7 min	1

5.2.2 Cell culture

Cells used in this thesis (see table 5.1) were cultured in DMEM supplemented with 10 % FBS at 37 °C in 5 % CO_2 and humidified air. For subcultures and transfection cells were detached using Accutase according to the suppliers manual. Cells were subcultured before reaching 80 % confluency and seeded at 30 %. Transfection with plasmids (see table 5.5) was performed using FuGENE 6 according to the suppliers manual. For microscopy and patch-clamp experiments, cells were seeded in 35mm glass-bottom dishes (MatTek) or on 20 mm glass coverslips, coated with poly-L-lysine 0.01 % solution (Sigma-Aldrich) for HEK293 and HEK 5x KO cells. Plasmids were transfected at equimolar ratios. Cells were measured 24-48 hours post-transfection.

5.2.3 Drug treatment

Drugs stored at -20 °C were allowed to reach room temperature for 20 minutes before solvation. All here described drugs are listed in table 5.3. To trap expressed proteins in the ER, 5 μg/ml BFA (pre-solved solution, 10 mg/ml) was added to the transfection mix containing culture medium. Depolymerization of the actin cytoskeleton was achieved by the addition of 2 μM LatB (dissolved in DMSO) to the culture medium and 1 hour incubation at 37 °C in 5 % CO_2. Depletion of the cholesterol content of the plasma membrane was done by addition of 5 mM MbCD (dissolved in DMEM by stirring for 30 min at room temperature and following sterile filtration) to the culture medium and incubation for 1 hour at 37 °C in 5 % CO_2.The following drugs were applied at the respective concentration at time points indicated in Results: 1 μM PMA (dissolved in DMSO), 5 μM CRT 0066101 (dissolved in H_2O), and 100 μM DOG (dissolved in DMSO).

5.2.4 FRET measurements

Acceptor photobleaching and seFRET experiments were performed on a high-speed setup from Leica microsystems (Dmi6000B stage, 63x/1.4 oil objective, high-speed

external Leica filter wheels with Leica FRET set filters (11522073), EL6000 light source, DFC360 FX camera, controlled by Las AF). All experiments were performed at room temperature.

Acceptor photobleaching

Cells were searched and focused using maximum gain and low illumination intensity to avoid pre-bleaching of fluorophores. FOVs were chosen that contained two or more cells sufficiently separated for one subset of cells being included in the illumination path of the almost closed field diaphragm, whereas the other cells were outside of the illumination path. The intensity of CFP and YFP was measured using the respective excitation and emission filters before and after bleaching steps. Bleaching was performed by closing the field diaphragm to only illuminate part of the cells in the FOV with the Leica filter cube N2.1 (excitation 515-560 nm) for 2.5-5 minutes per bleaching step. YFP intensity was monitored in Las AF after every step, and cells were bleached until YFP intensity decreased below 10 % of its value before bleaching. Evaluation of APB was done using FIJI [244] by measuring the intensity of CFP and YFP in bleached and unbleached cells in hand-drawn regions of interest (ROI).

seFRET

The cells were washed three times with isotonic buffer before the experiments. The sensitized emission of FRET constructs was assessed by measuring in short succession the CFP channel (I^{DD}), the YFP channel (I^{AA}), and the FRET channel (I^{DA}). Images were acquired every 10 seconds or 20 seconds for VRACs released with the reverse dimerization system to further minimize bleaching. Acquisition parameters were constant for all channels (100ms exposure, gain 1, illumination intensity 2) for correction factors to be constant as well. Spatial resolution was sacrificed for temporal resolution and sensitivity by 8x8 binning. Out of the three acquired channels, cFRET maps were calculated with the PixFRET plugin [245] according to the following equation [246]

$$cFRET = \frac{I^{DA} - I^{DD} \cdot \beta - I^{AA} \cdot \gamma}{I^{AA}}$$

With β being the correction factor for donor bleed through and γ the correction factor for acceptor cross excitation. Correction factors were determined with cells expressing either only donor (A-CFP or cytosolic CFP) or only acceptor (A-YFP or cytosolic YFP) constructs by the acquisition of I^{DD} and I^{DA} for donor only and I^{AA} and I^{DA} for acceptor only samples. Calculation of correction factors was done according to the fraction of intensity detected in I^{DA} to absolute detected intensity

I^{DD} or I^{AA} ($\beta = \frac{I^{DA}}{I^{DD}}$ and $\gamma = \frac{I^{DA}}{I^{AA}}$). The mean of correction factors determined on three different days of at least five samples per day was used for all performed experiments ($\beta = 0.614$ and $\gamma = 0.097$).

Images were processed in PixFRET using a gaussian blur of 2 and threshold of 1. Since PixFRET does only process stacks of a single timepoint, a macro was programmed that ordered stacks according to the input demands of PixFRET and calculated automatically cFRET maps for all time points of an experiment. All cells were evaluated that did show membrane-localized signals in all three channels with hand-drawn ROIs. To minimize selection biases, high-intensity regions of cells, that by morphology were channels residing in the Golgi, were only spared from ROIs if they were oversaturated in one of the three channels. Measured absolute cFRET values were normalized to the mean cFRET of the first timepoints in an experiment in isotonic buffer.

Ratiometric FRET

The ionic strength in cells was measured using the FRET RD-sensor (see table 5.5). Since acceptor and donor have a fixed stoichiometry in that sensor, the ratio of $\frac{I^{DA}}{I^{DD}}$ is a reliable measure of the strength of occurring FRET. Therefore, images of I^{DA} and I^{DD} channels were acquired every 10 seconds of RD-sensor expressing cells. Images were subtracted of background and every pixel of the I^{DA} image divided by the respective pixel in the I^{DD} channel to create a ratio map. Ratios were measured from hand drawn ROIs and normalized to isotonic values of that individual cell to account for ionic strength variations between cells and inhomogeneties in the detection.

Patch-clamp fluorometry

For patch-clamp fluorometry experiments, either FRET and currents of A-CFP/E-YFP expressing HEK 5x KO or of endogenous VRACs in HEK293 or HeLa cells were measured. Thin wall borosilicate capillaries (Warner instruments, Hamden, USA) were pulled on the P1000 micropipette puller (Sutter Instruments) and polished using a heat filament. Pulled pipettes had a resistance of 3-5 MΩ after filling with the intracellular solution. Pipettes were spanned in an ISO-type holder (G23 Instruments) for minimized drifting. Experiments were performed on an Olympus IX81 stage, equipped with a 40x/0.6 Olympus objective, and a Prime 95B CMOS camera (Photometrics). Excitation of CFP and YFP was achieved by 445 and 514 nm diode lasers (iChrome MLE, Toptica Photonics) coupled to the stage via a manual TIRF input. Laser angles were adjusted to pass the objective parallel to the optical path for epifluorescence detection. Filter cubes in the turret contained

only dichroic mirrors for either CFP or YFP. Emission light was split by a Cairn OptoSplit-II, equipped with a T495Ipxr dichroic mirror and emission filters for CFP (Em: 470/24) and YFP (Em: 520/40) and detected simultaneously on the same camera chip.

The monitoring of sealing and capacitance correction was performed with an Axopatch200B amplifier. Currents of cells were recorded using Axograph X (Axograph Scientific) and an Instrutech ITC-18 D-A interface (HEKA Elektronik). For patch-clamp fluorometric experiments, cells were chosen that where isolated from other cells (to avoid chemical cross-talk via tight-junction channels) and expressed all fluorescent fusion proteins to a detectable degree. After the successful establishment of the whole-cell configuration, cells were held at -30 mV. The protocol for a patch-clamp fluorometry experiment consisted of 9 cycles with 500 ms steps to -80 mV every 12 seconds. Cycle 10 consisted of a voltage step protocol, holding the potential for 300 ms at -40, 0, 40, 80, and 100 mV in turn. This protocol was repeated for the duration of the experiment. Before each voltage step to -80 mV, the emission of CFP and YFP was simultaneously detected after sequential excitation with either the 445 or 514 nm laser (exposure 100 ms, 2x2 binning).

Currents were analyzed with Axograph X. Outward flow of chloride was measured at -80 mV, subtracted from basal currents at the holding potential, and currents at -80 mV in isotonic buffer. Voltage-steps were recorded for monitoring if measured currents were due to VRACs, by testing them for outward rectification and inactivation at positive potentials. Fluorescence images were split into stacks matching the input requirements for PixFRET and were treated as described above.

5.2.5 Reverse dimerization system

Cells expressing the GFP-FM_4 construct were measured 24-48 h after transfection using the Leica L5 filter cube (Ex: 480/40, DC: 505, Em: 527/30). Before imaging, cells were washed three times with isotonic buffer and imaged in isotonic buffer. After the acquisition of images before D/D-solubilizer addition, 500 nM of D/D-solubilizer were added to the isotonic buffer and images acquired every 1-5 minutes at room temperature.

To A-CFP-FM_2 or A-CFP-FM_2/E-YFP expressing cells the 500 nM D/D-solubilizer was added directly to the growth medium and cells incubated at 37 °C and 5 % CO_2. Exemplary pictures of A-CFP-FM_2 aggregates were acquired before D/D-solubilizer addition. To perform a buffer switch experiment with VRACs localized in the respective organelles, dishes were washed and imaged in D/D-solubilizer containing isotonic buffer precisely 10 minutes after D/D-solubilizer addition for ER, after 80 minutes for Golgi, and after 165 minutes for plasma membrane (PM) measurements.

FRET measurements were performed with the first cell showing colocalizing signals in the CFP and YFP channel in the respective organelle (determined by visual inspection) as described above. For ER and PM localized complexes, cFRET was measured with hand-drawn ROIs in the cFRET map. To measure cFRET of complexes in the Golgi, a mask was generated with the CFP channel that was used on the cFRET map. The mask was thresholded to contain only the high-intensity juxtanuclear regions of all cells in the FOV. Cells showing signal at the plasma membrane were excluded from the mask.

5.2.6 Qualitative and quantitative microscopy

Imaging of intracellular localization, organelle markers, actin cytoskeleton, and cholesterol content was performed on a Leica Dmi8 (63x/1.4 oil objective, 20x/0.7 dry objective, EL6000 light source, Hamamatsu OcraFlash4.0 camera, controlled by LasX). All experiments were performed at room temperature. Cholesterol content determination was performed using the 20x/0.7 objective. All other images were acquired using the 63x/1.4 oil objective. Coverslips were cleaned by sonication for 15 minutes in 70 % before sterilization and cell seeding.

Intracellular localization of A-GFP/E-RFP

HeLa cells treated and untreated with BFA, expressing A-GFP/E-RFP were grown on glass-bottom dishes. For imaging, cells were washed three times with PBS and imaged in isotonic buffer. Acquisition of A-GFP signals was performed using the GFP filter cube (Ex: 480/40, DC: 505, Em:527/30) and E-RFP using the rhodamine filter cube (Ex: 540/23, DC: 580, Em: 590 LP). Images were processed with FIJI. For better visualization of the ER meshwork, images of BFA treated cells were background-subtracted using a rolling ball algorithm (radius = 50 pixels), and the contrast was enhanced by an unsharp mask (sigma = 3, weight = 0.7).

Co-localization of A-CFP-FM_2 with organelle markers

HeLa cells were cotransfected with A-CFP-FM_2 and either ER-YFP (ER), GalNAc-T2-RFP (Golgi), or CD4-YFP (PM) on coverslips (5 mm diameter). 24 h after transfection, aggregates were released with D/D-solubilizer for 10 (ER), 80 (Golgi), or 165 minutes (PM). Cells were fixed after these times by washing three times with PBS, fixation with 4 % paraformaldehyde (PFA) for 15 minutes at room temperature, washing three times with PBS, neutralization with DMEM containing 10 % FBS at 37 °C for 10 minutes and final washing three times with PBS before air drying and mounting using Fluoromount-G (Southern Biotech). A-CFP-FM_2 was imaged using a CFP filter cube (Ex: 436/20, DC: 455, Em: 480/40) together with

a YFP filter cube (Ex: 500/20, DC:515, Em: 535/30) for ER-YFP and CD4-YFP, and a rhodamine filter cube for GalNAc-T2-RFP.

Actin cytoskeleton

To stain the actin cytoskeleton, HeLa cells treated and untreated with LatB were PFA fixed as described above. After the final wash with PBS, cells were permeabilized with 0.1 % Triton-X100 in PBS containing 1 % BSA for 5 minutes, before staining with Alexa Fluor 546-phalloidin (Thermo Fisher Scientific) diluted 1:1000 in PBS containing 1 % BSA for 1 h at room temperature. After staining, cells were washed three times with PBS before mounting as described above. Cells were imaged with a rhodamine filter cube. Images of untreated cells were deconvolved using the blind algorithm of LasX with 15 iterations.

Cholesterol content determination

For determination of the cholesterol content of the plasma membrane, cells treated and untreated with MbCD were fixed as described above. After the final wash with PBS, cells were stained with 125 μg/ml filipin (dissolved in DMSO, diluted in PBS) for 45 minutes at room temperature, before washing three times with PBS. Images were acquired directly after staining using a DAPI filter cube (Ex: 360/40, DC: 400, Em: 425 LP). Images were segmented into signal and background by manual thresholding and mean intensities of all cells in one FOV in the treshhold measured as a data point.

5.2.7 Homology analysis of PKD motifs in LRRC8 proteins

To study the conservation of potential PKD motifs, I used the consensus motif of PKD1 and 2 L/V/I-X-R/K-X-X-S/T [217, 218]. This motif was searched in all human LRRC8 paralogs with the web-tool ScanProsite [219]. To test for the conservation of these motifs in the vertebrate subphylum, 34 entries of LRRC8A of different species were collected (summary of UniProt identifiers for all subunits and species in table 5.4). The other paralog sequences were searched for that set of species as well. Sequences of LRRC8 family members of all species were aligned using Clustal Omega [247]. Alignments created with Clustal Omega were analyzed using Jalview 2 [248] and conservation histograms for the predicted PKD motifs of human LRRC8 proteins generated.

5.2.8 Statistical analysis

Data are represented as mean of individual cells ± standard deviation (s.d.) or mean of n (number of independent experiments) ± standard error of the mean (s.e.m.) as indicated. P values were determined by two-tailed Student's t-test and are indicated in all figures according to convention: n.s. = not significant, *p≤0.05, **p≤0.005 and ***p≤0.0005.

Appendix

Protocol for seFRET experiments

This protocol refers to a Leica microscope using LasF and the FRET wizard package, but it is general enough to be adapted to any widefield platform to perform seFRET experiments with living cells. I recommend you to use a positive as well as a negative control for your first experiments to learn what "real" cFRET and what false positive signals created by background or autofluorescence looks like. A good positive control could be the CFP-18AA-YFP construct used in this thesis.

- Day 1 - Seeding
  - Coat your glass-bottom dishes or coverslips with poly-L-lysine if you are going to work with cells hardly attaching to glass (e.g., HEK293) as follows:
    - add 400 μl of 0.01 % poly-L-lysine solution to the 10 mm glass window of a glass-bottom dish (or 10 mm coverslip) and incubate for 15 minutes at room temperature, scale volumes according to the glass surface in use
    - aspirate poly-L-lysine solution and wash intensively 3 times with H_2O or PBS [1]
    - air dry (under the clean bench) for 2 h
  - Seed cells in 35 mm glass-bottom dishes at an appropriate density, for HeLa and HEK293 seed roughly $0.3 \cdot 10^6$ cells per dish
  - (Optional) For robust cell lines, as are HEK293 and HeLa, the transfection mix can be directly added after seeding, see day 2 for a description of transfection and continue with day 3
- Day 2 - Transfection
  - The following numbers refer to the transfection of a 35 mm dish, scale up according to your numbers of dishes or dish size

[1] High concentrations of poly-L-lysine are very effective at killing cells, so don't use too highly concentrated solutions and wash intensively.

  - FuGENE is used at a ratio to DNA of 3:1 with a total DNA mass of 1 μg
  - Prepare FuGENE 6 mix by adding 3 μl FuGENE to 145 μl pre-warmed OptiMem
  - Incubate for 5 minutes at room temperature
  - Add DNA to a total amount of 1 μg, for two plasmids add 500 ng of each
  - (Mandatory for first experiments) transfect acceptor and donor only samples as well to determine correction factors [2]
  - Vortex DNA-FuGENE mix for 10 seconds and incubate for 20 minutes at room temperature
  - Add 150 μl of your transfection mix dropwise to your cells

- Day 3 - FRET measurement
  - Prepare imaging buffers and eventually drugs as described in the materials part
  - Start microscopy platform and wash perfusion system first with H_2O and then with your imaging buffers
  - Start LasF with the widefield tree option, switch to the FRET wizard
  - The FRET wizard is an intuitive plugin for LasF that guides you through an experiment, I will briefly describe some functions but for a detailed report refer to: https://www.leica-microsystems.com/science-lab/fret-sensitized-emission-wizard-widefield/
  - Configure your experiment by creating three channels in the "setup" panel, for better orientation and metadata generation name them meaningfully (suggestion: Donor, FRET, Acceptor), filter sets should be as follows:
    * Filter cube for all three channels: FRE (FRET cube containing only a dichroic mirror)
    * Donor channel: Excitation filter: CFP; Emission filter: CFP
    * FRET channel: Excitation filter: CFP; Emission filter: YFP
    * Acceptor channel: Excitation filter: YFP; Emission filter: YFP
  - Make sure that "Same exposure for all channels" is enabled, thereby a change of any parameter in one channel will automatically be applied to

[2] Take care that both are expressed correctly, e.g., using E-YFP alone as an acceptor only sample would lead to E-YFP being retained in the ER and consequently changed intensities you would encounter in a regular experiment

all channels of your experiment (a prerequisite for your correction factors to be working)

- Now follows the most delicate step of the setup: determination of the acquisition parameters
  - Take a sample expressing the FRET pair under investigation
  - Adjust light intensity, gain, and exposure for the first channel (e.g., Donor) in the first field of view until detected signals are in the mid detector range of the camera[3], make sure not to use long exposure times (exceeding 300 ms) since seFRET of living cells relies on short successive images of your sample
  - Inspect your sample in different field of views to see how homogenous the expression of your proteins and therefore how reliable your acquisition parameters are
  - Switch on the same sample to the second channel and check detected intensity levels; if you encounter overexposed cells reduce exposure time, gain or light intensity (keep in mind that this change affects all your channels)
  - If you changed the acquisition parameters, recheck the first channel if you can still detect enough or too much signal
  - Repeat detection test for the last channel
  - In the end, you need parameters that lead to detectable signals in all three channels, some trial and error is unavoidable in this step
  - You can save your settings now to have them later fastly available again
  - In some cases, it might be wise to determine several acquisition parameters if your sample is very heterogeneous in signal intensity, but keep in mind that you will need separate sets of correction factors for these acquisition sets!
- Now switch from "setup" to "Corr. Images" and change the sample on the microscope to a donor only sample
- Choose the "Donor" sample type and acquire several images of your cells with the acquisition parameters you determined before, sample type determines the names of acquired images and that LasF automatically uses them for correction factor calculation

[3] I highly recommend to use the "Over/Under-exposed LUT", since it is easier for your eyes to discriminate the intensity distribution of your sample and if you have oversaturated pixels. You find it at the upper left corner of the screen where your images are shown.

- Choose the "Acceptor" sample type and do the same with an acceptor only sample
- The "FRET" sample type would enable you to acquire images that are named by LasF accordingly; it is not different from the other sample types by any means, and you won't probably need it
- (Optional) Switch from "Corr. Images" to "Corr. Factors" and follow the instructions on the screen to determine the correction factors from the donor and acceptor only samples you just acquired. Alternatively, you can calculate them later by yourself using FIJI. It might be useful to get a quick estimation of your factors so that you can follow a live calculated cFRET map during image acquisition
- (Optional) If you already know your correction factors from other experiments you can enter them here manually without the need for real donor and acceptor only samples
- Now you are ready to go for your actual measurement:
  * Load a FRET pair sample (your sample) on the microscope and switch to "Evaluation"
  * Leave "method 1" as your calculation method, it generates cFRET maps normalized to overall acceptor signal (method 2 is for confocal setups, method 3 for ratiometric FRET sensors)
  * Activate "Acquisition mode" if you want to acquire time-lapse or z-Stacks, otherwise the button "Run Experiment" only acquires a single stack of one-time point
  * Define and run your experiment, if you entered correction factors before, the last window shows you a cFRET map of the current frame
  * To remove the background signal from that frame, draw a ROI in any channel and hit "Accept" under "Background Subtractions"
  * To follow cFRET (and the other channels) during your experiment, switch the upper header to Graphs, draw a ROI around your cell and the graphs update the signals of every frame [4]
  * after your measurement, save the .lif file (do NOT export tiff, you loose thereby the metadata of your experiment!) and go on with the evaluation using FIJI

[4] The FRET wizard uses the background information of a single frame for your whole stack. Since these values can vary highly during your experiment do not take time-lapse graphs too serious. Rather trust on those you calculate with FIJI.

- Evaluation
  - Having your images acquired, you need to set up your FIJI for calculating cFRET maps
  - I used the plugin PixFRET[5], which is quite useful for calculating single maps for one time point; to process time-lapse or z-stacks, you need a macro that adds this. If you need it, write me a message on www.researchgate.net (there is only one other Benjamin König until now, I am the one with green hair) or an E-mail at bennik2@freenet.de, and I send it to you.
  - For PixFRET to work you need to create single stacks for every time point in the following order: FRET, Donor, Acceptor
  - Enter your correction factors in the tabs "Donor model" and "acceptor model", if you don't have them yet you can calculate them as follows:
    - Remove background from all donor and acceptor only samples
    - For a donor only sample measure the intensity of a cell in the FRET channel and divide this value by the intensity of the same ROI in the donor channel. This percentage is your donor bleed through β
    - For an acceptor only sample measure the intensity of a cell in the FRET channel and divide this value by the intensity of the same ROI in the acceptor channel. This is the percentage of cross-excitation γ
  - To avoid artificial cFRET spikes at the boundaries of cells use the gaussian filter option in PixFRET. The default value of 2 usually works fine.
  - In PixFRET you can choose between different normalization methods. Which to choose depends on your sample and your question. I recommend to read this paper [145] if you are unsure which one would be the best for your application
  - Now draw a ROI in your FRET stack (in the order FRET, Donor, Acceptor) to determine background values and hit "Get" in the background section, then draw a ROI around your signal and hit "compute FRET"[6]
  - This is your cFRET map from which you can get the cFRET value

[5]It appears that a company tries to commercialize protocols and plugins, including PixFRET. So it is possible that you will not find a download link for PixFRET without paying for it. In this case: write me as described above. It is possible to write a code that does the same as PixFRET

[6]As already mentioned, this can be done automatically with a macro.

References

[1] Clay M. Armstrong. The na/k pump, cl ion, and osmotic stabilization of cells. *Proceedings of the National Academy of Sciences of the United States of America*, 100(10):6257–6262, 2003.

[2] Alexander Leaf. Maintenance of concentration gradients and regulation of cell volume. *Annals of the New York Academy of Sciences*, 72(12):396–404, 1959.

[3] D. C. Tosteson and J. F. Hoffman. Regulation of cell volume by active cation transport in high and low potassium sheep red cells. *J Gen Physiol*, 44:169–94, 1960.

[4] M. Wickson-Ginzburg and A. K. Solomon. Electrolyte metabolism in hela cells. *The Journal of general physiology*, 46(6):1303–1315, 1963.

[5] S. H. Khan, N. Ahmad, F. Ahmad, and R. Kumar. Naturally occurring organic osmolytes: from cell physiology to disease prevention. *IUBMB Life*, 62(12):891–5, 2010.

[6] C. W. Bourque. Central mechanisms of osmosensation and systemic osmoregulation. *Nat Rev Neurosci*, 9(7):519–31, 2008.

[7] F. Lang, G. L. Busch, M. Ritter, H. Volkl, S. Waldegger, E. Gulbins, and D. Haussinger. Functional significance of cell volume regulatory mechanisms. *Physiol Rev*, 78(1):247–306, 1998.

[8] E. K. Hoffmann, I. H. Lambert, and S. F. Pedersen. Physiology of cell volume regulation in vertebrates. *Physiol Rev*, 89(1):193–277, 2009.

[9] Kevin Strange, Toshiki Yamada, and Jerod S. Denton. A 30-year journey from volume-regulated anion currents to molecular structure of the lrrc8 channel. *The Journal of General Physiology*, 151(2):100–117, 2019.

[10] J C Parker, P B Dunham, and A P Minton. Effects of ionic strength on the regulation of na/h exchange and k-cl cotransport in dog red blood cells. *The Journal of General Physiology*, 105(6):677–699, 1995.

[11] Hélène Guizouarn and René Motais. Swelling activation of transport pathways in erythrocytes: effects of cl, ionic strength, and volume changes. *American Journal of Physiology-Cell Physiology*, 276(1):C210–C220, 1999.

[12] R. Motais, H. Guizouarn, and F. Garcia-Romeu. Red cell volume regulation: the pivotal role of ionic strength in controlling swelling-dependent transport systems. *Biochim Biophys Acta*, 1075(2):169–80, 1991.

[13] C. A. Hubner, V. Stein, I. Hermans-Borgmeyer, T. Meyer, K. Ballanyi, and T. J. Jentsch. Disruption of kcc2 reveals an essential role of k-cl cotransport already in early synaptic inhibition. *Neuron*, 30(2):515–24, 2001.

[14] A. Mercado, V. Broumand, K. Zandi-Nejad, A. H. Enck, and D. B. Mount. A c-terminal domain in kcc2 confers constitutive k+-cl- cotransport. *J Biol Chem*, 281(2):1016–26, 2006.

[15] J. E. Capo-Aponte, P. Iserovich, and P. S. Reinach. Characterization of regulatory volume behavior by fluorescence quenching in human corneal epithelial cells. *J Membr Biol*, 207(1):11–22, 2005.

[16] Kenneth B. E. Gagnon, Roger England, and Eric Delpire. Volume sensitivity of cation-cl cotransporters is modulated by the interaction of two kinases: Ste20-related proline-alanine-rich kinase and wnk4. *American Journal of Physiology-Cell Physiology*, 290(1):C134–C142, 2006.

[17] A. Mercado, L. Song, N. Vazquez, D. B. Mount, and G. Gamba. Functional comparison of the k+-cl- cotransporters kcc1 and kcc4. *J Biol Chem*, 275(39):30326–34, 2000.

[18] D. B. Mount, A. Mercado, L. Song, J. Xu, Jr. George, A. L., E. Delpire, and G. Gamba. Cloning and characterization of kcc3 and kcc4, new members of the cation-chloride cotransporter gene family. *J Biol Chem*, 274(23):16355–62, 1999.

[19] Joanne E. Race, Fadi N. Makhlouf, Paul J. Logue, Frederick H. Wilson, Philip B. Dunham, and Eli J. Holtzman. Molecular cloning and functional characterization of kcc3, a new k-cl cotransporter. *American Journal of Physiology-Cell Physiology*, 277(6):C1210–C1219, 1999.

[20] Kevin Strange, Thomas D. Singer, Rebecca Morrison, and Eric Delpire. Dependence of kcc2 k-cl cotransporter activity on a conserved carboxy terminus tyrosine residue. *American Journal of Physiology-Cell Physiology*, 279(3):C860–C867, 2000.

[21] M. B. Rust, S. L. Alper, Y. Rudhard, B. E. Shmukler, R. Vicente, C. Brugnara, M. Trudel, T. J. Jentsch, and C. A. Hubner. Disruption of erythroid k-cl cotransporters alters erythrocyte volume and partially rescues erythrocyte dehydration in sad mice. *J Clin Invest*, 117(6):1708–17, 2007.

[22] T. J. Jentsch. Vracs and other ion channels and transporters in the regulation of cell volume and beyond. *Nat Rev Mol Cell Biol*, 17(5):293–307, 2016.

[23] H. C. Hartzell, Z. Qu, K. Yu, Q. Xiao, and L. T. Chien. Molecular physiology of bestrophins: multifunctional membrane proteins linked to best disease and other retinopathies. *Physiol Rev*, 88(2):639–72, 2008.

[24] N. Pedemonte and L. J. Galietta. Structure and function of tmem16 proteins (anoctamins). *Physiol Rev*, 94(2):419–59, 2014.

[25] M. D. Cahalan and R. S. Lewis. Role of potassium and chloride channels in volume regulation by t lymphocytes. *Soc Gen Physiol Ser*, 43:281–301, 1988.

[26] A. Hazama and Y. Okada. Ca2+ sensitivity of volume-regulatory k+ and cl- channels in cultured human epithelial cells. *J Physiol*, 402:687–702, 1988.

[27] Bernd Nilius, Jan Sehrer, Felix Viana, Christine De Greef, Luc Raeymaekers, Jan Eggermont, and Guy Droogmans. Volume-activated cl- currents in different mammalian non-excitable cell types. *Pflügers Archiv*, 428(3):364–371, 1994.

[28] Toshiki Yamada, Robert Wondergem, Rebecca Morrison, Viravuth P. Yin, and Kevin Strange. Leucine-rich repeat containing protein lrrc8a is essential for swelling-activated cl currents and embryonic development in zebrafish. *Physiological Reports*, 4(19):e12940, 2016.

[29] Z. Qiu, A. E. Dubin, J. Mathur, B. Tu, K. Reddy, L. J. Miraglia, J. Reinhardt, A. P. Orth, and A. Patapoutian. Swell1, a plasma membrane protein, is an essential component of volume-regulated anion channel. *Cell*, 157(2):447–458, 2014.

[30] F. K. Voss, F. Ullrich, J. Munch, K. Lazarow, D. Lutter, N. Mah, M. A. Andrade-Navarro, J. P. von Kries, T. Stauber, and T. J. Jentsch. Identification of lrrc8 heteromers as an essential component of the volume-regulated anion channel vrac. *Science*, 344(6184):634–8, 2014.

[31] Jennifer C. Lueck, Dmytro Puchkov, Florian Ullrich, and Thomas J. Jentsch. Lrrc8/vrac anion channels are required for late stages of spermatid development in mice. *Journal of Biological Chemistry*, 293(30):11796–11808, 2018.

[32] F. Formaggio, E. Saracino, M. G. Mola, S. B. Rao, M. Amiry-Moghaddam, M. Muccini, R. Zamboni, G. P. Nicchia, M. Caprini, and V. Benfenati. Lrrc8a is essential for swelling-activated chloride current and for regulatory volume decrease in astrocytes. *Faseb j*, 33(1):101–113, 2019.

[33] C. Kang, L. Xie, S. K. Gunasekar, A. Mishra, Y. Zhang, S. Pai, Y. Gao, A. Kumar, A. W. Norris, S. B. Stephens, and R. Sah. Swell1 is a glucose sensor regulating beta-cell excitability and systemic glycaemia. *Nat Commun*, 9(1):367, 2018.

[34] María C. Hyzinski-García, Alena Rudkouskaya, and Alexander A. Mongin. Lrrc8a protein is indispensable for swelling-activated and atp-induced release of excitatory amino acids in rat astrocytes. *The Journal of physiology*, 592(22):4855–4862, 2014.

[35] D. Lutter, F. Ullrich, J. C. Lueck, S. Kempa, and T. J. Jentsch. Selective transport of neurotransmitters and modulators by distinct volume-regulated lrrc8 anion channels. *J Cell Sci*, 130(6):1122–1133, 2017.

[36] L. Chen, B. Konig, T. Liu, S. Pervaiz, Y. S. Razzaque, and T. Stauber. More than just a pressure relief valve: physiological roles of volume-regulated lrrc8 anion channels. *Biol Chem*, 2019.

[37] Carl D. Bortner, Francis M. Hughes, and John A. Cidlowski. A primary role for k+ and na+ efflux in the activation of apoptosis. *Journal of Biological Chemistry*, 272(51):32436–32442, 1997.

[38] C. D. Bortner and J. A. Cidlowski. A necessary role for cell shrinkage in apoptosis. *Biochem Pharmacol*, 56(12):1549–59, 1998.

[39] K. Kunzelmann. Ion channels in regulated cell death. *Cell Mol Life Sci*, 73(11-12):2387–403, 2016.

[40] T. Shimizu, H. Ohtake, T. Fujii, Y. Tabuchi, and H. Sakai. Volume-sensitive outwardly rectifying cl(-) channels contribute to butyrate-triggered apoptosis of murine colonic epithelial mce301 cells. *J Physiol Sci*, 65(2):151–7, 2015.

[41] Yuesheng Xia, Yan Liu, Tong Xia, Xing Li, Cong Huo, Xin Jia, Lin Wang, Rong Xu, Ning Wang, Mingming Zhang, Hong Li, and Xiaoming Wang. Activation of volume-sensitive cl-channel mediates autophagy-related cell death in myocardial ischaemia/reperfusion injury. *Oncotarget*, 7(26):39345–39362, 2016.

[42] K. Kumagai, F. Toyoda, C. A. Staunton, T. Maeda, N. Okumura, H. Matsuura, Y. Matsusue, S. Imai, and R. Barrett-Jolley. Activation of a chondrocyte volume-sensitive cl(-) conductance prior to macroscopic cartilage lesion formation in the rabbit knee anterior cruciate ligament transection osteoarthritis model. *Osteoarthritis Cartilage*, 24(10):1786–1794, 2016.

[43] R. Planells-Cases, D. Lutter, C. Guyader, N. M. Gerhards, F. Ullrich, D. A. Elger, A. Kucukosmanoglu, G. Xu, F. K. Voss, S. M. Reincke, T. Stauber, V. A. Blomen, D. J. Vis, L. F. Wessels, T. R. Brummelkamp, P. Borst, S. Rottenberg, and T. J. Jentsch. Subunit composition of vrac channels determines substrate specificity and cellular resistance to pt-based anti-cancer drugs. *Embo j*, 34(24):2993–3008, 2015.

[44] T. Shimizu, T. Numata, and Y. Okada. A role of reactive oxygen species in apoptotic activation of volume-sensitive cl(-) channel. *Proc Natl Acad Sci U S A*, 101(17):6770–3, 2004.

[45] L. Sirianant, P. Wanitchakool, J. Ousingsawat, R. Benedetto, A. Zormpa, I. Cabrita, R. Schreiber, and K. Kunzelmann. Non-essential contribution of lrrc8a to volume regulation. *Pflugers Arch*, 468(5):805–16, 2016.

[46] F. Lang, E. Shumilina, M. Ritter, E. Gulbins, A. Vereninov, and S. M. Huber. Ion channels and cell volume in regulation of cell proliferation and apoptotic cell death. *Contrib Nephrol*, 152:142–160, 2006.

[47] W. Liang, L. Huang, D. Zhao, J. Z. He, P. Sharma, J. Liu, A. O. Gramolini, M. E. Ward, H. C. Cho, and P. H. Backx. Swelling-activated cl- currents and intracellular clc-3 are involved in proliferation of human pulmonary artery smooth muscle cells. *J Hypertens*, 32(2):318–30, 2014.

[48] B. Nilius, J. Eggermont, T. Voets, G. Buyse, V. Manolopoulos, and G. Droogmans. Properties of volume-regulated anion channels in mammalian cells. *Prog Biophys Mol Biol*, 68(1):69–119, 1997.

[49] T. Voets, G. Szucs, G. Droogmans, and B. Nilius. Blockers of volume-activated cl- currents inhibit endothelial cell proliferation. *Pflugers Arch*, 431(1):132–4, 1995.

[50] Jerzy M. Dziekan, Han Yu, Dan Chen, Lingyun Dai, Grennady Wirjanata, Andreas Larsson, Nayana Prabhu, Radoslaw M. Sobota, Zbynek Bozdech, and Pär Nordlund. Identifying purine nucleoside phosphorylase as the target of quinine using cellular thermal shift assay. *Science Translational Medicine*, 11(473):eaau3174, 2019.

[51] T. A. Bogush, B. B. Polezhaev, I. A. Mamichev, E. A. Bogush, B. E. Polotsky, S. A. Tjulandin, and A. B. Ryabov. Tamoxifen never ceases to amaze: New findings on non-estrogen receptor molecular targets and mediated effects. *Cancer Invest*, 36(4):211–220, 2018.

[52] Nicole H. Bowens, Preeti Dohare, Yu-Hung Kuo, and Alexander A. Mongin. Dcpib, the proposed selective blocker of volume-regulated anion channels, inhibits several glutamate transport pathways in glial cells. *Molecular pharmacology*, 83(1):22–32, 2013.

[53] T. Liu and T. Stauber. The volume-regulated anion channel lrrc8/vrac is dispensable for cell proliferation and migration. *Int J Mol Sci*, 20(11), 2019.

[54] A. Schwab, A. Fabian, P. J. Hanley, and C. Stock. Role of ion channels and transporters in cell migration. *Physiol Rev*, 92(4):1865–913, 2012.

[55] R. Wong, W. Chen, X. Zhong, J. T. Rutka, Z. P. Feng, and H. S. Sun. Swelling-induced chloride current in glioblastoma proliferation, migration, and invasion. *J Cell Physiol*, 233(1):363–370, 2018.

[56] Haifeng Zhang, Zhiqin Deng, Dongxia Zhang, Huarong Li, Lei Zhang, Jin Niu, Wanhong Zuo, Rao Fu, Lihong Fan, Jiang-Hong Ye, and Junjun She. High expression of leucine-rich repeat-containing 8a is indicative of a worse outcome of colon cancer patients by enhancing cancer cell growth and metastasis. *Oncology reports*, 40(3):1275–1286, 2018.

[57] T. Akita and Y. Okada. Characteristics and roles of the volume-sensitive outwardly rectifying (vsor) anion channel in the central nervous system. *Neuroscience*, 275:211–31, 2014.

[58] Alexander A. Mongin. Volume-regulated anion channel–a frenemy within the brain. *Pflugers Archiv : European journal of physiology*, 468(3):421–441, 2016.

[59] A. L. Schober, C. S. Wilson, and A. A. Mongin. Molecular composition and heterogeneity of the lrrc8-containing swelling-activated osmolyte channels in primary rat astrocytes. *J Physiol*, 595(22):6939–6951, 2017.

[60] J. Yang, M. D. C. Vitery, J. Chen, J. Osei-Owusu, J. Chu, and Z. Qiu. Glutamate-releasing swell1 channel in astrocytes modulates synaptic transmission and promotes brain damage in stroke. *Neuron*, 102(4):813–827.e6, 2019.

[61] N. J. Allen and C. Eroglu. Cell biology of astrocyte-synapse interactions. *Neuron*, 96(3):697–708, 2017.

[62] N. B. Hamilton and D. Attwell. Do astrocytes really exocytose neurotransmitters? *Nat Rev Neurosci*, 11(4):227–38, 2010.

[63] L. Kumar, J. Chou, C. S. Yee, A. Borzutzky, E. H. Vollmann, U. H. von Andrian, S. Y. Park, G. Hollander, J. P. Manis, P. L. Poliani, and R. S. Geha. Leucine-rich repeat containing 8a (lrrc8a) is essential for t lymphocyte development and function. *J Exp Med*, 211(5):929–42, 2014.

[64] A. Lalouette, A. Lablack, J. L. Guenet, X. Montagutelli, and D. Segretain. Male sterility caused by sperm cell-specific structural abnormalities in ebouriffe, a new mutation of the house mouse. *Biol Reprod*, 55(2):355–63, 1996.

[65] C. D. Platt, J. Chou, P. Houlihan, Y. R. Badran, L. Kumar, W. Bainter, P. L. Poliani, C. J. Perez, S. Y. R. Dent, D. E. Clapham, F. Benavides, and R. S. Geha. Leucine-rich repeat containing 8a (lrrc8a)-dependent volume-regulated anion channel activity is dispensable for t-cell development and function. *J Allergy Clin Immunol*, 140(6):1651–1659.e1, 2017.

[66] H. E. Miley, E. A. Sheader, P. D. Brown, and L. Best. Glucose-induced swelling in rat pancreatic beta-cells. *The Journal of physiology*, 504 (Pt 1)(Pt 1):191–198, 1997.

[67] L. Best, P. D. Brown, A. Sener, and W. J. Malaisse. Electrical activity in pancreatic islet cells: The vrac hypothesis. *Islets*, 2(2):59–64, 2010.

[68] Till Stuhlmann, Rosa Planells-Cases, and Thomas J. Jentsch. Lrrc8/vrac anion channels enhance β-cell glucose sensing and insulin secretion. *Nature Communications*, 9(1):1974, 2018.

[69] D. Deneka, M. Sawicka, A. K. M. Lam, C. Paulino, and R. Dutzler. Structure of a volume-regulated anion channel of the lrrc8 family. *Nature*, 558(7709):254–259, 2018.

[70] G. Kasuya, T. Nakane, T. Yokoyama, Y. Jia, M. Inoue, K. Watanabe, R. Nakamura, T. Nishizawa, T. Kusakizako, A. Tsutsumi, H. Yanagisawa, N. Dohmae, M. Hattori, H. Ichijo, Z. Yan, M. Kikkawa, M. Shirouzu, R. Ishitani, and O. Nureki. Cryo-em structures of the human volume-regulated anion channel lrrc8. *Nat Struct Mol Biol*, 25(9):797–804, 2018.

[71] Jennifer M. Kefauver, Kei Saotome, Adrienne E. Dubin, Jesper Pallesen, Christopher A. Cottrell, Stuart M. Cahalan, Zhaozhu Qiu, Gunhee Hong, Christopher S. Crowley, Tess Whitwam, Wen-Hsin Lee, Andrew B. Ward, and Ardem Patapoutian. Structure of the human volume regulated anion channel. *eLife*, 7:e38461, 2018.

[72] David M. Kern, SeCheol Oh, Richard K. Hite, and Stephen G. Brohawn. Cryo-em structures of the dcpib-inhibited volume-regulated anion channel lrrc8a in lipid nanodiscs. *eLife*, 8:e42636, 2019.

[73] F. Abascal and R. Zardoya. Lrrc8 proteins share a common ancestor with pannexins, and may form hexameric channels involved in cell-cell communication. *Bioessays*, 34(7):551–60, 2012.

[74] Benjamin König and Tobias Stauber. Biophysics and structure-function relationships of lrrc8-formed volume-regulated anion channels. *Biophysical Journal*, 116(7):1185–1193, 2019.

[75] Julio F. Cordero-Morales and Valeria Vásquez. How lipids contribute to ion channel function, a fat perspective on direct and indirect interactions. *Current Opinion in Structural Biology*, 51:92–98, 2018.

[76] Atsunori Oshima, Kazutoshi Tani, and Yoshinori Fujiyoshi. Atomic structure of the innexin-6 gap junction channel determined by cryo-em. *Nature Communications*, 7(1):13681, 2016.

[77] S. Maeda, S. Nakagawa, M. Suga, E. Yamashita, A. Oshima, Y. Fujiyoshi, and T. Tsukihara. Structure of the connexin 26 gap junction channel at 3.5 a resolution. *Nature*, 458(7238):597–602, 2009.

[78] Pingzheng Zhou, Maya M Polovitskaya, and Thomas J. Jentsch. Lrrc8 amino-termini influence pore properties and gating of volume-regulated vrac anion channels. *Journal of Biological Chemistry*, 2018.

[79] R. Syeda, Z. Qiu, A. E. Dubin, S. E. Murthy, M. N. Florendo, D. E. Mason, J. Mathur, S. M. Cahalan, E. C. Peters, M. Montal, and A. Patapoutian. Lrrc8 proteins form volume-regulated anion channels that sense ionic strength. *Cell*, 164(3):499–511, 2016.

[80] H. Gaitan-Penas, A. Gradogna, L. Laparra-Cuervo, C. Solsona, V. Fernandez-Duenas, A. Barrallo-Gimeno, F. Ciruela, M. Lakadamyali, M. Pusch, and R. Estevez. Investigation of lrrc8-mediated volume-regulated anion currents in xenopus oocytes. *Biophys J*, 111(7):1429–1443, 2016.

[81] Tingting Yang, Qun Liu, Brian Kloss, Renato Bruni, Ravi C. Kalathur, Youzhong Guo, Edda Kloppmann, Burkhard Rost, Henry M. Colecraft, and Wayne A. Hendrickson. Structure and selectivity in bestrophin ion channels. *Science (New York, N.Y.)*, 346(6207):355–359, 2014.

[82] Y. Okada. Volume expansion-sensing outward-rectifier cl- channel: fresh start to the molecular identity and volume sensor. *Am J Physiol*, 273(3 Pt 1):C755–89, 1997.

[83] Jianqiang Bao, Carlos J. Perez, Jeesun Kim, Huan Zhang, Caitlin J. Murphy, Tewfik Hamidi, Jean Jaubert, Craig D. Platt, Janet Chou, Meichun Deng, Meng-Hua Zhou, Yuying Huang, Héctor Gaitán-Peñas, Jean-Louis Guénet, Kevin Lin, Yue Lu, Taiping Chen, Mark T. Bedford, Sharon Yr Dent, John H. Richburg, Raúl Estévez, Hui-Lin Pan, Raif S. Geha, Qinghua Shi, and Fernando Benavides. Deficient lrrc8a-dependent volume-regulated anion channel activity is associated with male infertility in mice. *JCI insight*, 3(16):e99767, 2018.

[84] Human genomics. the genotype-tissue expression (gtex) pilot analysis: multitissue gene regulation in humans. *Science*, 348(6235):648–60, 2015.

[85] P. S. Jackson and K. Strange. Volume-sensitive anion channels mediate swelling-activated inositol and taurine efflux. *American Journal of Physiology-Cell Physiology*, 265(6):C1489–C1500, 1993.

[86] P. S. Jackson, K. Churchwell, N. Ballatori, J. L. Boyer, and K. Strange. Swelling-activated anion conductance in skate hepatocytes: regulation by cell cl- and atp. *Am J Physiol*, 270(1 Pt 1):C57–66, 1996.

[87] V. G. Manolopoulos, T. Voets, P. E. Declercq, G. Droogmans, and B. Nilius. Swelling-activated efflux of taurine and other organic osmolytes in endothelial cells. *American Journal of Physiology-Cell Physiology*, 273(1):C214–C222, 1997.

[88] S. H. Boese, F. Wehner, and R. K. Kinne. Taurine permeation through swelling-activated anion conductance in rat imcd cells in primary culture. *Am J Physiol*, 271(3 Pt 2):F498–507, 1996.

[89] O. P. Hamill, A. Marty, E. Neher, B. Sakmann, and F. J. Sigworth. Improved patch-clamp techniques for high-resolution current recording from cells and cell-free membrane patches. *Pflügers Archiv*, 391(2):85–100, 1981.

[90] A. Huxley. From overshoot to voltage clamp. *Trends Neurosci*, 25(11):553–8, 2002.

[91] Erwin Neher and Bert Sakmann. The patch clamp technique. *Scientific American*, 266(3):44–51, 1992.

[92] P. S. Jackson and K. Strange. Characterization of the voltage-dependent properties of a volume-sensitive anion conductance. *J Gen Physiol*, 105(5):661–76, 1995.

[93] T. Voets, G. Droogmans, and B. Nilius. Modulation of voltage-dependent properties of a swelling-activated cl- current. *J Gen Physiol*, 110(3):313–25, 1997.

[94] Victor G. Romanenko, George H. Rothblat, and Irena Levitan. Sensitivity of volume-regulated anion current to cholesterol structural analogues. *The Journal of general physiology*, 123(1):77–87, 2004.

[95] P. S. Jackson and K. Strange. Single-channel properties of a volume-sensitive anion conductance. current activation occurs by abrupt switching of closed channels to an open state. *The Journal of general physiology*, 105(5):643–660, 1995.

[96] J. E. Linley. Perforated whole-cell patch-clamp recording. *Methods Mol Biol*, 998:149–57, 2013.

[97] L. Best and P. D. Brown. Studies of the mechanism of activation of the volume-regulated anion channel in rat pancreatic beta-cells. *J Membr Biol*, 230(2):83–91, 2009.

[98] L. Best and A. P. Yates. Electrophysiological effects of osmotic cell shrinkage in rat pancreatic beta-cells. *Islets*, 2(5):303–7, 2010.

[99] M. Jakab, M. Grundbichler, J. Benicky, A. Ravasio, S. Chwatal, S. Schmidt, V. Strbak, J. Fürst, M. Paulmichl, and M. Ritter. Glucose induces anion conductance and cytosol-to-membrane transposition of icln in ins-1e rat insulinoma cells. *Cellular Physiology and Biochemistry*, 18(1-3):21–34, 2006.

[100] Y. E. Han, J. Kwon, J. Won, H. An, M. W. Jang, J. Woo, J. S. Lee, M. G. Park, B. E. Yoon, S. E. Lee, E. M. Hwang, J. Y. Jung, H. Park, S. J. Oh, and C. J. Lee. Tweety-homolog (ttyh) family encodes the pore-forming subunits of the swelling-dependent volume-regulated anion channel (vracswell) in the brain. *Exp Neurobiol*, 28(2):183–215, 2019.

[101] M. C. Hyzinski-Garcia, M. Y. Vincent, R. E. Haskew-Layton, P. Dohare, Jr. Keller, R. W., and A. A. Mongin. Hypo-osmotic swelling modifies glutamate-glutamine cycle in the cerebral cortex and in astrocyte cultures. *J Neurochem*, 118(1):140–52, 2011.

[102] S. Broer. Adaptation of plasma membrane amino acid transport mechanisms to physiological demands. *Pflugers Arch*, 444(4):457–66, 2002.

[103] Henry A. Polach. Evaluation and status of liquid scintillation counting for radiocarbon dating. *Radiocarbon*, 29(1):1–11, 1987.

[104] C. S. Wilson, M. D. Bach, Z. Ashkavand, K. R. Norman, N. Martino, A. P. Adam, and A. A. Mongin. Metabolic constraints of swelling-activated glutamate release in astrocytes and their implication for ischemic tissue damage. *J Neurochem*, 2019.

[105] H. K. Kimelberg, S. K. Goderie, S. Higman, S. Pang, and R. A. Waniewski. Swelling-induced release of glutamate, aspartate, and taurine from astrocyte cultures. *J Neurosci*, 10(5):1583–91, 1990.

[106] D. L. Martin, V. Madelian, B. Seligmann, and W. Shain. The role of osmotic pressure and membrane potential in k(+)-stimulated taurine release from cultured astrocytes and lrm55 cells. *J Neurosci*, 10(2):571–7, 1990.

[107] L. J. Galietta, P. M. Haggie, and A. S. Verkman. Green fluorescent protein-based halide indicators with improved chloride and iodide affinities. *FEBS Lett*, 499(3):220–4, 2001.

[108] A. Ghosh, N. Khandelwal, A. Kumar, and A. K. Bera. Leucine-rich repeat-containing 8b protein is associated with the endoplasmic reticulum ca(2+) leak in hek293 cells. *J Cell Sci*, 130(22):3818–3828, 2017.

[109] Michael A. Model. Methods for cell volume measurement. *Cytometry Part A*, 93(3):281–296, 2018.

[110] Else K. Hoffmann, Lars Ole Simonsen, and Ian H. Lambert. Volume-induced increase of k+ and cl- permeabilities in ehrlich ascites tumor cells. role of internal ca2+. *The Journal of Membrane Biology*, 78(3):211–222, 1984.

[111] Janina Trothe, Dirk Ritzmann, Victoria Lang, Paul Scholz, Ümit Pul, Roland Kaufmann, Claudia Buerger, and Torsten Ertongur-Fauth. Hypotonic stress response of human keratinocytes involves lrrc8a as component of volume-regulated anion channels. *Experimental Dermatology*, 27(12):1352–1360, 2018.

[112] Jonas Friard, Michel Tauc, Marc Cougnon, Vincent Compan, Christophe Duranton, and Isabelle Rubera. Comparative effects of chloride channel inhibitors on lrrc8/vrac-mediated chloride conductance. *Frontiers in Pharmacology*, 8(328), 2017.

[113] W. E. Crowe, J. Altamirano, L. Huerto, and F. J. Alvarez-Leefmans. Volume changes in single n1e-115 neuroblastoma cells measured with a fluorescent probe. *Neuroscience*, 69(1):283–96, 1995.

[114] Steffen Hamann, Jens Folke Kiilgaard, Thomas Litman, Francisco J. Alvarez-Leefmans, Benny R. Winther, and Thomas Zeuthen. Measurement of cell volume changes by fluorescence self-quenching. *Journal of Fluorescence*, 12(2):139–145, 2002.

[115] Carolyn L. Cannon, Srisaila Basavappa, and Kevin Strange. Intracellular ionic strength regulates the volume sensitivity of a swelling-activated anion channel. *American Journal of Physiology-Cell Physiology*, 275(2):C416–C422, 1998.

[116] Tamara Bond, Srisaila Basavappa, Michael Christensen, and Kevin Strange. Atp dependence of the i¡sub¿cl, swell¡/sub¿ channel varies with rate of cell swelling. *Evidence for Two Modes of Channel Activation*, 113(3):441–456, 1999.

[117] Antonella Gradogna, Paola Gavazzo, Anna Boccaccio, and Michael Pusch. Subunit-dependent oxidative stress sensitivity of lrrc8 volume-regulated anion channels. *The Journal of Physiology*, 595(21):6719–6733, 2017.

[118] A. A. Mongin and S. N. Orlov. Mechanisms of cell volume regulation and possible nature of the cell volume sensor. *Pathophysiology*, 8(2):77–88, 2001.

[119] T. Voets, G. Droogmans, G. Raskin, J. Eggermont, and B. Nilius. Reduced intracellular ionic strength as the initial trigger for activation of endothelial volume-regulated anion channels. *Proc Natl Acad Sci U S A*, 96(9):5298–303, 1999.

[120] R. Z. Sabirov, J. Prenen, T. Tomita, G. Droogmans, and B. Nilius. Reduction of ionic strength activates single volume-regulated anion channels (vrac) in endothelial cells. *Pflugers Arch*, 439(3):315–20, 2000.

[121] J. Zhang and M. Lieberman. Chloride conductance is activated by membrane distention of cultured chick heart cells. *Cardiovasc Res*, 32(1):168–79, 1996.

[122] L. Best and P. D. Brown. Studies of the mechanism of activation of the volume-regulated anion channel in rat pancreatic beta-cells. *J Membr Biol*, 230(2):83–91, 2009.

[123] P. S. Jackson, R. Morrison, and K. Strange. The volume-sensitive organic osmolyte-anion channel vsoac is regulated by nonhydrolytic atp binding. *Am J Physiol*, 267(5 Pt 1):C1203–9, 1994.

[124] H. E. Miley, P. D. Brown, and L. Best. Regulation of a volume-sensitive anion channel in rat pancreatic beta-cells by intracellular adenine nucleotides. *J Physiol*, 515 (Pt 2):413–7, 1999.

[125] S. Oiki, M. Kubo, and Y. Okada. Mg2+ and atp-dependence of volume-sensitive cl- channels in human epithelial cells. *Jpn J Physiol*, 44 Suppl 2:S77–9, 1994.

[126] A. J. Patel, I. Lauritzen, M. Lazdunski, and E. Honore. Disruption of mitochondrial respiration inhibits volume-regulated anion channels and provokes neuronal cell swelling. *J Neurosci*, 18(9):3117–23, 1998.

[127] A. Bryan-Sisneros, V. Sabanov, S. M. Thoroed, and P. Doroshenko. Dual role of atp in supporting volume-regulated chloride channels in mouse fibroblasts. *Biochimica et Biophysica Acta (BBA) - Biomembranes*, 1468(1):63–72, 2000.

[128] D. W. Hilgemann. Cytoplasmic atp-dependent regulation of ion transporters and channels: mechanisms and messengers. *Annu Rev Physiol*, 59:193–220, 1997.

[129] S. Sorota. Tyrosine protein kinase inhibitors prevent activation of cardiac swelling-induced chloride current. *Pflugers Arch*, 431(2):178–85, 1995.

[130] V. Crepel, W. Panenka, M. E. Kelly, and B. A. MacVicar. Mitogen-activated protein and tyrosine kinases in the activation of astrocyte volume-activated chloride current. *J Neurosci*, 18(4):1196–206, 1998.

[131] T. Voets, V. Manolopoulos, J. Eggermont, C. Ellory, G. Droogmans, and B. Nilius. Regulation of a swelling-activated chloride current in bovine endothelium by protein tyrosine phosphorylation and g proteins. *J Physiol*, 506 (Pt 2):341–52, 1998.

[132] P. Doroshenko. Pervanadate inhibits volume-sensitive chloride current in bovine chromaffin cells. *Pflugers Arch*, 435(2):303–9, 1998.

[133] S. M. Thoroed, A. Bryan-Sisneros, and P. Doroshenko. Protein phosphotyrosine phosphatase inhibitors suppress regulatory volume decrease and the volume-sensitive cl- conductance in mouse fibroblasts. *Pflugers Arch*, 438(2):133–40, 1999.

[134] A. Rudkouskaya, A. Chernoguz, R. E. Haskew-Layton, and A. A. Mongin. Two conventional protein kinase c isoforms, alpha and beta i, are involved in the atp-induced activation of volume-regulated anion channel and glutamate release in cultured astrocytes. *J Neurochem*, 105(6):2260–70, 2008.

[135] M. Hermoso, P. Olivero, R. Torres, A. Riveros, A. F. Quest, and A. Stutzin. Cell volume regulation in response to hypotonicity is impaired in hela cells expressing a protein kinase calpha mutant lacking kinase activity. *J Biol Chem*, 279(17):17681–9, 2004.

[136] I. Ben Soussia, F. Mies, R. Naeije, and V. Shlyonsky. Melatonin down-regulates volume-sensitive chloride channels in fibroblasts. *Pflugers Arch*, 464(3):273–85, 2012.

[137] L. Catacuzzeno, A. Michelucci, L. Sforna, F. Aiello, M. Sciaccaluga, B. Fioretti, E. Castigli, and F. Franciolini. Identification of key signaling molecules involved in the activation of the swelling-activated chloride current in human glioblastoma cells. *J Membr Biol*, 247(1):45–55, 2014.

[138] Gregory M. Dick, Karri K. Bradley, Burton Horowitz, Joseph R. Hume, and Kenton M. Sanders. Functional and molecular identification of a novel chloride conductance in canine colonic smooth muscle. *American Journal of Physiology-Cell Physiology*, 275(4):C940–C950, 1998.

[139] Sophia F. von Weikersthal, Margery A. Barrand, and Stephen B. Hladky. Functional and molecular characterization of a volume-sensitive chloride current in rat brain endothelial cells. *The Journal of Physiology*, 516(1):75–84, 1999.

[140] Alexander Zholos, Benjamin Beck, Vadym Sydorenko, Loïc Lemonnier, Pascal Bordat, Natalia Prevarskaya, and Roman Skryma. Ca(2+)- and volume-sensitive chloride currents are differentially regulated by agonists and store-operated ca2+ entry. *The Journal of general physiology*, 125(2):197–211, 2005.

[141] Katia Hiersemenzel, Euan Brown, and Rory Duncan. Imaging large cohorts of single ion channels and their activity. *Frontiers in Endocrinology*, 4(114), 2013.

[142] Ekaterina A. Bykova, Xiao-Dong Zhang, Tsung-Yu Chen, and Jie Zheng. Large movement in the c terminus of clc-0 chloride channel during slow gating. *Nature Structural &Amp; Molecular Biology*, 13:1115, 2006.

[143] T. Y. Chen. Structure and function of clc channels. *Annu Rev Physiol*, 67:809–39, 2005.

[144] Linda G. Zachariassen, Ljudmila Katchan, Anna G. Jensen, Darryl S. Pickering, Andrew J. R. Plested, and Anders S. Kristensen. Structural rearrangement of the intracellular domains during ampa receptor activation. *Proceedings of the National Academy of Sciences*, 113(27):E3950–E3959, 2016.

[145] A. D. Elder, A. Domin, G. S. Kaminski Schierle, C. Lindon, J. Pines, A. Esposito, and C. F. Kaminski. A quantitative protocol for dynamic measurements of protein interactions by förster resonance energy transfer-sensitized fluorescence emission. *Journal of the Royal Society Interface*, 6(Suppl 1):S59–S81, 2009.

[146] I. Levitan, C. Almonte, P. Mollard, and S. S. Garber. Modulation of a volume-regulated chloride current by f-actin. *The Journal of Membrane Biology*, 147(3):283–294, 1995.

[147] B. Liu, B. Poolman, and A. J. Boersma. Ionic strength sensing in living cells. *ACS Chem Biol*, 12(10):2510–2514, 2017.

[148] C. T. Rollins, V. M. Rivera, D. N. Woolfson, T. Keenan, M. Hatada, S. E. Adams, L. J. Andrade, D. Yaeger, M. R. van Schravendijk, D. A. Holt, M. Gilman, and T. Clackson. A ligand-reversible dimerization system for controlling protein-protein interactions. *Proc Natl Acad Sci U S A*, 97(13):7096–101, 2000.

[149] V. M. Rivera, X. Wang, S. Wardwell, N. L. Courage, A. Volchuk, T. Keenan, D. A. Holt, M. Gilman, L. Orci, Jr. Cerasoli, F., J. E. Rothman, and T. Clackson. Regulation of protein secretion through controlled aggregation in the endoplasmic reticulum. *Science*, 287(5454):826–30, 2000.

[150] S. Morishima, T. Shimizu, H. Kida, and Y. Okada. Volume expansion sensitivity of swelling-activated cl(-) channel in human epithelial cells. *Jpn J Physiol*, 50(2):277–80, 2000.

[151] E. M. Schwiebert, J. W. Mills, and B. A. Stanton. Actin-based cytoskeleton regulates a chloride channel and cell volume in a renal cortical collecting duct cell line. *J Biol Chem*, 269(10):7081–9, 1994.

[152] T. K. Klausen, C. Hougaard, E. K. Hoffmann, and S. F. Pedersen. Cholesterol modulates the volume-regulated anion current in ehrlich-lettre ascites cells via effects on rho and f-actin. *Am J Physiol Cell Physiol*, 291(4):C757–71, 2006.

[153] M. Caramia, L. Sforna, F. Franciolini, and L. Catacuzzeno. The volume-regulated anion channel in glioblastoma. *Cancers (Basel)*, 11(3), 2019.

[154] J. Mao, L. Wang, A. Fan, J. Wang, B. Xu, T. J. C. Jacob, and L. Chen. Blockage of volume-activated chloride channels inhibits migration of nasopharyngeal carcinoma cells. *Cellular Physiology and Biochemistry*, 19(5-6):249–258, 2007.

[155] P. J. Robinson. Differential stimulation of protein kinase c activity by phorbol ester or calcium/phosphatidylserine in vitro and in intact synaptosomes. *J Biol Chem*, 267(30):21637–44, 1992.

[156] E. Tahara, H. Kadara, L. Lacroix, D. Lotan, and R. Lotan. Activation of protein kinase c by phorbol 12-myristate 13-acetate suppresses the growth of lung cancer cells through klf6 induction. *Cancer Biol Ther*, 8(9):801–7, 2009.

[157] M. G. Kazanietz. Eyes wide shut: protein kinase c isozymes are not the only receptors for the phorbol ester tumor promoters. *Mol Carcinog*, 28(1):5–11, 2000.

[158] Gongyi Zhang, Marcelo G. Kazanietz, Peter M. Blumberg, and James H. Hurley. Crystal structure of the cys2 activator-binding domain of protein kinase cδ in complex with phorbol ester. *Cell*, 81(6):917–924, 1995.

[159] Jun Chen, Fan Deng, Jun Li, and Q. Jane Wang. Selective binding of phorbol esters and diacylglycerol by individual c1 domains of the pkd family. *Biochemical Journal*, 411(2):333–342, 2008.

[160] Valentina Benfenati, Marco Caprini, Grazia Paola Nicchia, Andrea Rossi, Melania Dovizio, Chiara Cervetto, Mario Nobile, and Stefano Ferroni. Carbenoxolone inhibits volume-regulated anion conductance in cultured rat cortical astroglia. *Channels*, 3(5):323–336, 2009.

[161] Benjamin König and Tobias Stauber. Biophysics and structure-function relationships of lrrc8-formed volume-regulated anion channels. *Biophysical Journal*, 116(7):1185–1193, 2019.

[162] Steven S. Vogel, B. Wieb van der Meer, and Paul S. Blank. Estimating the distance separating fluorescent protein fret pairs. *Methods (San Diego, Calif.)*, 66(2):131–138, 2014.

[163] A. Hoppe, K. Christensen, and J. A. Swanson. Fluorescence resonance energy transfer-based stoichiometry in living cells. *Biophys J*, 83(6):3652–64, 2002.

[164] S. Muallem, B. X. Zhang, P. A. Loessberg, and R. A. Star. Simultaneous recording of cell volume changes and intracellular ph or ca2+ concentration in single osteosarcoma cells umr-106-01. *J Biol Chem*, 267(25):17658–64, 1992.

[165] Rebekka M. Wachter and S. James Remington. Sensitivity of the yellow variant of green fluorescent protein to halides and nitrate. *Current Biology*, 9(17):R628–R629, 1999.

[166] G. J. Kremers, J. Goedhart, E. B. van Munster, and Jr. Gadella, T. W. Cyan and yellow super fluorescent proteins with improved brightness, protein folding, and fret forster radius. *Biochemistry*, 45(21):6570–80, 2006.

[167] S. F. Pedersen, T. K. Klausen, and B. Nilius. The identification of a volume-regulated anion channel: an amazing odyssey. *Acta Physiologica*, 213(4):868–881, 2015.

[168] Doralicia Casares, Pablo V. Escribá, and Catalina Ana Rosselló. Membrane lipid composition: Effect on membrane and organelle structure, function and compartmentalization and therapeutic avenues. *International journal of molecular sciences*, 20(9):2167, 2019.

[169] B. Nilius, J. Prenen, T. Voets, J. Eggermont, and G. Droogmans. Activation of volume-regulated chloride currents by reduction of intracellular ionic strength in bovine endothelial cells. *J Physiol*, 506 (Pt 2):353–61, 1998.

[170] Paolo Arosio, Baptiste Jaquet, Hua Wu, and Massimo Morbidelli. On the role of salt type and concentration on the stability behavior of a monoclonal antibody solution. *Biophysical Chemistry*, 168-169:19–27, 2012.

[171] A. L. Moore, M. W. Roe, R. F. Melnick, and S. D. Lidofsky. Calcium mobilization evoked by hepatocellular swelling is linked to activation of phospholipase cgamma. *J Biol Chem*, 277(37):34030–5, 2002.

[172] C. Ruwhof, J. T. van Wamel, L. A. Noordzij, S. Aydin, J. C. Harper, and A. van der Laarse. Mechanical stress stimulates phospholipase c activity and intracellular calcium ion levels in neonatal rat cardiomyocytes. *Cell Calcium*, 29(2):73–83, 2001.

[173] J. H. Nam, H. S. Lee, Y. H. Nguyen, T. M. Kang, S. W. Lee, H. Y. Kim, S. J. Kim, Y. E. Earm, and S. J. Kim. Mechanosensitive activation of k+ channel via phospholipase c-induced depletion of phosphatidylinositol 4,5-bisphosphate in b lymphocytes. *J Physiol*, 582(Pt 3):977–90, 2007.

[174] M. Fujii, M. Ohtsubo, T. Ogawa, H. Kamata, H. Hirata, and H. Yagisawa. Real-time visualization of ph domain-dependent translocation of phospholipase c-delta1 in renal epithelial cells (mdck): response to hypo-osmotic stress. *Biochem Biophys Res Commun*, 254(2):284–91, 1999.

[175] D. M. Browe and C. M. Baumgarten. Stretch of beta 1 integrin activates an outwardly rectifying chloride current via fak and src in rabbit ventricular myocytes. *J Gen Physiol*, 122(6):689–702, 2003.

[176] J. A. Felix, M. L. Woodruff, and E. R. Dirksen. Stretch increases inositol 1,4,5-trisphosphate concentration in airway epithelial cells. *Am J Respir Cell Mol Biol*, 14(3):296–301, 1996.

[177] W. Deng, L. Baki, and C. M. Baumgarten. Endothelin signalling regulates volume-sensitive cl- current via nadph oxidase and mitochondrial reactive oxygen species. *Cardiovasc Res*, 88(1):93–100, 2010.

[178] D. M. Browe and C. M. Baumgarten. Angiotensin ii (at1) receptors and nadph oxidase regulate cl- current elicited by beta1 integrin stretch in rabbit ventricular myocytes. *J Gen Physiol*, 124(3):273–87, 2004.

[179] X. T. Wang, K. D. McCullough, X. J. Wang, G. Carpenter, and N. J. Holbrook. Oxidative stress-induced phospholipase c-gamma 1 activation enhances cell survival. *J Biol Chem*, 276(30):28364–71, 2001.

[180] Xiao-Chun Bai, Fan Deng, An-Ling Liu, Zhi-Peng Zou, Yu Wang, Zhi-Yong Ke, Qun-Sheng Ji, and Shen-Qiu Luo. Phospholipase c-gamma1 is required for cell survival in oxidative stress by protein kinase c. *The Biochemical journal*, 363(Pt 2):395–401, 2002.

[181] A. M. Domijan, S. Kovac, and A. Y. Abramov. Lipid peroxidation is essential for phospholipase c activity and the inositol-trisphosphate-related ca(2)(+) signal. *J Cell Sci*, 127(Pt 1):21–6, 2014.

[182] Joan-Marc Servitja, Roser Masgrau, Raúl Pardo, Elisabet Sarri, and Fernando Picatoste. Effects of oxidative stress on phospholipid signaling in rat cultured astrocytes and brain slices. *Journal of Neurochemistry*, 75(2):788–794, 2000.

[183] I. H. Lambert. Reactive oxygen species regulate swelling-induced taurine efflux in nih3t3 mouse fibroblasts. *J Membr Biol*, 192(1):19–32, 2003.

[184] R. Crutzen, V. Shlyonsky, K. Louchami, M. Virreira, E. Hupkens, A. Boom, A. Sener, W. J. Malaisse, and R. Beauwens. Does nad(p)h oxidase-derived h2o2 participate in hypotonicity-induced insulin release by activating vrac in beta-cells? *Pflugers Arch*, 463(2):377–90, 2012.

[185] J. B. Holm, R. Grygorczyk, and I. H. Lambert. Volume-sensitive release of organic osmolytes in the human lung epithelial cell line a549: role of the 5-lipoxygenase. *Am J Physiol Cell Physiol*, 305(1):C48–60, 2013.

[186] P. Doroshenko and E. Neher. Volume-sensitive chloride conductance in bovine chromaffin cell membrane. *J Physiol*, 449:197–218, 1992.

[187] A. Y. Estevez, T. Bond, and K. Strange. Regulation of i(cl,swell) in neuroblastoma cells by g protein signaling pathways. *Am J Physiol Cell Physiol*, 281(1):C89–98, 2001.

[188] Bernd Nilius, Thomas Voets, Jean Prenen, Holger Barth, Klaus Aktories, Kozo Kaibuchi, Guy Droogmans, and Jan Eggermont. Role of rho and rho kinase in the activation of volume-regulated anion channels in bovine endothelial cells. *The Journal of Physiology*, 516(1):67–74, 1999.

[189] Viktoriya Syrovatkina, Kamela O. Alegre, Raja Dey, and Xin-Yun Huang. Regulation, signaling, and physiological functions of g-proteins. *Journal of molecular biology*, 428(19):3850–3868, 2016.

[190] M. Mederos y Schnitzler, U. Storch, S. Meibers, P. Nurwakagari, A. Breit, K. Essin, M. Gollasch, and T. Gudermann. Gq-coupled receptors as mechanosensors mediating myogenic vasoconstriction. *Embo j*, 27(23):3092–103, 2008.

[191] G. L. Waldo, T. K. Ricks, S. N. Hicks, M. L. Cheever, T. Kawano, K. Tsuboi, X. Wang, C. Montell, T. Kozasa, J. Sondek, and T. K. Harden. Kinetic scaffolding mediated by a phospholipase c-beta and gq signaling complex. *Science*, 330(6006):974–80, 2010.

[192] T. Kendall Harden, Gary L. Waldo, Stephanie N. Hicks, and John Sondek. Mechanism of activation and inactivation of gq/phospholipase c-β signaling nodes. *Chemical reviews*, 111(10):6120–6129, 2011.

[193] B. Ruhfus, H. Tinel, and R. K. Kinne. Role of g-proteins in the regulation of organic osmolyte efflux from isolated rat renal inner medullary collecting duct cells. *Pflugers Arch*, 433(1-2):35–41, 1996.

[194] P. Burow, M. Klapperstuck, and F. Markwardt. Activation of atp secretion via volume-regulated anion channels by sphingosine-1-phosphate in raw macrophages. *Pflugers Arch*, 467(6):1215–26, 2015.

[195] G. J. Duan, J. Zhu, C. Y. Xu, J. Y. Wan, L. Zhang, X. D. Ge, L. M. Liu, and Y. S. Liu. Protective effect of go6976, a pkd inhibitor, on lps/d: -galn-induced acute liver injury in mice. *Inflamm Res*, 60(4):357–66, 2011.

[196] Nicholas C. Zachos, Luke J. Lee, Olga Kovbasnjuk, Xuhang Li, and Mark Donowitz. Plc-γ directly binds activated c-src, which is necessary for carbachol-mediated inhibition of nhe3 activity in caco-2/bbe cells. *American journal of physiology. Cell physiology*, 305(3):C266–C275, 2013.

[197] F. J. Johannes, J. Prestle, S. Eis, P. Oberhagemann, and K. Pfizenmaier. Pkcu is a novel, atypical member of the protein kinase c family. *J Biol Chem*, 269(8):6140–8, 1994.

[198] A. M. Valverde, J. Sinnett-Smith, J. Van Lint, and E. Rozengurt. Molecular cloning and characterization of protein kinase d: a target for diacylglycerol and phorbol esters with a distinctive catalytic domain. *Proc Natl Acad Sci U S A*, 91(18):8572–6, 1994.

[199] E. Rozengurt, O. Rey, and R. T. Waldron. Protein kinase d signaling. *J Biol Chem*, 280(14):13205–8, 2005.

[200] M. Cobbaut and J. Van Lint. Function and regulation of protein kinase d in oxidative stress: A tale of isoforms. *Oxid Med Cell Longev*, 2018:2138502, 2018.

[201] Daniel J Elsner, Katharina M Siess, Thomas Gossenreiter, Markus Hartl, and Thomas A Leonard. A ubiquitin-like dimerization domain controls protein kinase d dimerization and activation by trans-autophosphorylation. *Journal of Biological Chemistry*, 2019.

[202] L. Paolucci, J. Sinnett-Smith, and E. Rozengurt. Lysophosphatidic acid rapidly induces protein kinase d activation through a pertussis toxin-sensitive pathway. *Am J Physiol Cell Physiol*, 278(1):C33–9, 2000.

[203] R. T. Waldron, O. Rey, E. Zhukova, and E. Rozengurt. Oxidative stress induces protein kinase c-mediated activation loop phosphorylation and nuclear redistribution of protein kinase d. *J Biol Chem*, 279(26):27482–93, 2004.

[204] P. Storz and A. Toker. Protein kinase d mediates a stress-induced nf-kappab activation and survival pathway. *Embo j*, 22(1):109–20, 2003.

[205] J. Igarashi, M. Miyoshi, T. Hashimoto, Y. Kubota, and H. Kosaka. Hydrogen peroxide induces s1p1 receptors and sensitizes vascular endothelial cells to sphingosine 1-phosphate, a platelet-derived lipid mediator. *Am J Physiol Cell Physiol*, 292(2):C740–8, 2007.

[206] Richard T. Waldron, Giulio Innamorati, M. Eugenia Torres-Marquez, James Sinnett-Smith, and Enrique Rozengurt. Differential pkc-dependent and -independent pkd activation by g protein α subunits of the gq family: selective stimulation of pkd ser autophosphorylation by gαq. *Cellular signalling*, 24(4):914–921, 2012.

[207] Lingye Chen, Thorsten M. Becker, Ursula Koch, and Tobias Stauber. The lrrc8/vrac anion channel facilitates myogenic differentiation of murine myoblasts by promoting membrane hyperpolarization. *Journal of Biological Chemistry*, 2019.

[208] Alexander Kleger, Christiane Loebnitz, Ganesh Pusapati, Milena Armacki, Martin Müller, Stefan Tümpel, Anett Illing, Daniel Hartmann, Cornelia Brunner, Stefan Liebau, Karl L Rudolph, Guido Adler, and Thomas Seufferlein. Protein kinase d2 is an essential regulator of murine myoblast differentiation. *PloS one*, 6:e14599, 2011.

[209] Yulia V. Shulga, Matthew K. Topham, and Richard M. Epand. Regulation and functions of diacylglycerol kinases. *Chemical Reviews*, 111(10):6186–6208, 2011.

[210] Aiko Kume, Koki Kawase, Suguru Komenoi, Takako Usuki, Ena Takeshita, Hiromichi Sakai, and Fumio Sakane. The pleckstrin homology domain of diacylglycerol kinase η strongly and selectively binds to phosphatidylinositol 4,5-bisphosphate. *The Journal of biological chemistry*, 291(15):8150–8161, 2016.

[211] J. V. Olsen, B. Blagoev, F. Gnad, B. Macek, C. Kumar, P. Mortensen, and M. Mann. Global, in vivo, and site-specific phosphorylation dynamics in signaling networks. *Cell*, 127(3):635–48, 2006.

[212] H. Zhou, S. Di Palma, C. Preisinger, M. Peng, A. N. Polat, A. J. Heck, and S. Mohammed. Toward a comprehensive characterization of a human cancer cell phosphoproteome. *J Proteome Res*, 12(1):260–71, 2013.

[213] N. Dephoure, C. Zhou, J. Villen, S. A. Beausoleil, C. E. Bakalarski, S. J. Elledge, and S. P. Gygi. A quantitative atlas of mitotic phosphorylation. *Proc Natl Acad Sci U S A*, 105(31):10762–7, 2008.

[214] J. V. Olsen, M. Vermeulen, A. Santamaria, C. Kumar, M. L. Miller, L. J. Jensen, F. Gnad, J. Cox, T. S. Jensen, E. A. Nigg, S. Brunak, and M. Mann. Quantitative phosphoproteomics

reveals widespread full phosphorylation site occupancy during mitosis. *Sci Signal*, 3(104):ra3, 2010.

[215] K. T. Rigbolt, T. A. Prokhorova, V. Akimov, J. Henningsen, P. T. Johansen, I. Kratchmarova, M. Kassem, M. Mann, J. V. Olsen, and B. Blagoev. System-wide temporal characterization of the proteome and phosphoproteome of human embryonic stem cell differentiation. *Sci Signal*, 4(164):rs3, 2011.

[216] Toshiki Yamada and Kevin Strange. Intracellular and extracellular loops of lrrc8 are essential for volume-regulated anion channel function. *The Journal of General Physiology*, 150(7):1003–1015, 2018.

[217] Kiyotaka Nishikawa, Alex Toker, Franz-Josef Johannes, Zhou Songyang, and Lewis C. Cantley. Determination of the specific substrate sequence motifs of protein kinase c isozymes. *Journal of Biological Chemistry*, 272(2):952–960, 1997.

[218] Tim Eiseler, Angelika Hausser, Line De Kimpe, Johan Van Lint, and Klaus Pfizenmaier. Protein kinase d controls actin polymerization and cell motility through phosphorylation of cortactin. *The Journal of biological chemistry*, 285(24):18672–18683, 2010.

[219] E. de Castro, C. J. Sigrist, A. Gattiker, V. Bulliard, P. S. Langendijk-Genevaux, E. Gasteiger, A. Bairoch, and N. Hulo. Scanprosite: detection of prosite signature matches and prorule-associated functional and structural residues in proteins. *Nucleic Acids Res*, 34(Web Server issue):W362–5, 2006.

[220] Mirita Franz-Wachtel, Stephan A. Eisler, Karsten Krug, Silke Wahl, Alejandro Carpy, Alfred Nordheim, Klaus Pfizenmaier, Angelika Hausser, and Boris Macek. Global detection of protein kinase d-dependent phosphorylation events in nocodazole-treated human cells. *Molecular & Cellular Proteomics*, 11(5):160–170, 2012.

[221] Todd Scheuer. Regulation of sodium channel activity by phosphorylation. *Seminars in cell & developmental biology*, 22(2):160–165, 2011.

[222] M. J. Davis, X. Wu, T. R. Nurkiewicz, J. Kawasaki, P. Gui, M. A. Hill, and E. Wilson. Regulation of ion channels by protein tyrosine phosphorylation. *Am J Physiol Heart Circ Physiol*, 281(5):H1835–62, 2001.

[223] II Ismailov and D. J. Benos. Effects of phosphorylation on ion channel function. *Kidney Int*, 48(4):1167–79, 1995.

[224] DAVID N. SHEPPARD and MICHAEL J. WELSH. Structure and function of the cftr chloride channel. *Physiological Reviews*, 79(1):S23–S45, 1999.

[225] M. C. Winter and M. J. Welsh. Stimulation of cftr activity by its phosphorylated r domain. *Nature*, 389(6648):294–6, 1997.

[226] M. M. Reddy and P. M. Quinton. camp-independent phosphorylation activation of cftr by g proteins in native human sweat duct. *Am J Physiol Cell Physiol*, 280(3):C604–13, 2001.

[227] S. Inayat, L. H. Pinto, and J. B. Troy. Minimizing cytosol dilution in whole-cell patch-clamp experiments. *IEEE Transactions on Biomedical Engineering*, 60(7):2042–2051, 2013.

[228] Michael Pusch and Erwin Neher. Rates of diffusional exchange between small cells and a measuring patch pipette. *Pflügers Archiv*, 411(2):204–211, 1988.

[229] Iraj Laffafian and M. B. Hallett. Lipid-assisted microinjection: Introducing material into the cytosol and membranes of small cells. *Biophysical Journal*, 75(5):2558–2563, 1998.

[230] K. Irie, A. Nakahara, Y. Nakagawa, H. Ohigashi, M. Shindo, H. Fukuda, H. Konishi, U. Kikkawa, K. Kashiwagi, and N. Saito. Establishment of a binding assay for protein kinase c isozymes using synthetic c1 peptides and development of new medicinal leads with protein kinase c isozyme and c1 domain selectivity. *Pharmacol Ther*, 93(2-3):271–81, 2002.

[231] Iskandar F. Abdullaev, Alena Rudkouskaya, Gary P. Schools, Harold K. Kimelberg, and Alexander A. Mongin. Pharmacological comparison of swelling-activated excitatory amino acid release and cl- currents in cultured rat astrocytes. *The Journal of physiology*, 572(Pt 3):677–689, 2006.

[232] T. Okada, M. R. Islam, N. A. Tsiferova, Y. Okada, and R. Z. Sabirov. Specific and essential but not sufficient roles of lrrc8a in the activity of volume-sensitive outwardly rectifying anion channel (vsor). *Channels (Austin)*, pages 1–12, 2016.

[233] Adrian R. Black and Jennifer D. Black. Protein kinase c signaling and cell cycle regulation. *Frontiers in immunology*, 3:423–423, 2013.

[234] E. Galperin, V. V. Verkhusha, and A. Sorkin. Three-chromophore fret microscopy to analyze multiprotein interactions in living cells. *Nat Methods*, 1(3):209–17, 2004.

[235] A. D. Hoppe, B. L. Scott, T. P. Welliver, S. W. Straight, and J. A. Swanson. N-way fret microscopy of multiple protein-protein interactions in live cells. *PLoS One*, 8(6):e64760, 2013.

[236] Brandon L. Scott and Adam D. Hoppe. Optimizing fluorescent protein trios for 3-way fret imaging of protein interactions in living cells. *Scientific Reports*, 5:10270, 2015.

[237] L. J. Fulcher, T. Macartney, P. Bozatzi, A. Hornberger, A. Rojas-Fernandez, and G. P. Sapkota. An affinity-directed protein missile system for targeted proteolysis. *Open Biol*, 6(10), 2016.

[238] Luke J. Fulcher, Luke D. Hutchinson, Thomas J. Macartney, Craig Turnbull, and Gopal P. Sapkota. Targeting endogenous proteins for degradation through the affinity-directed protein missile system. *Open biology*, 7(5):170066, 2017.

[239] Derek W. Bartlett and Mark E. Davis. Insights into the kinetics of sirna-mediated gene silencing from live-cell and live-animal bioluminescent imaging. *Nucleic acids research*, 34(1):322–333, 2006.

[240] L. Leisle, C. F. Ludwig, F. A. Wagner, T. J. Jentsch, and T. Stauber. Clc-7 is a slowly voltage-gated 2cl(-)/1h(+)-exchanger and requires ostm1 for transport activity. *Embo j*, 30(11):2140–52, 2011.

[241] N. Le Bot, C. Antony, J. White, E. Karsenti, and I. Vernos. Role of xklp3, a subunit of the xenopus kinesin ii heterotrimeric complex, in membrane transport between the endoplasmic reticulum and the golgi apparatus. *J Cell Biol*, 143(6):1559–73, 1998.

[242] M. L. Markwardt, G. J. Kremers, C. A. Kraft, K. Ray, P. J. Cranfill, K. A. Wilson, R. N. Day, R. M. Wachter, M. W. Davidson, and M. A. Rizzo. An improved cerulean fluorescent protein with enhanced brightness and reduced reversible photoswitching. *PLoS One*, 6(3):e17896, 2011.

[243] T. Nagai, K. Ibata, E. S. Park, M. Kubota, K. Mikoshiba, and A. Miyawaki. A variant of yellow fluorescent protein with fast and efficient maturation for cell-biological applications. *Nat Biotechnol*, 20(1):87–90, 2002.

[244] J. Schindelin, I. Arganda-Carreras, E. Frise, V. Kaynig, M. Longair, T. Pietzsch, S. Preibisch, C. Rueden, S. Saalfeld, B. Schmid, J. Y. Tinevez, D. J. White, V. Hartenstein, K. Eliceiri, P. Tomancak, and A. Cardona. Fiji: an open-source platform for biological-image analysis. *Nat Methods*, 9(7):676–82, 2012.

[245] J. N. Feige, D. Sage, W. Wahli, B. Desvergne, and L. Gelman. Pixfret, an imagej plug-in for fret calculation that can accommodate variations in spectral bleed-throughs. *Microsc Res Tech*, 68(1):51–8, 2005.

[246] X. Jiang and A. Sorkin. Coordinated traffic of grb2 and ras during epidermal growth factor receptor endocytosis visualized in living cells. *Mol Biol Cell*, 13(5):1522–35, 2002.

[247] Fabian Sievers, Andreas Wilm, David Dineen, Toby J. Gibson, Kevin Karplus, Weizhong Li, Rodrigo Lopez, Hamish McWilliam, Michael Remmert, Johannes Söding, Julie D. Thompson, and Desmond G. Higgins. Fast, scalable generation of high-quality protein multiple sequence alignments using clustal omega. *Molecular systems biology*, 7:539–539, 2011.

[248] Andrew M. Waterhouse, James B. Procter, David M. A. Martin, Michèle Clamp, and Geoffrey J. Barton. Jalview version 2—a multiple sequence alignment editor and analysis workbench. *Bioinformatics*, 25(9):1189–1191, 2009.